THE UNIVERSITY OF CALGARY

LOSS OF PRESTRESS AND STRESS REDISTRIBUTION WITH TIME IN POST-TENSIONED HOLLOW MASONRY WALLS

by

RAJESH TANEJA

A THESIS

SUBMITTED TO THE FACULTY OF GRADUATE STUDIES IN PARTIAL FULFILLMENT OF THE REQUIREMENTS FOR THE DEGREE OF MASTER OF SCIENCE IN ENGINEERING

DEPARTMENT OF CIVIL ENGINEERING

CALGARY, ALBERTA

MAY, 1986

ISBN Ø-315-3ØØØ6-X

THE UNIVERSITY OF CALGARY

FACULTY OF GRADUATE STUDIES

The undersigned certify that they have read, and recommend to the Faculty of Graduate Studies for acceptance, a thesis entitled "Loss of Prestress and Stress Redistribution with Time in Post-Tensioned Hollow Masonry Walls", submitted by Rajesh Taneja in partial fulfillment of the requirements for the degree of Master of Science in Engineering.

N. G. Shrive

Dr. N.G. Shrive
Department of Civil Engineering
(Supervisor)

A. Huizer

Mr. A. Huizer
Department of Civil Engineering

A. Ghali

Dr. A. Ghali
Department of Civil Engineering

O Vin

Dr. O. Vinogradov
Dept. of Mechanical Engineering

2nd May 1986

Date

ABSTRACT

A three-dimensional finite element model of masonry for calculating the potential loss of prestress in post-tensioned hollow masonry walls is developed. The model allows for creep and shrinkage in the mortar and concrete block units, and stress relaxation in the prestressing steel. Short-term experimental creep and shrinkage data of masonry components, available in the literature, are fitted into mathematical expressions and extrapolated to the desired long-term times.

Fully bedded and face-shell bedded specimens of concrete block and brick wall models are analysed. Long-term as well as short-term upper and lower bounds to loss of prestress are calculated. Upper and lower limits correspond respectively to the worst and the best case of creep and shrinkage strains in mortar and block units. Short-term computed losses are compared with experimental values reported in the literature. Finally, the redistribution of stresses in post-tensioned hollow masonry wall models is studied and the mechanisms causing redistributions are discussed in detail.

The overall results indicate that post-tensioning is a viable method of increasing the long-term flexural capacity in masonry walls.

ACKNOWLEDGEMENTS

I am very grateful to my supervisors, Dr. N.G. Shrive and Mr. A. Huizer, for their willing assistance and guidance at all times. I am much indebted to Dr. N.G. Shrive for his suggestion of the problem. His encouragement and constructive criticisms were invaluable in the development of this study. Special recognition is due to Mr. Fred J. Griffiths for his friendship, and valuable help during the final stages of this work. Thanks are also due to Ms. Carolyn Macarthur for spending her evenings and weekends typing this thesis.

The financial assistance provided by the Department of Civil Engineering and the Natural Sciences and Engineering Research Council of Canada is gratefully acknowledged.

Last but not least, I wish to dedicate this work to my parents for providing the educational opportunities, and for their love from across the miles.

To my parents

TABLE OF CONTENTS

PAGE

LIST OF TABLES

LIST OF FIGURES

FIGURE		PAGE

FIGURE | PAGE

LIST OF SYMBOLS

$\{\ \}$	column vector
$\{\ \}^T$	row vector
$[\ ]$	matrix
a_i	time function coefficient (scale factor)
$\{a\}$	scale factors matrix
A	stress storage factor
A_m	mortar bedded area
A_{ps}	nominal area of prestressing steel
b_i	exponential constant
$[b]$	exponential terms matrix
$[B]$	strain-displacement transformation matrix
$[B]_H$	hybrid equivalent of matrix $[B]$
C	specific creep strain
$C(t,t_i)$	specific creep strain at time t due to a load applied at time t_i
$[C]$	material compliances matrix
C_e	eccentricity coefficient
C_s	slenderness coefficient
$\{d\}$	nodal displacements vector
$\{D\}$	nodal displacements vector at global level
E	modulus of elasticity
$[E]$	material stiffness (rigidities) matrix
f	stress in the steel bar
f_m	allowable compressive stress
f'_m	ultimate compressive strength
f_{pi}	initial prestress
$f_{ps}(t)$	stress in the prestressed bar at time t

f_{pu}	ultimate strength of the prestressing steel
f_{py}	yield strength of the prestressing steel
Δf^r_{ps}	steel stress loss due to relaxation
$\Delta f^r_{n-1,n}$	steel stress loss due to relaxation in n^{th} time interval, i.e. from time t_{n-1} to t_n
$\{F\}$	structural load vector
$[H]$	product of matrices in hybrid stress approach
k	age coefficient
$[K]$	structural stiffness matrix
$[L]$	linear differential operator matrix
m	a constant (number of terms)
$[M]$	multiplication factors matrix
$[N]$	shape functions matrix
P	vertical compressive load
$[P]$	stress functions matrix
P_a or P_b	force in prestressing bar
$\{s\}$	specific creep strains vector
t_i	time at the end of i time steps
t_o	age at application of loading
t_s	age at start of drying
Δt_i	i^{th} time interval $(t_i - t_{i-1})$
$\{\Delta t^r\}$	equivalent thermal loads vector due to relaxation
$\{u\}$	displacements within an element
u, v, w	displacements in x, y and z directions respectively
X	least square error
$\{\beta\}$	stress parameters vector
γ^c	shear creep strain

ε	normal strain
$\{\varepsilon\}$	strain vector
$\varepsilon^{e\ell}$	elastic strain
ε_e	effective strain
ε^c	normal creep strain
ε_e^c	effective creep strain
$\varepsilon^c(t,t_o)$	creep strain at time t due to a load applied at t_o
$\Delta\varepsilon^c$	incremental creep strain
$\Delta\varepsilon^c_{n-1,n}$	incremental creep strain in n^{th} time interval, i.e. from t_{n-1} to t_n
ε^s	shrinkage strain
$\varepsilon^s(t,t_s)$	shrinkage strain at time t where t_s is the age at the start of drying
$\Delta\varepsilon^s_{n-1,n}$	incremental shrinkage strain in n^{th} time interval, i.e. from time t_{n-1} to t_n
$\{\varepsilon_o\}$	initial strain vector
ν_c	creep Poisson's ratio
σ	normal stress
$\{\sigma\}$	stress vector
$\bar{\sigma}$	effective stress
σ_e	effective stress
σ_i	stress in i^{th} time step
$\Delta\sigma_i$	incremental stress for i^{th} time step
$\{\sigma_o\}$	initial stress vector
τ	shear stress
$\phi(t,t_o)$	creep coefficient at time t due to a load applied at time t_o
χ	aging coefficient
χ_r	reduced relaxation coefficient

CHAPTER 1

INTRODUCTION

1.1 Statement of the Problem

In recent years, prestressed masonry wall systems have gained a new recognition as a structural option. The use of prestressing in masonry structures increases the tensile capacity as well as overcoming the problem of crack size limitation. Furthermore, it has been observed that prestressed designs are more economical than other structural systems.

In prestressed structures, a significant loss of prestress occurs with time and the initial tensile capacity is reduced. Thus, it is important to estimate prestress losses before applying a prestressing force. Very little is known regarding the prestress loss in masonry. Therefore, the author's purpose in this research is to calculate the potential loss of prestress in post-tensioned hollow masonry walls. To achieve this, a three-dimensional finite element model of masonry is developed. This work involved study of creep and shrinkage in mortar and concrete blocks or brick units, and stress relaxation in prestressing steel.

Creep is the time-dependent increase in strain induced in a material at constant temperature by a constant sustained stress. Contrary to creep, shrinkage does not depend on loading and is simply the time-dependent contraction of material due to loss of moisture to the environment. Like creep, relaxation is time dependent and is the decrease in stress under a constant deformation at constant temperature. Both creep and shrinkage strains have been observed in concrete blocks, mortars and brick units by Lenczner (1969, 1971 and 1974) and Ameny (1979 and 1982). In composite materials, the creep in steel is neglected as it is insignificant as compared to the creep in the other components. However, a significant relaxation of stress in the prestressing steel takes place for stresses more than fifty percent of the ultimate strength of the prestressing steel.

Creep and shrinkage cause a continuous redistribution of stresses in masonry units, mortar and steel in any reinforced, prestressed or composite masonry system. In the case of prestressed hollow masonry walls, creep and shrinkage cause a contraction which leads to a significant loss of the initial prestressing force. Furthermore, stress relaxation of the prestressing steel also contributes to the problem of prestress loss.

Experimental values of the loss of prestress in hollow masonry walls have been reported by Tatsa et al (1973), Lenczner (1983), Huizer and Shrive (1984) and Lenczner and Davis (1984). These values are for a relatively short period of time (200 days only). Lenczner (1969, 1971 and 1974) and Ameny (1979 and 1982) obtained the short-term time dependent deformational behaviour of masonry experimentally. But in order to design masonry walls safely, stress loss in the steel over time and long-term deformations must be estimated before applying a prestressing force.

In "Masonry Designer's Manual" by Curtin et al (1982), 20% ultimate prestress loss is suggested for post-tensioned brickwork masonry. In the literature, a few approximate numerical methods have been proposed to estimate long-term deformations of masonry from the properties of its different constituents by Jessop et al (1978b) and Shrive and England (1981). Their solutions were based on several assumptions and simplifications. Ameny et al (1984) suggested a few models to estimate long-term deformations based on analytical solution procedures. Lenczner (1981) gave an approximate expression to calculate the ultimate creep strain in brickwork assuming a constant stress state at all times. In order to predict results more accurately, more precise numerical solutions have to be developed. Anand et al (1983 and 1984) developed a two-dimensional finite element model which incorporated a numerical solution technique to calculate the influence of redistribution of stresses due to creep and shrinkage in composite masonry walls. The numerical solution required creep and shrinkage properties of the different components of masonry structures.

Since the nature of stresses in masonry walls is essentially triaxial, there was a need to develop a three-dimensional model into which the effects of prestressing of steel could be incorporated.

1.2 Objectives of the Research

Accordingly, the objective of this study was to develop a numerical technique for a three-dimensional model capable of:

1. computing the redistribution of stresses in post-tensioned hollow masonry walls due to creep and shrinkage;
2. including prestress force numerically with the effects of stress relaxation taken into account; and
3. calculating both long and short-term, upper and lower bounds to loss of prestress, given our current knowledge of creep, shrinkage and relaxation properties.

1.3 Outline of the Research

To achieve the research objectives, the following work was carried out and is described in this thesis.

1. Review the detailed relevant literature (Chapter 2).
2. Evolve a method of analysis for creep, shrinkage and relaxation effects. Select and develop the numerical procedure and modify an existing finite element program in order to incorporate the relevant time-dependent non-linear effects (Chapter 3).
3. Fit mathematical expressions to the short-term data of creep and shrinkage of mortar, concrete blocks and brick units available in the literature, such that the data could be stored efficiently in the computer program. Further, the expressions were used to extrapolate for the long-term behaviour of masonry (Chapter 4).
4. Develop model specimens to represent both actual hollow concrete masonry and brickwork masonry walls. Different models were selected to represent different mortar combinations with concrete blocks and brick units respectively (Chapter 5).
5. Study the redistribution of stresses between mortar and masonry units using the modified program and prestressed hollow masonry wall models. Further, upper and lower bounds to prestress loss in the stretched steel bars were obtained. Finally, short-term prestress loss values were compared with experimental values reported in the literature (Chapter 6).

CHAPTER 2

LITERATURE REVIEW

2.1 Introduction

In the author's opinion, the literature review was not complete until the research was over. As the study proceeded, certain points needed to be studied and probed further. Those areas were researched and the literature is discussed in the relevant chapters. In this chapter, only that part of literature is reviewed which is relevant to the main objectives of the study.

The use of prestressing in masonry is quite recent. Some experimental observations and theoretical results regarding stress distribution in prestressed masonry have been reported in the literature but still there is a lot more to be done in this field. Very few observations have been made regarding loss of prestress in masonry due to time-dependent effects. Nothing has been done to find the long-term prestress loss. On the other hand, in prestressed concrete structures, a lot of research work has been reported. Thus, in this chapter, some work related to concrete is also reviewed.

2.2 Finite Element Models for Masonry

Khalil (1983) made an extensive search of existing literature about finite element models in his Ph.D. work. His main finding was that although masonry walls had been analysed with finite element models, most analyses had involved two-dimensional plane elements only. Also most of the analyses involved solid homogeneous units only. There were very few reports of three-dimensional stress analyses and those were limited in scope. Khalil (1983) used a three-dimensional finite element model to analyse hollow masonry walls. He concluded that finite element computer programs can work really well for the analysis of both concrete block and clay brick walls provided that reliable material properties are used. He verified the values of stress and strain obtained analytically by comparing with experimental values. In his analysis Khalil used material properties determined by Ameny (1979 and 1982). Khalil assumed perfect bond between units and mortar. He also assumed that both unit and mortar were homogeneous, isotropic and linear-elastic. The assumption of linear-elastic behaviour was justified by analysing the model under a uniformly distributed load equal to 0.35 of the ultimate strength.

In the area of hollow masonry, the work was carried further by Simbeya (1985). He also used three-dimensional models to assess the stress distributions in masonry due to concentrated load. He modelled different types of masonry wall to obtain an understanding of the stress distributions. In his finite element analysis, Simbeya made the same assumptions as Khalil.

2.3 Creep and Shrinkage Properties

A significant number of observations have been made in the past concerning creep and shrinkage strains in masonry. An extensive review of published material on elastic, thermal, shrinkage and creep properties of masonry has been made by Jessop et al (1978a). Although Ameny (1979) also made a detailed survey of the literature in this field, points related specifically to this study are reviewed again here.

Poljakov (1962) made some important contributions to creep in masonry. He studied creep strains of some brickwork prisms which were subjected to a sustained stress of 0.4 to 0.6 of the estimated ultimate strength of the test specimens. He noticed that the ultimate creep strains developed in the prisms were 85-155% of the instantaneous elastic strain. He tried to fit a mathematical expression to the experimental creep data and found that an approximate logarithmic relationship existed between creep strains and the stress/strength ratio. Further, if the stress/strength ratio was less than 0.6, this relationship could be a linear one. He also studied the effects of different ages at loading. More importantly he formed an exponential type expression for masonry creep as a function of age at loading, the duration of the load, stress over strength ratio and the brickwork type. The expression was of the form:

$$\varepsilon^{c}(t,t_o) = A \times \left(\frac{\text{stress}}{\text{strength}}\right) \left(0.1 + 1.82\, e^{-0.3 t_o^{\frac{1}{4}}}\right) (t-t_o)^{1/7}$$

where $\varepsilon^{c}(t,t_o)$ is the masonry creep at any time t, t_o is the age at loading and A is a coefficient depending on the type of brickwork. This was an important finding as it matches with the observations made by Bazant and Wu (1973) in the field of concrete structures. Poljakov also observed that the creep behaviour did not differ much due to eccentric loading.

Lenczner performed many tests on brick masonry as well as concrete masonry. Using half size model bricks Lenczner (1969) observed that creep strains in wall panels were lower than in the piers by 20%. He found that considerable creep occurred in the piers, though 80-96% of the creep strains at 70 days occurred in the first 28 days. Lenczner (1971) also concluded that creep in brickwork containing full size bricks was much smaller, even less than one-fifth of creep strains measured in model brickwork.

Lenczner et al (1975) performed tests to study the effects of stress levels using different types of units and mortars. They observed that creep strains increased with stress although the relationship was not linear, especially when stress/strength ratio exceeded 0.4. They concluded that creep could be expected to cease within a year.

The effects of age at loading and eccentricity in brick masonry were studied by Lenczner and Salahuddin (1976). They noticed that age at loading, provided it was greater than 14 days, did not change the creep strains very significantly. Small eccentricities had little influence on creep behaviour. Creep tests on isolated brick units were also performed. It was observed that there was not much creep in the individual units and most of the creep occurred in the first 30 days. This behaviour indicated that the major portion of creep in brickwork occurred in the mortar joints. The main point to be noted is that all their tests were conducted at a constant temperature of 20°C and approximately 50% relative humidity. In their tests shrinkage strains were also examined. Maximum shrinkage in brick walls was found to be only 54 $\times 10^{-6}$. On the other hand individual bricks showed some moisture expansion and the maximum expansion strains were 30 $\times 10^{-6}$.

Wyatt et al (1975) tried to fit the creep data of brick masonry obtained earlier by Lenczner to an equation or expression form. They obtained a logarithmic relationship between creep strains and age at observation of creep strains. The function was of the form:

$$\varepsilon^{c}(t) = 2500 \left(\frac{\text{stress}}{\text{strength}}\right)^{3} \ell n\ (t + 1)$$

Lenczner (1974) studied creep and shrinkage in blockwork. He observed that the creep strains which developed in the blockwork were considerably higher than those of the brickwork. He found that for his circumstances, creep ceased at all stress levels after approximately 300 days. Another point he observed was that creep strains in the mortar (1:1:6) were 4 to 5 times greater than those in the concrete block units. When the tests were conducted again at a constant temperature of 20°C and 50% relative humidity, it was observed that the shrinkage strain rate was very high in the beginning followed by a slow rate. After 320 days, shrinkage strains in blockwork were 525×10^{-6} while in individual block units the strains were 410×10^{-6}. At this time strains were still increasing but at a very reduced rate.

Ameny (1979 and 1982) in his M.Sc. and Ph.D. theses obtained a similar set of creep and shrinkage strain data for concrete and brick masonry compared with the data Lenczner had obtained. Ameny concluded that the order of magnitude of strains was the same as had been obtained by Lenczner. The main difference was that in Ameny's case, there was no provision to maintain constant temperature and humidity although the laboratory was centrally air heated and the observed temperature and humidity during the course of experiments did not vary much except on one occasion.

Ameny et al (1980) concluded that in concrete block masonry when the ratio of applied stress to masonry strength is in the range of 0.17-0.40, creep is linearly related to the stress/strength ratio and further that this relationship is not altered by eccentricity of loading. Creep strains in block masonry were 18-43% higher than creep measured in the individual blocks. Hence, the mortar crept more than the blocks.

Ameny et al (1984) reported that brick creep was very small with a creep coefficient of only 0.08-0.13 after one year. For convenience the creep coefficient has been defined as the ratio of the creep strain to the elastic strain.

$$\phi(t,t_o) = \varepsilon^c(t,t_o)/\varepsilon^{e\ell}(t_o)$$

Since there was no gauge available to measure the mortar strains individually, a few separate tests were conducted on mortar cylinders, although Ameny (1982) acknowledged that the behaviour of the mortar cylinders did not represent the true behaviour of mortar in masonry. In his test specimens two different mortar cases were taken. Creep strains of N-mortar were observed to be much higher than that of M-mortar. He observed very low shrinkage strains in brick masonry and concluded that it could be neglected. As per Jessop et al (1978a) there is a significant amount of moisture movement (expansion) reported in brickwork. In the early stages, bricks undergo significant reversible expansion. Ameny et al (1984) however, reported little moisture expansion in the brickwork, as the bricks used were thoroughly soaked in water before constructing the test specimens.

Tatsa et al (1973) noticed that in the case of concrete blockwork walls the ratio of the creep strains in the joints to the creep strains in the blocks was 4.4 when specimens were not presoaked and 16.8 when specimens were presoaked.

2.4 Prestress in Masonry

A few published reports about experimental observations of stress distribution due to prestress in masonry can be found in the literature but theoretical analyses are rare.

Suter et al (1983) tried to analyse prestressed masonry walls theoretically but that work was very limited in scope. In the stress analysis, only two-dimensional constant strain triangular plane finite elements were used. This did not represent the triaxial stress nature of prestressed masonry walls. Further, the prestressing steel stiffness was neglected and moreover, the prestressing force was represented as a concentrated load at the top of the wall. This did not represent the actual prestressing load system.

Simbeya (1985) continued work in this field by analysing masonry walls with a concentrated load using three-dimensional solid finite elements. He studied the stress distribution in a number of different masonry walls.

Tatsa et al (1973) made a few experimental observations in blockwork walls regarding prestress loss in masonry. Their main conclusion was that losses were of the same order of magnitude as in conventional prestressed concrete. In their tests all panels were prestressed to 45% of the ultimate strength and the post-tensioned steel bars were stressed to 83% of the ultimate tensile strength. After 180 days prestress loss due to creep and shrinkage was found to be 12.5% and due to stress relaxation of steel 6.5%. The overall short term losses after 180 days were in the order of 20%.

Recently Huizer and Shrive (1984) reported experimental values of short-term losses in a post-tensioned concrete block masonry wall. The block units used were over three years old and thus the mortar was expected to contribute most of the total creep or shrinkage. Post-tensioning steel wires were of high tensile strength and were prestressed to 70% of the ultimate strength. Over 200 days, the observed prestress loss due to creep, shrinkage and relaxation was 16% or less.

Short-term loss of prestress in post-tensioned brickwork has been observed by Lenczner and Davis (1984). His findings were that prestress loss in brickwork practically ceased after some 175 days and 50% of the loss occurred during the first 25-40 days. After about a year, 9-11% prestress loss was observed in brickwork walls. As the prestressing bars were not stressed more than 50% of the ultimate strength, loss due to relaxation of steel was negligible. Thus, the overall loss reported was essentially because of creep and shrinkage only.

Curtin et al (1982) recommend 20% ultimate loss of post-tensioned force to be considered in the design of post-tensioned brickwork masonry due to creep, shrinkage and relaxation effects. Wherein the losses due to relaxation may be taken as about 8% at the 70% stress level and 0% at 50% stress level.

2.5 Method of Analysis

In composite masonry, a numerical approach has been developed by Anand et al (1983 and 1984) for the solution of creep and shrinkage problems of a two-dimensional nature. A similar approach has been used by a number of authors in the field of concrete structures. On the same topic, several finite element texts, e.g. by Zienkiewicz (1977) and Cook (1981), are also available. It is a load incremental, iterative, step-by-step solution method in the time domain. The first step is an elastic analysis of the problem. At the end of the time step, creep and shrinkage strains are calculated. These are taken as initial strains for the next time step and the problem is analysed again. This procedure is continued until either the final requisite time is reached or the stress-strain distribution in two consequent time steps differs only slightly. This method is general and applicable for any form of creep and shrinkage input data.

CHAPTER 3

FINITE ELEMENT ANALYSIS FOR CREEP, SHRINKAGE AND RELAXATION EFFECTS

3.1 Introduction

Masonry is a composite type of construction wherein concrete blocks or brick units are joined together by thin layers of mortar. Different material characteristics of mortar, concrete blocks and brick units make the analysis of masonry walls very complicated especially when time-dependent effects due to creep, shrinkage and relaxation properties are also incorporated. The use of hollow units, prestressing steel and different mortar bedding types in between the masonry units increase the complexity of stress analysis in prestressed hollow masonry walls. Approximate solutions for the time-dependent analysis of masonry structures have been reported in the literature but are based on several assumptions and simplifications. In order to predict long-term behaviour of prestressed masonry accurately, the finite element method, a numerical solution procedure, was chosen for the present study. Modern age computers have popularized this method of analysis. The finite element program available to the author, had to be modified to perform time-dependent non-linear analysis as previously it only had the capacity of analysing linear elasto-static problems. A numerical solution technique was developed to include the effects of the creep, shrinkage and relaxation properties of masonry.

3.2 Creep, Shrinkage and Relaxation Effects

3.2.1 Creep and Shrinkage Phenomena

Basic definitions, theories of creep and shrinkage phenomena, their mechanisms and different methods have been given in detail in the text by Neville et al (1983). This text has been referenced throughout this study as an aid in understanding and applying the different concepts and analysis methods.

In this section, the basic assumptions made in the analysis for creep and shrinkage properties are discussed.

Creep has been defined as the strain in excess of the elastic strain at the time of application of load. In reality materials gain stiffness with aging so that true elastic strain decreases as time passes. Therefore, creep is actually the strain in excess of the true elastic strain. The change in elastic strain over time has been observed to be small. It has been neglected in past studies to simplify the analytical procedure. In this study, it is assumed that the elastic strain remains constant during the entire time analysis.

In the literature, creep and shrinkage phenomena, occurring at the same time, have been assumed to be additive. In reality the two are interdependent. In general, the effect of shrinkage (drying) on creep is to increase the magnitude of creep strains. For simplification, however, the creep strains are taken to be those in excess of the shrinkage strains. The input data of creep and shrinkage properties of masonry components used in this study were based on the assumption of the additive phenomena.

It has been reported by Bazant (1982) that creep and shrinkage strains do not remain constant throughout the depth of cross sections of test specimens. This uneven distribution across the section causes internal forces which may cause surface cracks. In the case of thick sections, these effects may be very severe. The sections of masonry walls, analysed in this study, as well as those of prism specimens which were used to obtain creep and shrinkage data, were not thick. Thus, the creep and shrinkage strains may be assumed to represent an overall or mean value across the cross section.

3.2.2 Creep

3.2.2.1 Influencing Factors

Creep strains are influenced by a large number of factors which have been given in detail in the text by Neville et al (1983). Only the main points are reviewed here and a comparison between laboratory tested specimens and the model specimens, analysed in this study, will be made in the next chapter through the following factors.

1. Compressive Strength: In general, creep deformations are inversely proportional to the ultimate compressive strength of the unit.
2. Relative Humidity: Creep strains decrease with an increase in the ambient relative humidity provided there are no fluctuations in the relative humidity after loading the specimens. It has been observed that creep increases if the specimens are exposed to variations in the relative humidity after the application of loading.
3. Size of Specimen: Creep deformations decrease with an increase in the thickness of the specimen, but when the thickness exceeds about 0.9 m the size effect becomes negligible.

4. Magnitude of Applied Stress: Creep strains increase with the magnitude of the sustained stress. This relationship is generally found to be linear for a stress level of 0.4 of the ultimate strength.

5. Time Since Loading: Creep strains increase with the duration of applied stress.

6. Age at Loading: Creep strains decrease with an increase in the age at which the load is applied.

7. Temperature: Creep strains increase with temperature, proportionally in the range of 20° to 70°C.

3.2.2.2 Creep under Compression and Tension

Most of the creep data in masonry have been obtained with uniaxial compression tests. In the literature as per Neville et al (1983), many researchers have observed the creep in tension and compression to be equal under an equal magnitude of stress. In the present study of prestressed masonry walls, all model specimens are in compression although local tensile stress may be present at some points. The average compressive stress is 0.25 of the ultimate strength of masonry, ensuring that the stresses remain in the working stress range. The low tensile stresses in the present analysis allow the assumption that the magnitude of total creep under both states of stress is the same and creep data obtained from compression tests have been used for tensile stress states too.

3.2.2.3 Creep under Multiaxial Stress State

It has been observed that during uniaxial compression tests, creep strains not only occur in the direction of applied stress, but also normal to it. This induced lateral deformation due to creep has been defined as lateral creep strain. Similar to the definition of elastic Poisson's ratio, creep Poisson's ratio has been expressed as the ratio of the lateral creep strain to the creep strain along the direction of the applied stress.

In the case of masonry structures, nothing has been reported about values of creep Poisson's ratio. In the field of concrete structures, a lot of research has been done. Some have observed creep Poisson's ratio to be very close to the elastic Poisson's ratio.

As only uniaxial creep test data are available, a multiaxial stress state has to be developed from the uniaxial stress state. To develop a three-dimensional stress state, two approaches have been reported.

In the first approach, creep Poisson's ratio is used. In any direction of three-dimensional multiaxial stress state, creep occurs due to stress applied in that direction as well as due to stresses in the other two normal directions. By assuming that all strains occur independently of one another, the principle of superposition can be applied and a multiaxial stress state can be developed and expressed as follows:

$$\varepsilon_i^c = \varepsilon_i^{cu} - \nu_{cu}\varepsilon_j^{cu} - \nu_{cu}\varepsilon_k^{cu} \tag{3.1}$$

where ε_i^{cu}, ε_j^{cu}, ε_k^{cu} are the axial creep strains due to the separate action of principal stresses σ_1, σ_2 and σ_3. ν_{cu} is the creep Poisson's ratio under uniaxial compression and ε_i^c is the total creep in the direction of σ_i under multiaxial stress state. If the stress in any direction is less than 0.4 f'_m, where f'_m is the ultimate compressive strength, then the observed experimental fact of a linear relationship between creep strains and sustained stress can be used. For convenience the specific creep term, which has been defined as the ratio of creep strains to the stress applied or creep strain per unit stress, can be used.

$$C = \varepsilon^{cu}/\sigma_u$$

where C is the specific creep and σ_u is the uniaxial stress.

Equation (3.1) can be rewritten as

$$\varepsilon_i^c = \frac{\varepsilon^{cu}}{\sigma_u} [\sigma_i - \nu_{cu}(\sigma_j + \sigma_k)]$$

$$\varepsilon_i^c = C[\sigma_i - \nu_{cu}(\sigma_j + \sigma_k)] \qquad (3.2)$$

ν_{cu} can either be taken equal to elastic Poisson's ratio or can be any experimental observed value. Further, it may be different in all three directions.

In the second approach an effective stress-strain relationship is used. It has been observed that the volumetric creep $(\varepsilon_1^{cu} + \varepsilon_2^{cu} + \varepsilon_3^{cu})$ has the same relationship with time as uniaxial creep. As per Neville et al (1983) a linear relationship has been found between

$$[(\varepsilon_1^{cu} - \varepsilon_2^{cu})^2 + (\varepsilon_2^{cu} - \varepsilon_3^{cu})^2 + (\varepsilon_3^{cu} - \varepsilon_1^{cu})^2]^{\frac{1}{2}} \quad \text{and}$$

$$[(\sigma_1 - \sigma_2)^2 + (\sigma_2 - \sigma_3)^2 + (\sigma_3 - \sigma_1)^2]$$

The same concept has been stated in the text by Crandall et al (1972) in the form of a relationship between equivalent stress and equivalent creep strain. Creep behaviour was associated with yield criterion of plasticity. This approach was used by Haque et al (1974) in the study of tensile creep analysis of concrete structures. Recently, using the concepts of this approach, Anand et al (1984) developed the multiaxial stress state of composite masonry.

This technique can be summarized as follows:

$$\sigma_e = \sqrt{\frac{1}{2}[(\sigma_1 - \sigma_2)^2 + (\sigma_2 - \sigma_3)^2 + (\sigma_3 - \sigma_1)^2]} \tag{3.3}$$

and $$\varepsilon_e = \sqrt{\frac{2}{9}[(\varepsilon_1 - \varepsilon_2)^2 + (\varepsilon_2 - \varepsilon_3)^2 + (\varepsilon_3 - \varepsilon_1)^2]} \tag{3.4}$$

where σ_e is the effective stress and ε_e is the effective strain which is equivalent to effective plastic strain. σ_1, σ_2 and σ_3 are the principal stresses and ε_1, ε_2 and ε_3 are the principal strains. The main assumption of this approach to creep analysis is that the equivalent plastic strain of Equation (3.4) has been replaced by experimentally observed uniaxial creep strain which has been defined as the equivalent creep strain.

$$\varepsilon_e = \varepsilon_e^c \tag{3.5}$$

where ε_e^c is the equivalent creep strain. Then multiaxial creep strains can be expressed as follows:

$$\varepsilon_x^c = \frac{\varepsilon_e^c}{\sigma_e} [\sigma_x - \frac{1}{2} (\sigma_y + \sigma_z)] \tag{3.6a}$$

$$\varepsilon_y^c = \frac{\varepsilon_e^c}{\sigma_e} [\sigma_y - \frac{1}{2} (\sigma_z + \sigma_x)] \tag{3.6b}$$

$$\varepsilon_z^c = \frac{\varepsilon_e^c}{\sigma_e} [\sigma_z - \frac{1}{2} (\sigma_x + \sigma_y)] \tag{3.6c}$$

$$\gamma^c_{xy} = 3 \frac{\varepsilon^c_e}{\sigma_e} \tau_{xy} \tag{3.6d}$$

$$\gamma^c_{yz} = 3 \frac{\varepsilon^c_e}{\sigma_e} \tau_{yz} \tag{3.6e}$$

$$\gamma^c_{zx} = 3 \frac{\varepsilon^c_e}{\sigma_e} \tau_{zx} \tag{3.6f}$$

where ε^c_x, ε^c_y and ε^c_z are the normal creep strain components and γ^c_{xy}, γ^c_{yz} and γ^c_{zx} are the shear creep strain components.

In the absence of any experimental data regarding creep Poisson's ratio in masonry, the second approach has been used in the present study to develop multiaxial creep strain components.

3.2.3 Method of Creep Analysis

Creep deformations are stress dependent but do not cause any change in the overall stress resultant under constant loading conditions. In the case of plain homogeneous sections subjected to a constant load, creep analysis is fairly simple as the stress always remains constant. In the case of reinforced or prestressed sections, however, complexity arises because of the presence of the steel. The steel restrains the creep deformations of the surrounding material and results in a redistribution of stresses as the overall stress resultant still remains the same. Redistribution of stresses changes the constant stress problem to one of variable stress with time. In the case of prestressed structures, this problem is further complicated. Due to creep deformations, contraction is produced which results in a drop in the initial prestress value and continuously varies the overall stress with time.

Various methods for creep analysis have been explained by Neville et al (1983). In the present study, a step-by-step numerical solution technique has been selected to deal with the problem of stress varying continuously with time. Formulation of the numerical technique is presented in the following sections.

3.2.3.1 Principle of Superposition

In relation to creep, the principle of superposition states that if a specimen is subjected to different stresses at different times, the creep strain produced at any time due to a stress applied before is independent of the effects of any other stress applied before or after. This principle which is well documented in a report by Anand et al (1984) can be explained with the help of Figure 3.1. Creep response is to be obtained for a specimen subjected to the stress state as shown in Figure 3.1a. This stress state is represented by two independent stress levels acting at different times as shown in Figures 3.1b and 3.1c. Their superposition gives the same value of stress at all times, as shown by Figure 3.1a. Creep responses to stress levels of Figures 3.1b and 3.1c are given by virgin specific creep* curves as shown in Figures 3.1d and 3.1e respectively. From the principle of superposition, the creep response to each stress level can be assumed to be independent of the other. The combined creep response can be obtained from the summation of the curves of Figures 3.1d and 3.1e as shown in Figure 3.1f.

---

* Specific creep is defined as the ratio of creep strain to the stress applied or creep strain per unit stress.

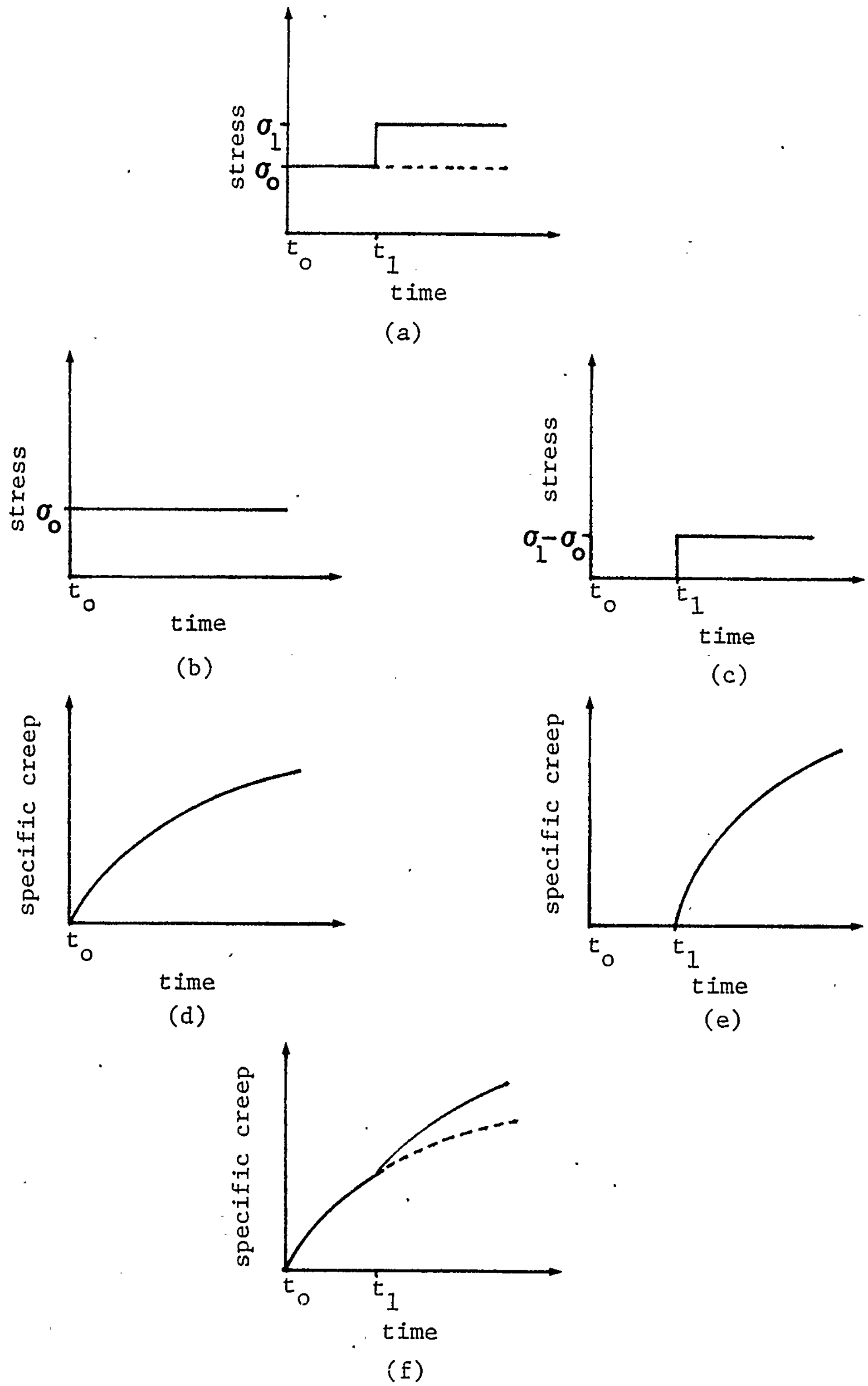

Figure 3.1 Principle of Superposition

Mathematically this can be expressed as:

at any time $t > t_1$, due to stress σ_o of Figure 3.1b

$$\varepsilon_o^c(t) = \sigma_o \, C(t,t_o) \tag{3.7}$$

where $\varepsilon_o^c(t)$ is the creep strain at time t due to a stress σ_o applied at time t_o and $C(t,t_o)$ is the specific creep strain at t due to stress applied at age t_o.

$$\Delta\varepsilon_1^c(t) = (\sigma_1 - \sigma_o) \, C(t,t_1) \tag{3.8}$$

where $\Delta\varepsilon_1^c(t)$ corresponds to stress $(\sigma_1 - \sigma_o)$ of Figure 3.1c. From the principle of superposition, the total creep strain due to a stress state of Figure 3.3a is

$$\varepsilon^c(t) = \varepsilon_o^c(t) + \Delta\varepsilon_1^c(t)$$

i.e. $$\varepsilon^c(t) = \sigma_o C(t,t_o) + (\sigma_1 - \sigma_o) C(t,t_1) \tag{3.9}$$

For a general case of (n-1) stress changes in n time intervals, the total creep strain at time t_n is equal to:

$$\varepsilon^c(t_n) = \sigma_o C(t_n,t_o) + \sum_{i=1}^{n-1} \Delta\sigma_i \, C(t_n,t_i) \tag{3.10}$$

$$\text{where } \Delta\sigma_i = \sigma_i - \sigma_{i-1} \tag{3.11}$$

Equation (3.10), derived from the principle of superposition, is used here in the step-by-step solution method. As per Dilger (1982), this principle gives good comparison with experimental results for increasing stress and slightly decreasing stress. For complete unloading, predicted results are overestimated. In this study, the principle of superposition has been assumed to be valid here as unloading is only due to the loss of prestress which is a small part of the total loading.

3.2.3.2 Step-by-Step Numerical Solution Method

The creep problem in prestressed structures has the varying stress state shown in Figure 3.2a. In this method, the total time is divided into a number of time steps. For a particular time interval, the stress at the beginning of the time interval is known. At the end of the time interval the new stress must be determined from the creep analysis procedure for the model specimen.

(a) Explicit and Implicit Schemes

Quite a few formulations of the step-by-step method have been reported but all of them can be classified into one of the two schemes known as explicit or implicit. In the case of elasto-viscoplastic solids, these schemes have been discussed by Owen and Hinton (1980). Since the creep case is similar to elasto-viscoplasticity, the two procedures for the creep problem are reviewed here.

The creep strain at time t_{n+1}, due to a step increment of stress $(\sigma_n - \sigma_{n-1})$ applied at time t_n can be found from Equation (3.8) and is equal to:

$$\Delta\varepsilon^c_n(t_{n+1}) = (\sigma_n - \sigma_{n-1})C(t_{n+1},t_n) = \Delta\sigma_n C(t_{n+1},t_n) \tag{3.12}$$

In general, for a continuously varying stress, Equation (3.12) can be written as:

$$\Delta\varepsilon^c_n(t_{n+1}) = [(1 - K)\Delta\sigma_n + K\,\Delta\sigma_{n+1}]C(t_{n+1},t_n) \tag{3.13}$$

where $\Delta\sigma_{n+1} = \sigma_{n+1} - \sigma_n$ and K is any constant. With K equal to zero a fully explicit scheme or forward difference method is obtained as the creep strain increment is determined from the stress existing at the

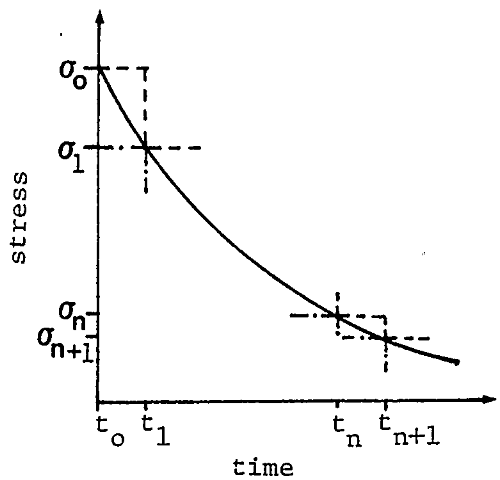

(a) Varying Stress State

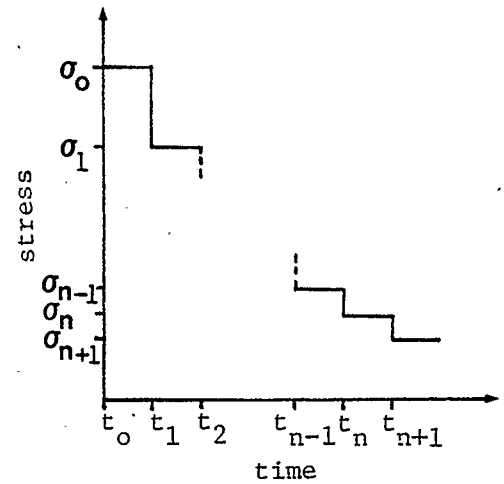

(b) Time Step Scheme

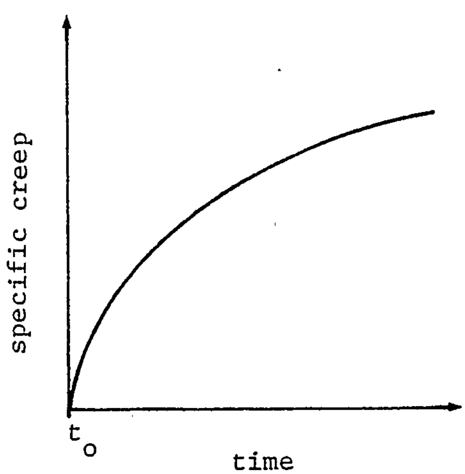

(c)

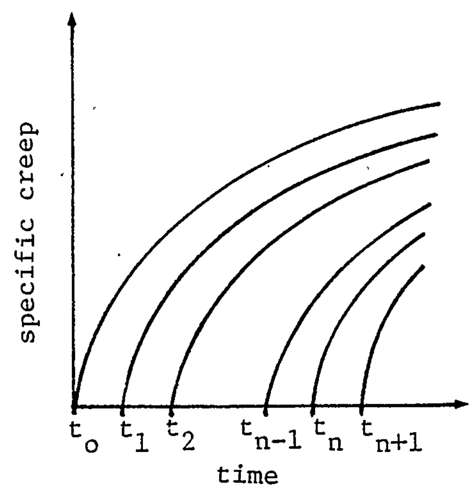

(d)

Specific Creep Curves

Figure 3.2 Step-by-Step Solution Method

beginning of the time interval, i.e. at time t_n. On the other hand K equal to unity results in a fully implicit scheme or backward difference method as the creep strain is determined from the final stress at the end of the time interval, i.e. at time t_{n+1}. In Figure 3.2a an explicit scheme has been shown by a dotted line while an implicit scheme is shown by a chain-dotted line.

As per Owen and Hinton (1980), for K less than 0.5, the numerical process is only conditionally stable and it can only proceed when the time interval, Δt_i, is less than some critical value, otherwise it results in numerical instability. For K greater than or equal to 0.5, the procedure is unconditionally stable but may not give accurate results unless there is a limit put on the time step length. On the other hand explicit methods simplify the analysis procedure, as in Equation (3.13) with K equal to zero, the only unknown to be solved is $\Delta\varepsilon_n^c$. In the implicit scheme (with K=1), besides $\Delta\varepsilon_n^c$, the other unknown to be solved is σ_{n+1}. Use of an implicit scheme requires the knowledge of creep flow rate criteria. Since few data are available about masonry creep behaviour, an explicit scheme was adopted for this study.

(b) Solution Method Used

The two-dimensional creep analysis procedure used by Anand et al (1984) has been modified here for a three-dimensional problem. The total time span is divided into a number of time steps. The continuously varying stress problem of Figure 3.2a has been transformed to one as shown in Figure 3.2b using the explicit scheme. The basic steps are as follows:

1. At time t_o, the elastic analysis is performed with resulting elastic stresses σ_x, σ_y, σ_z, τ_{xy}, τ_{yz}, τ_{zx} and the corresponding strains ε_x, ε_y,

ε_z, γ_{xy}, γ_{yz}, γ_{zx}. Principal stresses σ_1, σ_2 and σ_3 are obtained and using Equation (3.3) the effective stress, σ_e, is calculated. i.e. at time $t = t_o$, $\bar{\sigma}_o = \sigma_e$. This is assumed to remain constant for the first time interval from t_o to t_1.

2. Using Equation (3.7) creep strain ε^c at time t_1 is calculated as:

$$\varepsilon^c(t_1) = \varepsilon_o^c(t_1) = \bar{\sigma}_o\, C(t_1, t_o) \tag{3.14}$$

This requires input data of the specific creep curve for the specimen loaded at t_o, as shown in Figure 3.2c. Creep input data for the present study are discussed in detail in the next chapter. For the time being, it has been assumed that creep data in the form of specific creep curves are known. As $\varepsilon_o^c(t_1)$ is also the change in creep strain in the first time interval, Equation (3.14) can be rewritten as:

$$\Delta\varepsilon_{0,1}^c = \bar{\sigma}_o\, C(t_1, t_o) \tag{3.15}$$

where $\Delta\varepsilon_{o,1}^c$ is incremental creep strain from time t_o to t_1.

3. In Equations (3.6a) to (3.6f), ε_e^c is substituted by $\Delta\varepsilon_{o,1}^c$ and all six creep strain components are calculated at the end of first time interval Δt_1. At time t_1, these creep strains are taken as initial strains and the model specimen is analysed again yielding incremental displacements, stresses and strains. The details of the initial strain approach for this step are explained in the finite element analysis method. The new incremental stresses, strains and displacements obtained in this step are added to previous total values of stresses, strains and displacements respectively. From these known total stresses and using Equation (3.3), a new effective stress, σ_e, such that $\bar{\sigma}_1 = \sigma_e$, is calculated. It is assumed to remain constant for the next time interval i.e. from t_1 to t_2.

4. Using the principle of superposition from Equations (3.8) and (3.9), total creep strain, $\varepsilon^c(t_2)$, at time t_2 is calculated as:

$$\Delta\varepsilon_1^c(t_2) = (\bar{\sigma}_1 - \bar{\sigma}_o)C(t_2,t_1) \tag{3.16}$$

$$\varepsilon^c(t_2) = \bar{\sigma}_o C(t_2,t_o) + (\bar{\sigma}_1 - \bar{\sigma}_o)C(t_2,t_1) \tag{3.17}$$

This step requires a specific creep curve for the specimen loaded at t_1 as shown in Figure 3.2d. From Equations (3.14) and (3.17) the incremental creep strain for the second time interval can be calculated as:

$$\Delta\varepsilon_{1,2}^c = \varepsilon^c(t_2) - \varepsilon^c(t_1)$$

i.e. $$\Delta\varepsilon_{1,2}^c = \bar{\sigma}_o[C(t_2,t_o) - C(t_1,t_o)] + (\bar{\sigma}_1 - \bar{\sigma}_o)C(t_2,t_1) \tag{3.18}$$

For the next step $\Delta\varepsilon_{1,2}^c$ is substituted in Equation (3.6) and all components of incremental creep strains are obtained.

5. For the succeeding time intervals steps 3 and 4 are repeated. Equation (3.18), obtained in step 4, can be generalized for any time interval. For example, from time t_{n-1} to t_n, i.e. the n^{th} time interval, it generalizes to:

$$\Delta\varepsilon_{n-1,n}^c = \bar{\sigma}_o[C(t_n,t_o) - C(t_{n-1},t_o)] + \sum_{i=1}^{n-1} (\bar{\sigma}_i - \bar{\sigma}_{i-1})[C(t_n,t_i) - C(t_{n-1},t_i)] \tag{3.19}$$

Equation (3.19) requires input data of different virgin specific creep curves for specimens loaded at different ages t_o, t_1, ..., t_{n-1} and so on as shown in Figure 3.2d. The analysis procedure proceeds until the final time of interest is reached.

The only constraint by the explicit scheme is the selection of time step lengths. In the field of concrete structures subjected to continuously varying stress, it has been reported that for the best results, the lengths of the time intervals chosen should be approximately equal on a log-time plot.

3.2.4 Shrinkage

3.2.4.1 Influencing Factors

Shrinkage strains are influenced by the following factors:

1. Type of Unit: Shrinkage strains depend on the type of the main unit used. For example, in the case of brick units, during early stages shrinkage may be present in the form of expansion strains.
2. Relative Humidity: Shrinkage strains decrease with an increase in the ambient relative humidity.
3. Size of Member: Mean shrinkage strain decreases with an increase in the thickness of the section. The thicker the section is, the more non-uniform the shrinkage strains become.
4. Time of Drying: Shrinkage strains increase with an increase in the duration of drying or the age of the member.

In the next chapter, strains obtained from laboratory shrinkage specimens are related to the model specimens analysed in this study through the factors above.

3.2.5 Method of Shrinkage Analysis

Shrinkage analysis can easily be incorporated in a step-by-step solution method as the strains are independent of the applied stress and are assumed to be constant throughout the cross section. For the purpose of analysis, shrinkage strains can be assumed to be of the form of a curve as shown in Figure 3.3. Details of the input data are discussed in the next chapter.

The shrinkage strain at any time t can be read from Figure 3.3 as $\varepsilon^s(t,t_s)$ where t_s is the age at the start of drying. In a step-by-step solution method during any time interval, incremental shrinkage strains are taken as initial strains occurring at the end of that time interval. The model specimen is re-analysed for these initial strains. The resulting stresses, strains and displacements are added to previous stresses, strains and displacements respectively to yield new total values.

In general, for n^{th} time interval, i.e. from t_{n-1} to t_n, incremental shrinkage strains are calculated as:

$$\Delta\varepsilon^s_{n-1,n} = \varepsilon^s(t_n,t_s) - \varepsilon^s(t_{n-1},t_s) \tag{3.20}$$

3.2.6 Relaxation

Stress relaxation in the prestressing bars is the loss of tensile force with time, even though the sample is maintained at constant length and temperature. For the present study, stress-time functions for different steels have been taken. For normal relaxation steel, Magura

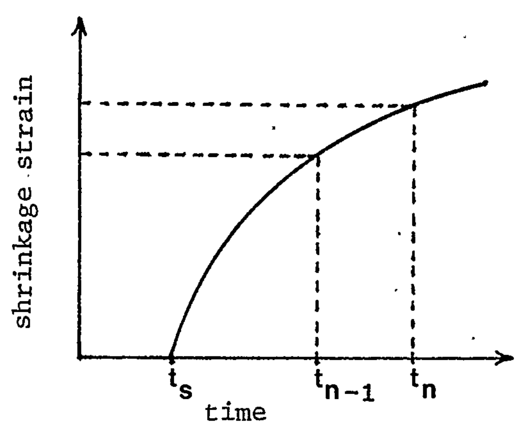

Figure 3.3 Shrinkage Strain vs. Time

et al (1964) suggested an expression of the form:

$$f_{ps}(t) = f_{pi}[1 - \frac{\log_{10} 24(t-t_o)}{10} (\frac{f_{pi}}{f_{py}} - 0.55)] \qquad (3.21)$$

For low relaxation steel the PCI Committee (1975) modified the above expression to:

$$f_{ps}(t) = f_{pi}[1 - \frac{\log_{10} 24(t-t_o)}{45} (\frac{f_{pi}}{f_{py}} - 0.55)] \qquad (3.22)$$

where $f_{ps}(t)$ is the stress in the prestressing steel at time t, f_{pi} is the initial prestress, $(t-t_o)$ is the time in days since the initial prestressing is applied and f_{py} is the yield strength of steel. It can be taken as:

$f_{py} = 0.85\, f_{pu}$ for normal relaxation steel and

$f_{pu} = 0.90\, f_{pu}$ for low relaxation steel

where f_{pu} is the ultimate strength of the prestressing steel. The stress loss Δf^r_{ps}, due to relaxation, at any time t can be computed as:

$$\Delta f^r_{ps}(t) = f_{pi} - f_{ps}(t) \qquad (3.23)$$

i.e. for normal relaxation steel

$$\Delta f^r_{ps}(t) = \frac{f_{pi}}{10} [\log_{10} 24(t-t_o)] (\frac{f_{pi}}{f_{py}} - 0.55) \qquad (3.24)$$

and for low relaxation steel

$$\Delta f^r_{ps}(t) = \frac{f_{pi}}{45} [\log_{10} 24(t-t_o)] (\frac{f_{pi}}{f_{py}} - 0.55) \qquad (3.25)$$

3.2.7 Method of Relaxation Analysis

Equation (3.21) or (3.22) can be plotted as shown in Figure 3.4a. For a step-by-step solution technique, the analysis method for relaxation effects with creep and shrinkage strains has been taken from Loov

(1984).

(a) For normal relaxation steel:

Assuming $t_o = 0$, from Equation (3.21) steel stress at time t_n is:

$$f_{ps}(t_n) = f_{pi}[1 - \frac{\log_{10}24t_n}{10}(\frac{f_{pi}}{f_{py}} - 0.55)] \tag{3.26}$$

At time t_{n+1}

$$f_{ps}(t_{n+1}) = f_{pi}[1 - \frac{\log_{10}24t_{n+1}}{10}(\frac{f_{pi}}{f_{py}} - 0.55)] \tag{3.27}$$

Steel stress loss due to relaxation in the $(n+1)^{th}$ time interval is equal to:

$$\Delta f^r_{n,n+1} = f_{ps}(t_{n+1}) - f_{ps}(t_n) \tag{3.28}$$

$$\text{i.e. } \Delta f^r_{n,n+1} = \frac{f_{pi}}{10}[\log_{10}(\frac{t_{n+1}}{t_n})](\frac{f_{pi}}{f_{py}} - 0.55) \tag{3.29}$$

Equation (3.29) is valid if only the relaxation effect is present. In the present case, steel relaxation loss is accompanied with losses due to creep and shrinkage effects as well. This combined effect for the $(n+1)^{th}$ time interval has been shown by Figure 3.4b. At time t_n, let the net stress in steel due to creep, shrinkage and relaxation effects be $f_{ps}(t_n)$, such that

$$f_{ps}(t_n) = f_{pin}[1 - \frac{\log_{10}24t_n}{10}(\frac{f_{pin}}{f_{py}} - 0.55)] \tag{3.30}$$

where f_{pin} is the modified initial prestress for the $(n+1)^{th}$ time interval. At time t_{n+1}

$$f_{ps}(t_{n+1}) = f_{pin}[1 - \frac{\log_{10}24t_{n+1}}{10}(\frac{f_{pin}}{f_{py}} - 0.55)] \tag{3.31}$$

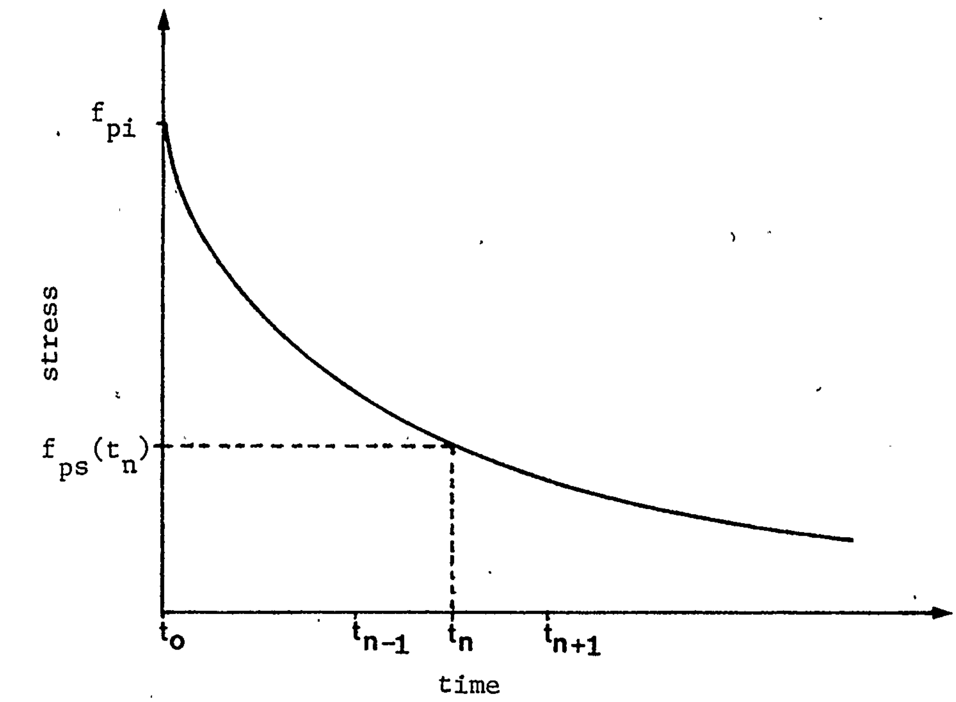

(a) without Creep and Shrinkage Effects

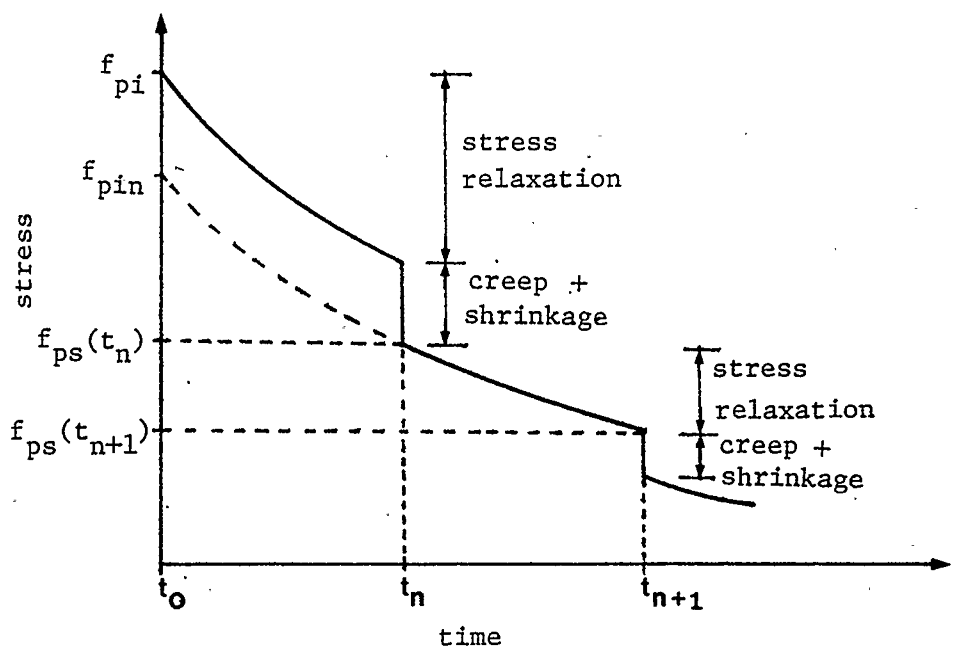

(b) with Creep and Shrinkage Effects

Figure 3.4 Stress Relaxation of Prestressing Steel and the loss of prestress due to relaxation only is equal to:

$$\Delta f^{r}_{n,n+1} = f_{ps}(t_{n+1}) - f_{ps}(t_n) \tag{3.32}$$

From Equation (3.30) f_{pin} can be determined as:

$$\frac{\log_{10}24t_n}{10f_{py}} f_{pin}^{\;2} - (1 + \frac{0.55\ \log_{10}24t_n}{10})\ f_{pin} + f_{ps}(t_n) = 0$$

$$f_{pin}^{\;2} - (\frac{10\ f_{py}}{\log_{10}24t_n} + 0.55) f_{pin} + \frac{10f_{py}f_{ps}(t_n)}{\log_{10}24t_n} = 0$$

$$f_{pin} = \frac{f_{py}}{2}\ [\frac{10}{\log_{10}24t_n} + 0.55 - \sqrt{(\frac{10}{\log_{10}24t_n} + 0.55)^2 - \frac{40f_{ps}(t_n)}{f_{py}\log_{10}24t_n}} \tag{3.33}$$

From Equations (3.31), (3.32) and (3.33) stress loss due to relaxation in $(n+1)^{th}$ time interval can be found.

(b) For low relaxation steel Equations for $f_{ps}(t_{n+1})$, f_{pin} and $\Delta f^{r}_{n,n+1}$ can be developed the same way as has been done in the normal relaxation steel case.

$$f_{pin} = \frac{f_{py}}{2}[\frac{45}{\log_{10}24t_n} + 0.55 - \sqrt{(\frac{45}{\log_{10}24t_n} + 0.55)^2 - \frac{180f_{ps}(t_n)}{f_{py}\log_{10}24t_n}} \tag{3.34}$$

$$f_{ps}(t_{n+1}) = f_{pin}[1 - \frac{\log_{10}24t_{n+1}}{45}\ (\frac{f_{pin}}{f_{py}} - 0.55)] \tag{3.35}$$

During the $(n+1)^{th}$ time interval, stress loss due to relaxation can be found by Equations (3.32), (3.34) and (3.35).

3.3 Finite Element Method

The definition of the finite element method has been adopted from the text by Zienkiewicz (1977) and is reviewed here. It is a general discretization procedure of continuum problems which approximates the solution process (a) by dividing the continuum into a finite number of elements whose behaviour is specified and (b) by solving the whole system as an assembly of its elements following the same rules as those applicable to standard discrete problems. Throughout this study the above mentioned text and the text by Cook (1981) have been referenced.

3.3.1 Computer Program Used

Two finite element programs (1) FINEPAK and (2) SMAC were available to the author. Both the programs were general and had the capacity to solve three-dimensional elasto-static problems. Program FINEPAK had one 3-dimensional 20-node solid displacement element while SMAC had the following three 3-dimensional elements:

(1) 8- to 21-node displacement element

(2) 8-node hybrid stress element

(3) 8-node incompatible modes element

The 20-node displacement element of FINEPAK was used previously by Khalil (1983) and Simbeya (1985). Clearly SMAC has the advantage of two additional 3-dimensional elements. Chieslar (1985b) made some theoretical comparisons of hybrid elements with conventional displacement elements. He concluded that in bending, hybrid elements give the most economic solution. He also proved the superiority of an 8-node hybrid stress element over an 8-node displacement element. An 8-node hybrid element has the advantage of fewer variables compared to a 20-node displacement element even though the final results were comparable. In the case of a non-linear analysis with a step-by-step solution technique, a large quantity of data in the form of stresses, strains and displacements from previous time step must be stored for all the nodal or Gauss integration points. The 8-node hybrid stress element, with fewer variables, was chosen for the present study. Thus, the computer program SMAC (Systematic Matrix Analysis of Continua) developed by Chieslar (1985a) was finally selected.

3.3.2 Finite Element Method in General

Finite element method formulation is based on the following two assumptions:

(1) The strain-displacement relationship is linear. In other words, the small displacement theory is valid.

(2) The stress-strain constitutive relationship is linear, i.e. the concept of material linearity is also valid.

Propagation of cracks is one of the factors which may cause material nonlinearity. This effect can be eliminated by changing the stiffness of the elements which undergo cracking. In the present study, the stiffness change due to cracking is not considered, as the average stresses are within the elastic range. The other factor which results in material nonlinearity is the creep and shrinkage effects of masonry. The solution to the non-linear problem is obtained by reducing it to a series of linear problems which are solved in successive time steps by adopting an incremental time step solution procedure.

As a hybrid element has been chosen for the present analysis, hybrid formulation is compared with displacement formulation in the following sections.

3.3.2.1 Displacement Model

In this approach displacements are taken as the primary unknowns. With the help of assumed shape functions, displacements within an element are defined in terms of displacement at the nodes. Through strain-displacement relations, stresses and strains within the element are also defined in terms of these displacements. At the global level, the system's total potential energy, expressed as a function of nodal displacements, is minimized. This results in equilibrium equations for the unknown displacement parameters. The basic steps can be summarized as follows:

$$\{u\} = [N]\{d\} \tag{3.36}$$

where $\{u\}$ is the displacement vector within an element, $[N]$ are the assumed shape functions and $\{d\}$ are nodal displacements. From strain-displacement relations, we have:

$$\begin{aligned}\{\varepsilon\} &= [L]\{u\} \\ &= [L][N]\{d\} \\ &= [B]\{d\}\end{aligned} \tag{3.37}$$

where $[L]$ is the linear differential operator matrix and $[B] = [L][N]$ is the strain-displacement transformation matrix. From stress-strain relations

$$\begin{aligned}\{\sigma\} &= [E]\{\varepsilon\} \\ &= [E][B]\{d\}\end{aligned} \tag{3.38}$$

where $[E]$ is the material stiffness matrix and $[E] = [C]^{-1}$ where $[C]$ is the material compliances matrix such that

$$\{\varepsilon\} = [C]\{\sigma\} \tag{3.39}$$

All the above relations have been expressed at the element level. Minimization of potential energy produces the equilibrium expression as:

$$[K]\{D\} = \{F\} \tag{3.40}$$

where $[K]$ is the structural stiffness matrix, $\{D\}$ is the structural displacement vector which contains all $\{d\}$ vectors and $\{F\}$ is the structural load vector due to all different loading cases of the system. Equation (3.40) is solved for the unknown displacements. Knowing $\{d\}$, values for $\{\varepsilon\}$ and $\{\sigma\}$ can be obtained from Equations (3.37) and (3.38).

3.3.2.2 Stress Hybrid Model

The stress hybrid model is a type of mixed model where there is more than one primary variable. It is based on an assumed stress field within the element and the displacements are assumed to vary according to Equation (3.36). Stresses are eliminated at the element level. At the global system level, equilibrium equations are solved for the displacement variables. As both assumptions are independent, stresses are obtained indirectly from the displacements.

Although the hybrid stress element concept was introduced by Pian (1964), the detailed information of the hybrid model used in the present analysis is described in Chieslar (1985b). As a comparison with the displacement formulation, only the main step is reviewed here.

$$\{\sigma\} = [P]\{\beta\} \tag{3.41}$$

where [P] is the assumed stress function matrix and $\{\beta\}$ is the stress parameters vector to be evaluated. Vector $\{\beta\}$ is related to the displacements at the nodes.

$$\{\beta\} = [H]\{d\} \tag{3.42}$$

Actually, [H] is a product of many matrices derived from the basic assumptions of the hybrid stress approach. From Equations (3.41) and (3.42), we have:

$$\{\sigma\} = [P][H]\{d\} \tag{3.43}$$

Equation (3.43) is very similar to Equation (3.38). [P][H] is the hybrid equivalent of the stress recovery matrix associated with the displacement formulation.

i.e. $[P][H] \cong [E][B]$ (3.44)

3.3.3 Finite Element Modelling of Prestressed Masonry Wall Specimens

3.3.3.1 Element Types Used

In finite element models of prestressed masonry walls, masonry units and mortar have to be represented by different elements because of their different material characteristics. In order to study the triaxial state of stress in masonry, 3-dimensional hybrid stress elements have been used for both mortar and units. Although details of the different models for the present study are discussed in Chapter 5, a typical vertically post-tensioned hollow masonry wall specimen has been shown in Figure 3.5. The wall is made of hollow units and is post-tensioned by vertical steel bars which pass through the inner core of the blocks. As axial prestressing is used, a uniaxial truss element was selected to represent the prestressing steel member. The prestressing force is transmitted to the wall, through steel plates anchored at the ends. A perfect bond has been assumed between prestressing bars, steel plates and masonry units at the ends. The steel plates were also represented by 3-dimensional solid hybrid elements.

3.3.3.2 Prestressing Concept in Finite Element Approach

In prestressed members, the steel bar carries the tensile force and transfers equal and opposite compressive force to the rest of the structural member. In the present case of axial prestressing, this behaviour has been achieved by taking the thermal loading case of a truss element. A negative temperature change, equivalent to the prestressing force, is applied to the truss member which results in a tensile force in the truss member and a compressive force to the rest of the model structure. This procedure can be explained with the help of a simple example of an axial column shown in Figure 3.6. A general case of two prestressed bars (a) and (b) has been taken. The main objective is to find the final temperature changes t_{af} and t_{bf} corresponding to the prestressing forces P_a and P_b (or stresses f_a and f_b) in the two bars respectively.

To achieve this, two trial elastic runs are made:

First Run: initial thermal load t_{ai} is applied in bar (a) which results in stresses f_{aa} and f_{ba} in the two bars, where f_{ij} is the stress in bar (i) due to a thermal load in bar (j).

Second Run: initial thermal load t_{bi} is applied in bar (b) which results in stresses f_{ab} and f_{bb} in the two bars.

The final stresses f_a and f_b in the two bars due to final thermal loads t_{af} and t_{bf} applied simultaneously can be obtained using the principle of superposition:

$$f_a = t_{af} \frac{f_{aa}}{t_{ai}} + t_{bf} \frac{f_{ab}}{t_{bi}} \tag{3.45a}$$

$$f_b = t_{af} \frac{f_{ba}}{t_{ai}} + t_{bf} \frac{f_{bb}}{t_{bi}} \tag{3.45b}$$

Equations (3.45a) and (3.45b) can be represented in matrix form as:

$$\begin{Bmatrix} f_a \\ f_b \end{Bmatrix} = \begin{bmatrix} f_{aa}/t_{ai} & f_{ab}/t_{bi} \\ f_{ba}/t_{ai} & f_{bb}/t_{bi} \end{bmatrix} \begin{Bmatrix} t_{af} \\ t_{bf} \end{Bmatrix} \tag{3.46a}$$

or

$$\{f\} = [M]\{t_f\} \tag{3.46b}$$

where [M] is defined here as the multiplication factor matrix. From Equation (3.46) unknowns t_{af} and t_{bf} corresponding to f_a and f_b can be

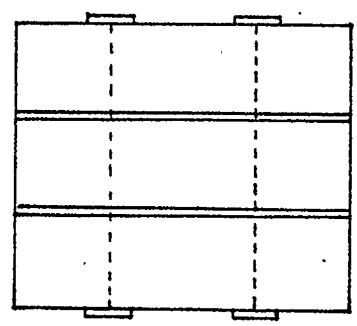

Figure 3.5 Prestressed Wall Specimen

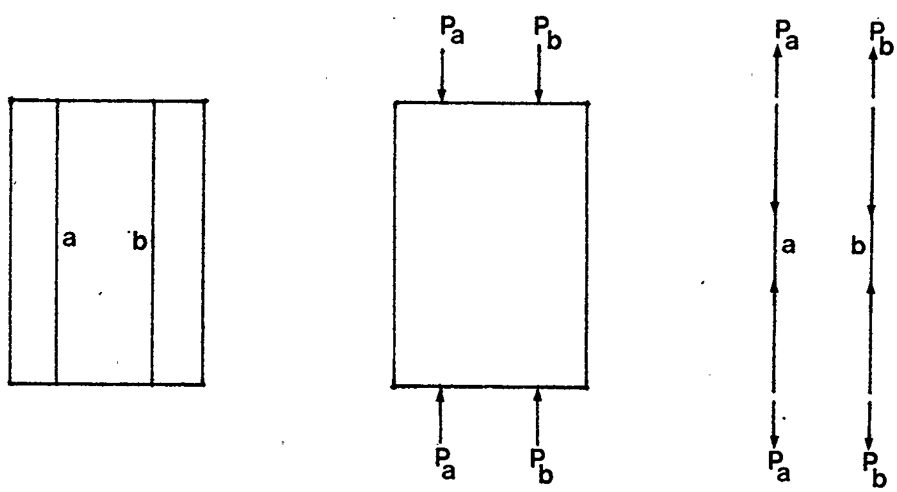

Figure 3.6 Axial Prestressing Concept

obtained as:

$$\begin{Bmatrix} t_{af} \\ t_{bf} \end{Bmatrix} = \begin{bmatrix} f_{aa}/t_{ai} & f_{ab}/t_{bi} \\ f_{ba}/t_{ai} & f_{bb}/t_{bi} \end{bmatrix}^{-1} \begin{Bmatrix} f_a \\ f_b \end{Bmatrix} \qquad (3.47a)$$

or

$$\{t_f\} = [M]^{-1}\{f\} \qquad (3.47b)$$

Equation (3.47) can be generalized for any number of prestressing bars. The number of trial elastic runs is equal to the number of prestressing bars. In the case of one axial prestressing tendon Equation (3.47) reduces to:

$$t_f = \frac{t_i}{f_i}\,\sigma_f \qquad (3.48)$$

where f_i is the initial stress corresponding to initial thermal load of t_i temperature change.

3.3.4 Modelling the Analysis Techniques

3.3.4.1 Creep and Shrinkage Analyses

In a step-by-step solution method, with constant stress state during any time interval, creep strain loading can be taken as equivalent to thermal loading. Similarly shrinkage or moisture induced swelling strain, being independent of the stress at all times, is also similar to a case of temperature loading. Thus, in the finite element technique, an initial stress-strain approach, similar to one for thermal loading, has been used to incorporate creep and shrinkage effects. The basic steps of the initial strain approach can be found from any text and are as follows:

1. Evaluate the initial strains at all Gauss integration points for all elements

$$\{\varepsilon_o\}^T = \{\varepsilon_{xo}\ \varepsilon_{yo}\ \varepsilon_{zo}\ \gamma_{xyo}\ \gamma_{yzo}\ \gamma_{zxo}\} \tag{3.49}$$

2. Evaluate the corresponding initial stresses and store them for the final stress evaluation step.

   $\{\sigma_o\} = -[E]\{\varepsilon_o\}$

3. Evaluate equivalent nodal loads due to initial strains for all the elements by either of the following two methods:

   (a) $\{f\} = \int_V [B]^T[E]\{\varepsilon_o\}dv$

or

   (b) $\{f\} = -\int_V [B]^T\{\sigma_o\}dv$.

4. At the global level, perform a summation of nodal loads for all the elements.

   $$\{F\} = \sum_{i=1}^{n} \{f_i\}$$

   where n is the number of elements.

5. After solving for nodal displacements {d}, obtain final stress as:

   $\{\sigma\} = [E][B]\{d\} + \{\sigma_o\}$

The hybrid formulation equivalent of matrix [E][B] is given by Equation (3.44). By pre-multiplying these matrices by $[E]^{-1}$, the hybrid equivalent of matrix [B] can be found.

i.e. $[E][B] \cong [P][H]$

$$[B]_H \cong [E]^{-1}[P][H] \tag{3.50}$$

where $[B]_H$ is the hybrid equivalent of matrix [B].

For the creep analysis of Step 3 in the step-by-step solution of Section (3.2.3.2), initial creep strain components are obtained as:

$$\{\varepsilon_o^c\}^T = \{\varepsilon_x^c \ \varepsilon_y^c \ \varepsilon_z^c \ \gamma_{xy}^c \ \gamma_{yz}^c \ \gamma_{zx}^c\} \tag{3.51}$$

In the case of shrinkage analysis, initial strains are obtained from Equation (3.20). Only normal strain components are present.

i.e. $$\{\varepsilon_o^s\}^T = \{\varepsilon_x^s \ \varepsilon_y^s \ \varepsilon_z^s \ 0 \ 0 \ 0\} \tag{3.52}$$

For combined creep and shrinkage analyses, initial strains of Equations (3.51) and (3.52) are added to form total initial strains as:

$$\{\varepsilon_o\}^T = \{\varepsilon_o^c\}^T + \{\varepsilon_o^s\}^T \tag{3.53}$$

Initial strains obtained from Equation (3.51) or (3.52) or (3.53) are substituted in Equation (3.49) and their equivalent nodal loads are obtained. After this step, the creep analysis procedure of Section (3.2.3.2) or the shrinkage analysis procedure of Section (3.2.5) or their combined analysis is carried further.

3.3.4.2 Relaxation Analysis

At the end of any time interval, the loss of prestress in steel due to stress relaxation can be found by Equation (3.32). The prestress loss concept is similar to the concept of application of prestress force, the only difference between the two is the reversal of stress sign. Thus the technique developed for prestressing concept in Section (3.3.3.2) has also been used to represent stress relaxation effect.

For convenience Equation (3.47b) is rewritten here.

$$\{\Delta t^r\} = [M]^{-1}\{\Delta f^r\} \tag{3.54}$$

where $\{\Delta f^r\}$ is prestress loss due to relaxation and is computed by Equation (3.32). Using the inverse of multiplication factors matrix $\{M\}^{-1}$, developed in Section (3.3.3.2), equivalent thermal loads $\{\Delta t^r\}$

(positive temperature change) due to the relaxation effect, are computed from Equation (3.54).

When creep and shrinkage analyses are to be combined with relaxation effects, the equivalent nodal loads obtained due to (1) the initial strains of Equations (3.53) and (2) the temperature changes of Equation (3.54) are added together. Then the analysis of model specimens, due to these combined nodal loads, yields the final results due to creep, shrinkage and relaxation properties of masonry.

3.4 Results of Analysis for Prestressed Wall Models

At the end of all time steps, the finite element analysis results in

(1) the total displacements at all nodal points,

(2) the stress-strain distribution at all nodal or integration points and

(3) the total stress in the axial truss members.

The stress in the steel at any time corresponds to the net prestressing force at that time. Thus, the changes of stress in the truss member represents the loss of prestress.

CHAPTER 4

CREEP, SHRINKAGE AND STRESS RELAXATION INPUT DATA, AND COMPUTER PROGRAMMING

4.1 Introduction

With a step-by-step numerical solution technique, finite element analysis for creep, shrinkage and stress relaxation of post-tensioned hollow masonry walls results in the prediction of actual structural behaviour. However, such an analysis requires the input data of stress-time functions for prestressing steel, shrinkage strain curves and specific creep curves at various ages of loading for concrete blocks, brick units and different mortars. The short-term creep and shrinkage properties of masonry components are available in the literature as a set of laboratory measured values at discrete times. Mathematical expressions were fitted to the available data to allow extrapolation for long-term behaviour and for efficient computer storage. The detailed procedures and numerical expressions will be described in the following sections.

4.2 Creep and Shrinkage Properties

4.2.1 Input Data

Creep and shrinkage data for masonry components have been obtained by Lenczner (1969, 1971 and 1974) and Ameny (1979 and 1982). The experimental results were similar, so Ameny's data have been used in conjunction with certain results of Lenczner for the present analysis.

Using stack-bonded prism specimens with full mortar bedding, Ameny (1979) obtained the creep and shrinkage data of concrete blockwork. He also obtained the creep and shrinkage behaviour of brickwork specimens

(Ameny, 1982). The experiments were conducted in a laboratory where there was little control over temperature and humidity. In both studies, the observed temperature did not vary much and was in the range of 17-22°C. During the course of the concrete blockwork tests, the relative humidity was in the range of 30-60%. In the case of the brickwork tests, the relative humidity varied from 15 to 40% for most of the time period except at one occasion. At the age of 200 days after loading, the relative humidity rose to 75% and this continued for the next sixty days. In the creep and shrinkage tests, two mortar cases were taken.

(1) N-mortar (1:3; masonry cement:sand);

(2) M-mortar (1:1:6; portland cement:masonry cement:sand).

In the concrete blockwork tests, prism specimens were loaded axially at the age of seven days and strain measurements were made for the next 100-120 days. Two separate loading cases were taken. Prism specimens were loaded axially to a maximum stress of (1) 0.4 f'_m and (2) 0.2 f'_m, where f'_m is the ultimate compressive strength. Creep and shrinkage strain measurements were made (1) across the whole length of the prisms, (2) in the individual units and (3) across the mortar joints. Strains across the mortar joint were measured over a 50.8 mm gauge length covering the 10 mm mortar joint thickness. Thus the measured strains across the joint were not the actual strains in the mortar joint.

In the case of the brickwork tests, specimens were axially loaded at the age of nine days and strain measurements were made for the next 330-460 days. Creep and shrinkage strains of individual brick units were measured on small brick specimens cut from the main units while those of mortar were obtained from mortar cylinders. Ameny postulated that the actual strains in the mortar joint would be higher than those of the mortar cylinders because of the lower stiffness of the mortar joints due to poor curing conditions.

In Ameny's tests, the age at the start of drying in the shrinkage specimens coincided with the age at application of loading for the creep specimens.

4.2.2 Comparison with Wall Model Specimens

The masonry wall specimens modelled in this study were assumed to have the same range of temperatures and relative humidity as was observed during Ameny's experiments to determine creep and shrinkage properties. Furthermore, the walls were of the same thickness as the experimental test specimens. Thus, the creep and shrinkage data obtained from the test specimens were used for the wall models. As the average compressive stress in the wall models is 0.25 f'_m, the creep strains have been assumed to be linearly proportional to the magnitude of the sustained stress and have been derived from the specific creep curves obtained from the experimental results. For the creep analysis in the step-by-step solution method of Section (3.2.3.2), input data of different specific creep curves for specimen loaded at different ages are required. It was found that the creep strains of individual concrete block units, obtained by Ameny, were of the same order as predicted by the CEB-FIP (1970 and 1978) models for conventional concrete. In the CEB-FIP (1978) model, creep is obtained as a summation of two components, an irreversible creep (age at application of load effect) and a reversible creep (duration effect) whereas in the CEB-FIP (1970) model, creep strain expression is represented in the form of a product of age and duration effects. Since the creep strain expressions developed in the present study are of the same type as those of the CEB-FIP (1970) model, the coefficient for age at application of load given by the CEB-FIP (1970) model has been adopted for this study and virgin specific creep curves for different ages have been derived from the available input data.

4.2.3 Fitting the Data to Logarithmic Expressions

Wyatt et al (1975) obtained a logarithmic relationship between creep strains and time under load for brick masonry. In the field of concrete structures, the US Bureau of Reclamation (1956) developed a similar logarithmic expression based on experimental data for concrete. It was observed that specific creep is a linear function of the logarithm of the time under load provided the stress/strength ratio did not exceed 0.35. For the present study, creep data obtained by Ameny were plotted against the log (time) scale. Most of the creep data could be fitted very well by one or two straight lines in the specific creep strain versus log (time under load) plot. Shrinkage data were also fitted to a similar form of logarithmic relationship. A linear relationship of short-term data was thus easily extrapolated to the desired long-term times. As the main objective was to obtain long-term prestress losses for a period of about 10-15 years, the extrapolation of short-term data would be assumed to hold good for that time only. In the case of creep data, beyond fifteen years time creep strain curves will have to be reassessed in order to predict a finite ultimate value.

4.2.3.1 Creep

(A) Specific Creep Functions for Specimens Loaded at the Age of Seven Days

In Ameny's work on concrete blockwork specimens, loading was applied at the age of seven days while brickwork specimens were loaded at the age of nine days. For the present study the age at initial loading, t_o, has been assumed to be seven days for both cases.

(a) Concrete Block Units

It was observed that the specific creep strains of the individual block units obtained from the prisms tests with N-mortar were higher than those with M-mortar. Data from the N-mortar case were taken as upper bound values while those from the M-mortar were considered as lower bound. A regression analysis using the least square method was performed and the best-fit straight-line expressions were obtained. Specific creep data for all the different cases are plotted in Figure 4.1. As the data obtained by Ameny were only for 100-120 days, they had to be extrapolated to predict the long-term behaviour. Lenczner (1974) reported that creep in concrete blockwork masonry ceased after approximately 300 days. For this study, the second straight line obtained for time greater than 14 days, was extended up to 300 days and then a third line was plotted with the slope of the first line. The extrapolation of the data is shown in Figure 4.1. The different expressions obtained are as follows:

(1) Upper Bound

(i) for $(t-t_o) \leq 14$ days

$$C(t,t_o) = [14.484\ \ell n(t-t_o) + 15.692] \times 10^{-6}. \tag{4.1}$$

FIG. 4.1 SPECIFIC CREEP STRAIN VERSUS TIME FOR CONCRETE BLOCK UNITS

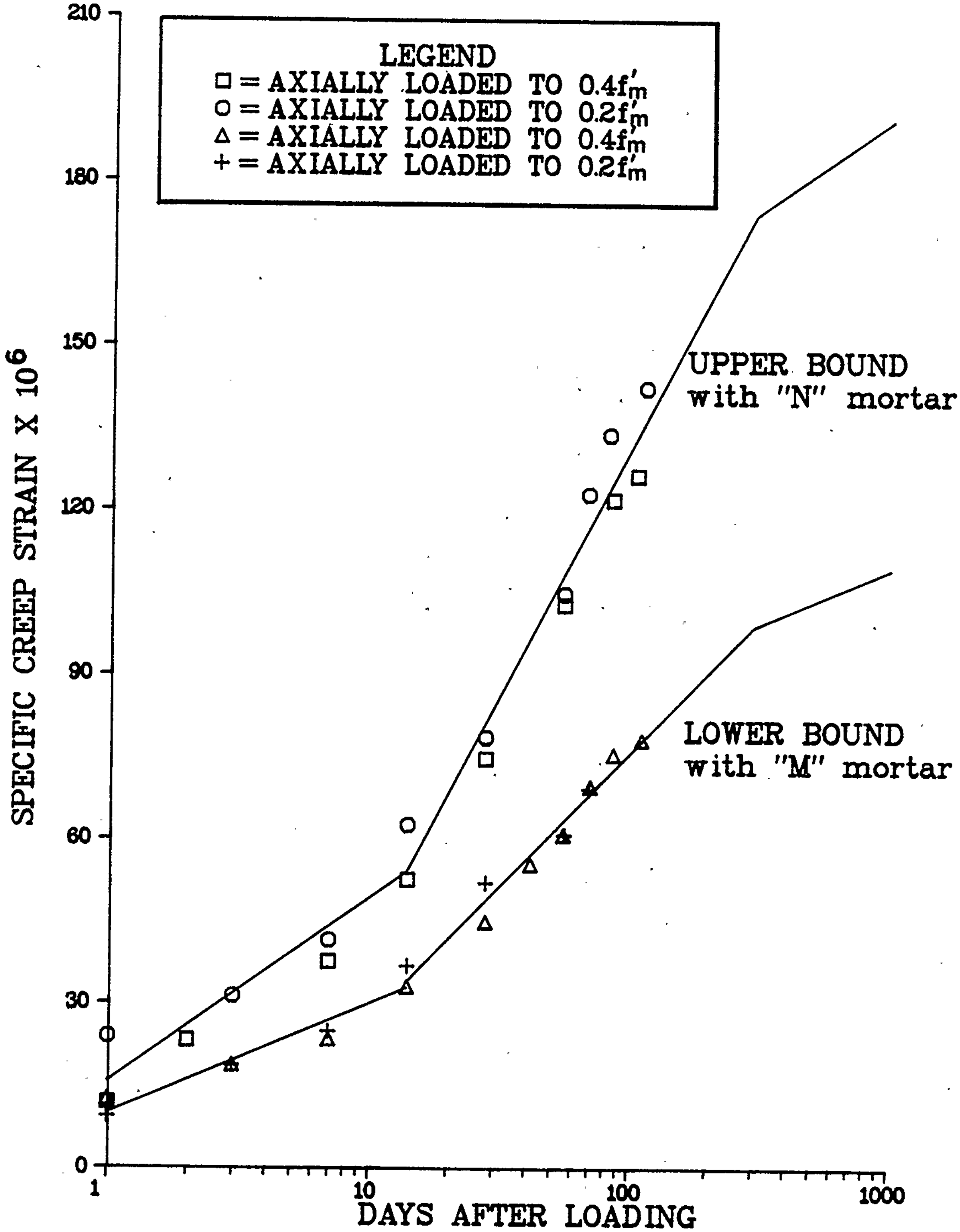

(ii) for 14 days $< (t-t_o) \leq 300$ days

$$C(t,t_o) = [39.057\ \ell n(t-t_o) - 49.067] \times 10^{-6}. \tag{4.2}$$

(iii) and for $(t-t_o) > 300$ days

$$C(t,t_o) = [14.484\ \ell n(t-t_o) + 91.096] \times 10^{-6}. \tag{4.3}$$

(2) Lower Bound

(i) for $(t-t_o) \leq 14$ days

$$C(t,t_o) = [8.6774\ \ell n(t-t_o) + 9.8579] \times 10^{-6}. \tag{4.4}$$

(ii) for 14 days $< (t-t_o) \leq 300$ days

$$C(t,t_o) = [21.121\ \ell n(t-t_o) - 21.816] \times 10^{-6}. \tag{4.5}$$

(iii) and for $(t-t_o) > 300$ days

$$C(t,t_o) = [8.6774\ \ell n(t-t_o) + 49.160] \times 10^{-6}. \tag{4.6}$$

where $C(t,t_o)$ is the specific creep strain observed at time t, t_o is the time at application of load and is equal to seven days in the present case, $(t-t_o)$ is the duration of loading.

(b) N-Mortar

Two sets of data were available. From the first set of data obtained by Ameny (1979), actual strains in the mortar joint were calculated as:

$$\varepsilon_j = (50.8\ \varepsilon_a - 40.8\ \varepsilon_u)/10 \tag{4.7}$$

where ε_j is the strain in the joint, ε_a is the measured strain across the joint, ε_u is the measured strain in the individual unit. The strain gauge length was 50.8 mm and the mortar joint thickness was 10 mm.

In the second set of data obtained by Ameny (1982), mortar cylinders were used. The ratio of the specific creep strains in the mortar joint to those of the concrete block units was in the order of 10-12 for the first set of data and 4-5 for the second set. Lenczner (1974) also reported this ratio to be in the range of 4-5. Tatsa et al (1973) observed the same ratio to be 16.8 when the specimens were presoaked and 4.4 when the specimens were not.

For the present study, specific creep strains derived from the first set of data are taken as an upper bound while those from the second set of data are a lower bound. Different expressions derived from regression analysis have been plotted in Figure 4.2 and are as follows.

(1) Upper Bound

(i) when specimens were subjected to a compressive stress of 0.4 f'_m, for all times

$$C(t,t_o) = [141.59 \ln(t-t_o) + 493.21] \times 10^{-6}. \tag{4.8}$$

(ii) when specimens were subjected to a compressive stress of 0.2 f'_m, for all times

$$C(t,t_o) = [355.56 \ln(t-t_o) + 158.48] \times 10^{-6}. \tag{4.9}$$

The average of the above two equations has been taken as the upper bound expression.

i.e. for all times

$$C(t,t_o) = [248.58 \ln(t-t_o) + 325.85] \times 10^{-6}. \tag{4.10}$$

(2) Lower Bound

for $(t-t_o) \leq 14$ days

$$C(t,t_o) = [127.41 \ln(t-t_o) + 235.61] \times 10^{-6}, \tag{4.11}$$

and for $(t-t_o) > 14$ days

$$C(t,t_o) = [42.462 \ln(t-t_o) + 474.47] \times 10^{-6}. \tag{4.12}$$

In the case of lower bound values, creep strains after 200 days were found to deviate up from the straight line relationship. The sudden rise of creep strains was neglected. This was probably due to

FIG. 4.2 SPECIFIC CREEP STRAIN VERSUS TIME

FOR "N" MORTAR

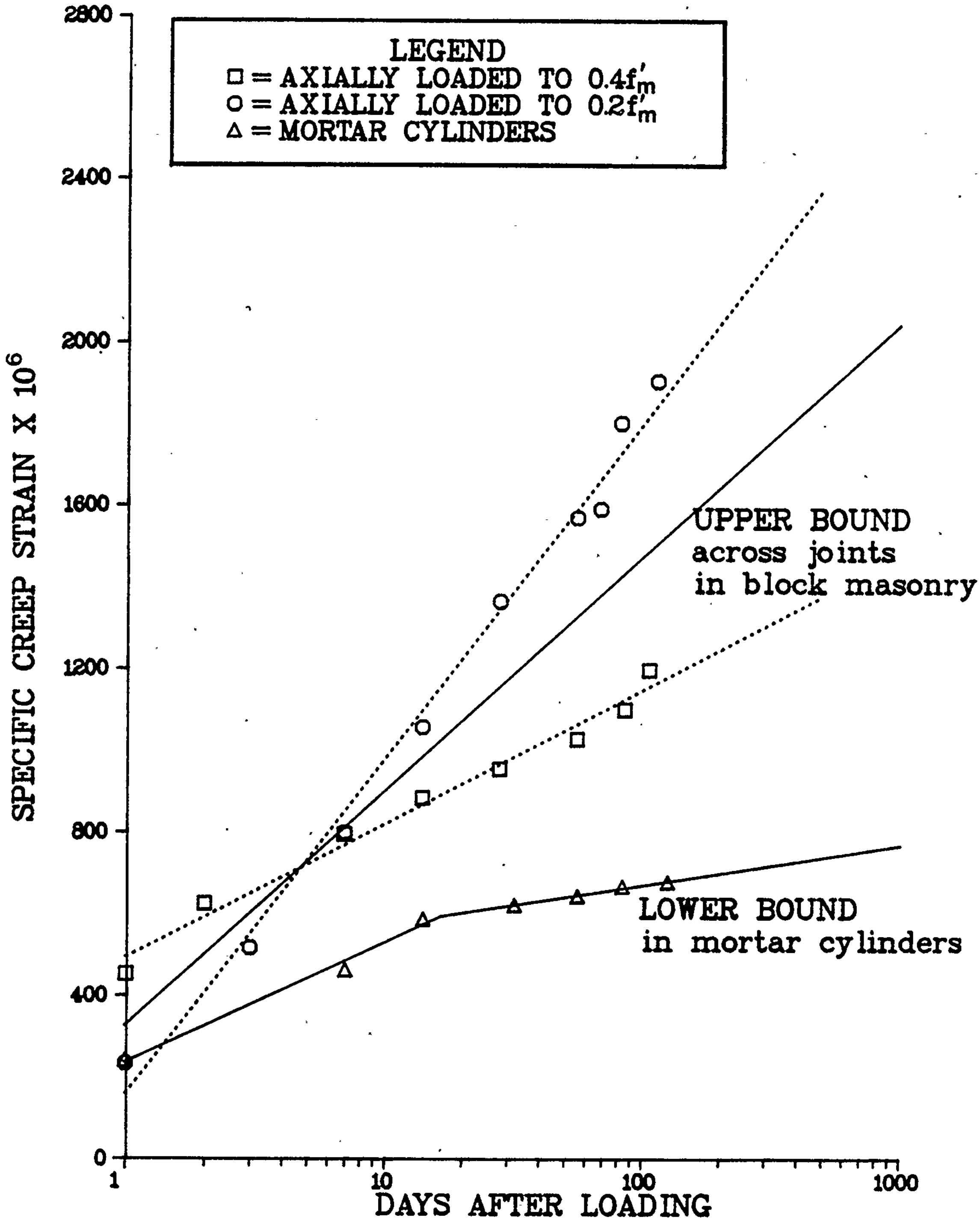

the abrupt variation in the relative humidity.

(c) M-Mortar

Similar to the N-mortar case, upper and lower bound expressions were obtained and are plotted in Figure 4.3.

(1) Upper Bound

(i) when specimens were subjected to a compressive stress of 0.4 f'_m, for all times

$$C(t,t_o) = [163.24 \ln(t-t_o) + 555.49] \times 10^{-6}. \tag{4.13}$$

(ii) when specimens were subjected to a compressive stress of 0.2 f'_m, for all times

$$C(t,t_o) = [142.73 \ln(t-t_o) + 189.96] \times 10^{-6}. \tag{4.14}$$

For this study, Equation (4.13) has been taken as an upper bound expression.

(2) Lower Bound

for all times

$$C(t,t_o) = [56.123 \ln(t-t_o) + 81.826] \times 10^{-6}. \tag{4.15}$$

In this case also, variation in the creep strains after 200 days was neglected.

(d) Brick Units

Both Ameny and Lenczner observed very low creep strains in the brick units. Ameny (1982) reported that the creep strain after a year was only 10% of the instantaneous elastic strain. For the present study, creep strains in the brick units have been neglected.

(B) Specific Creep Functions for Specimens Loaded at Any Age

Using the age coefficient recommended by the CEB-FIP (1970) model, specific creep curves for specimens loaded at different ages have been

FIG. 4.3 SPECIFIC CREEP STRAIN VERSUS TIME

FOR "M" MORTAR

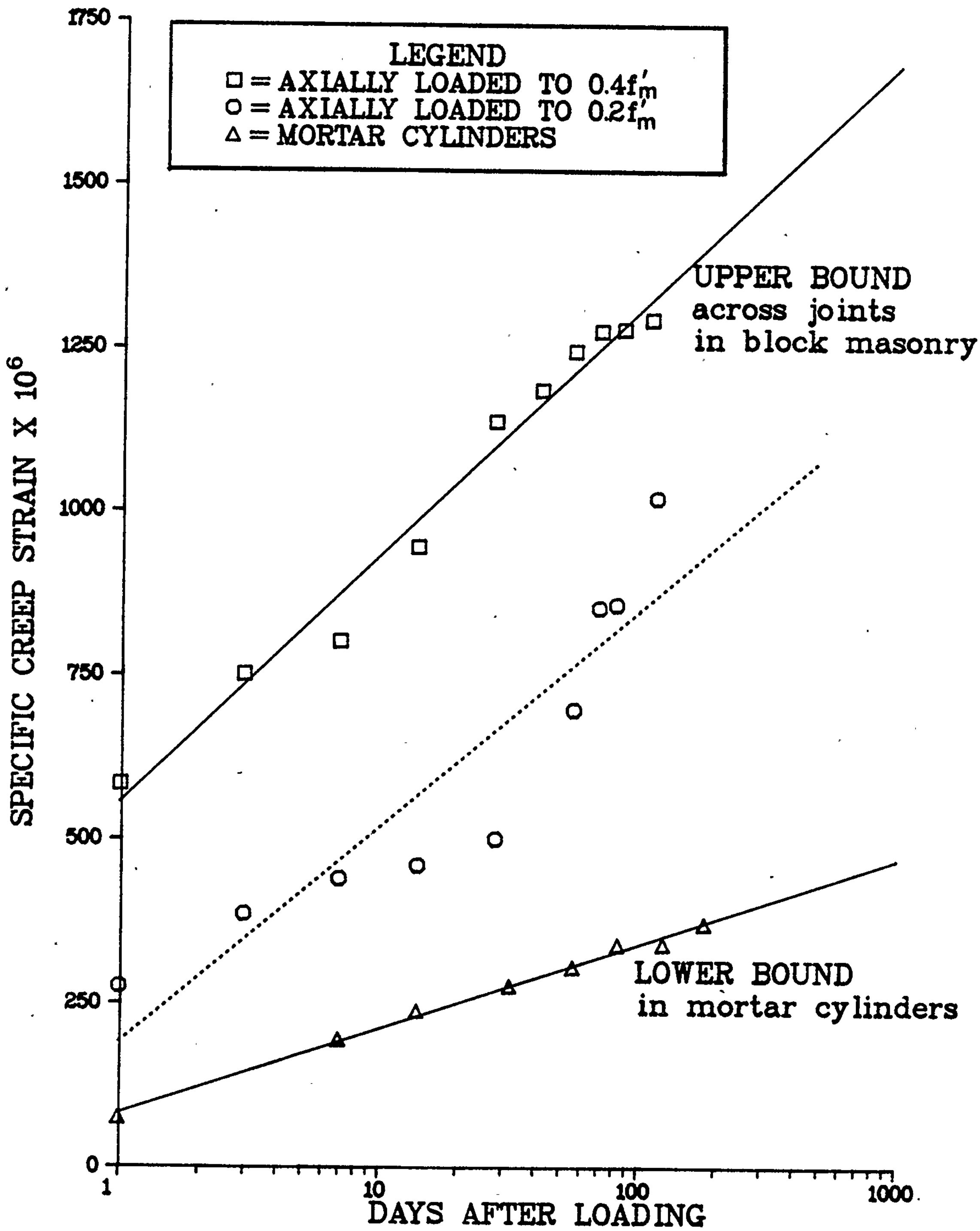

derived as follows:

$$C(t,t_o) = k \times C(t,7) \tag{4.16}$$

where k is the age coefficient, C(t,7) is the specific creep strain at time t (days) for a specimen loaded at the age of seven days and t_o is any age at loading.

C(t,7) values can be obtained from Expressions (4.1) to (4.15). Values of the age coefficient, k, are plotted in Figure 4.4 and are given by the following expression.

(i) for 1 day $\leq t_o \leq$ 7 days

$$k = -0.1470 \ \ln(t_o) + 1.286 \tag{4.17}$$

(ii) for 7 days $< t_o \leq$ 28 days

$$k = -0.2063 \ \ln(t_o) + 1.4015 \tag{4.18}$$

(iii) for 28 days $< t_o \leq$ 360 days

$$k = -0.1398 \ \ln(t_o) + 1.1798) \tag{4.19}$$

For $t_o >$ 360 days, the CEB-FIP (1970) model does not suggest any value of age coefficient, k. To be on the conservative side, no further decrease in k value is assumed in the present analysis. Thus,

(iv) for $t_o >$ 360 days

$$k = 0.357. \tag{4.20}$$

4.2.3.2 <u>Shrinkage</u>

In the present study the age at the start of drying, t_s, was assumed to be seven days to coincide with the age at application of loading.

It has been experimentally verified for concrete that shrinkage tends to a limiting value earlier than creep strains. This effect was confirmed by Lenczner (1974) for masonry structures. For the present analysis, shrinkage strains were extrapolated to an ultimate finite

FIG. 4.4 CEB–FIP(1970) , CREEP PREDICTION CURVE

COEFFICIENT FOR AGE AT APPLICATION OF LOAD

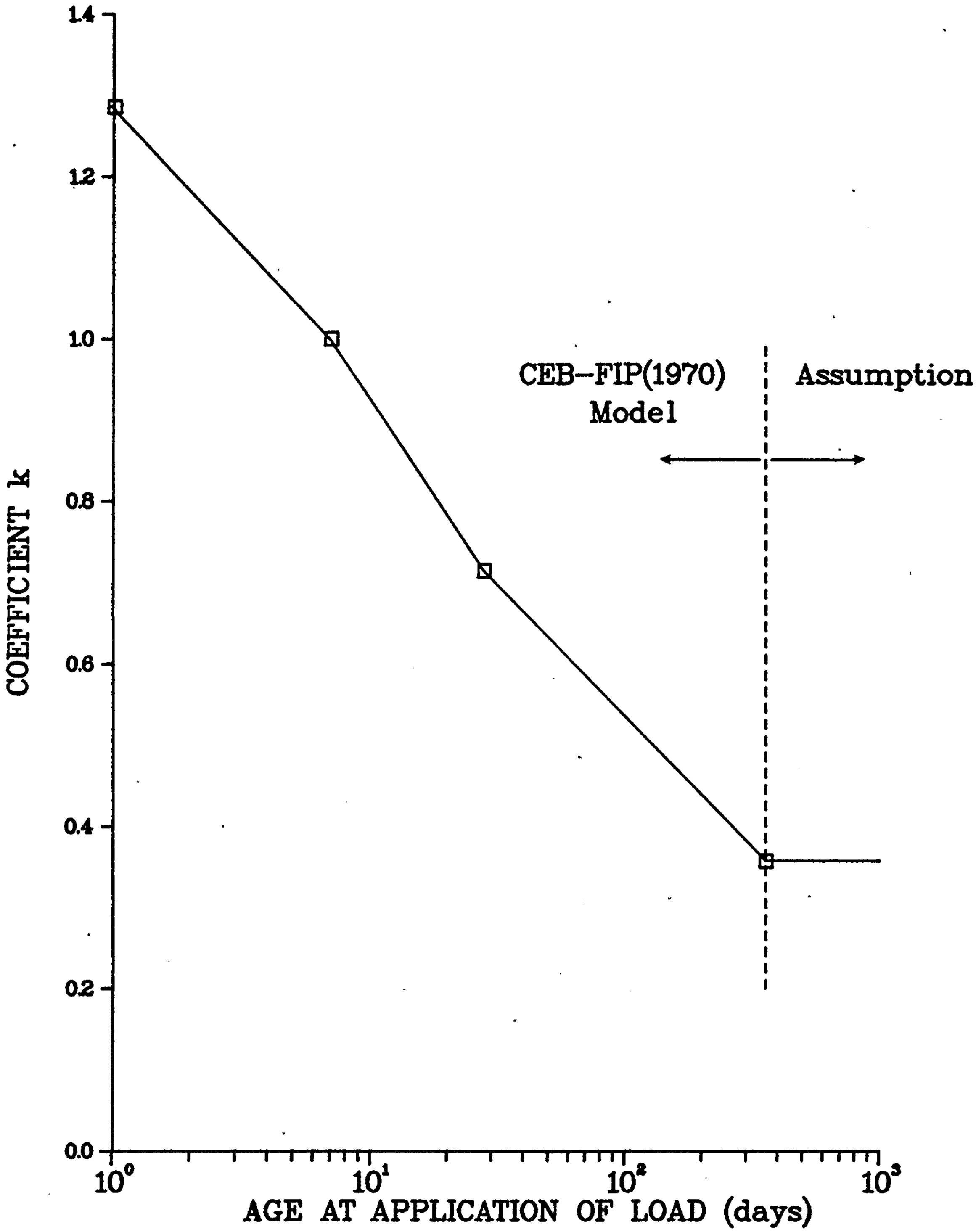

value and then no further shrinkage increase was assumed.

(a) Concrete Block Units

Results of six test specimens are plotted in Figure 4.5. The line of best fit, obtained from all the data points, was extrapolated to 200 days and then a horizontal line indicating no further shrinkage was assumed. Derived expressions are as follows:

Both Upper and Lower Bounds

(i) for $(t-t_s) \leqq 10$ days

$$\varepsilon^s(t,t_s) = [23.188 \ \ell n(t-t_s) + 23.882] \times 10^{-6} \tag{4.21}$$

(ii) for 10 days $< (t-t_s) \leqq 200$ days

$$\varepsilon^s(t,t_s) = [139.22 \ \ell n(t-t_s) - 228.64] \times 10^{-6} \tag{4.22}$$

(iii) and for $(t-t_s) > 200$ days

$$\varepsilon^s(t,t_s) = 510.0 \times 10^{-6}. \tag{4.23}$$

Lenczner (1974) obtained an ultimate shrinkage strain of 410×10^{-6} after 320 days. Thus, the input data used in the present study, are on the conservative side.

(b) N-Mortar

Similar to the case of creep in mortars, Equation (4.7) was used to obtain the shrinkage strains in the mortar joint. Results of different test specimens are plotted in Figure 4.6. In the upper bound case, shrinkage strains for different test specimens differed quite a bit. An upper bound envelope to all the test data points has been used for the present study. In the lower bound case, the shrinkage drop from 160 to 220 days was neglected because of the sudden rise of relative humidity.

FIG. 4.5 SHRINKAGE STRAIN VERSUS TIME

FOR CONCRETE BLOCK UNITS

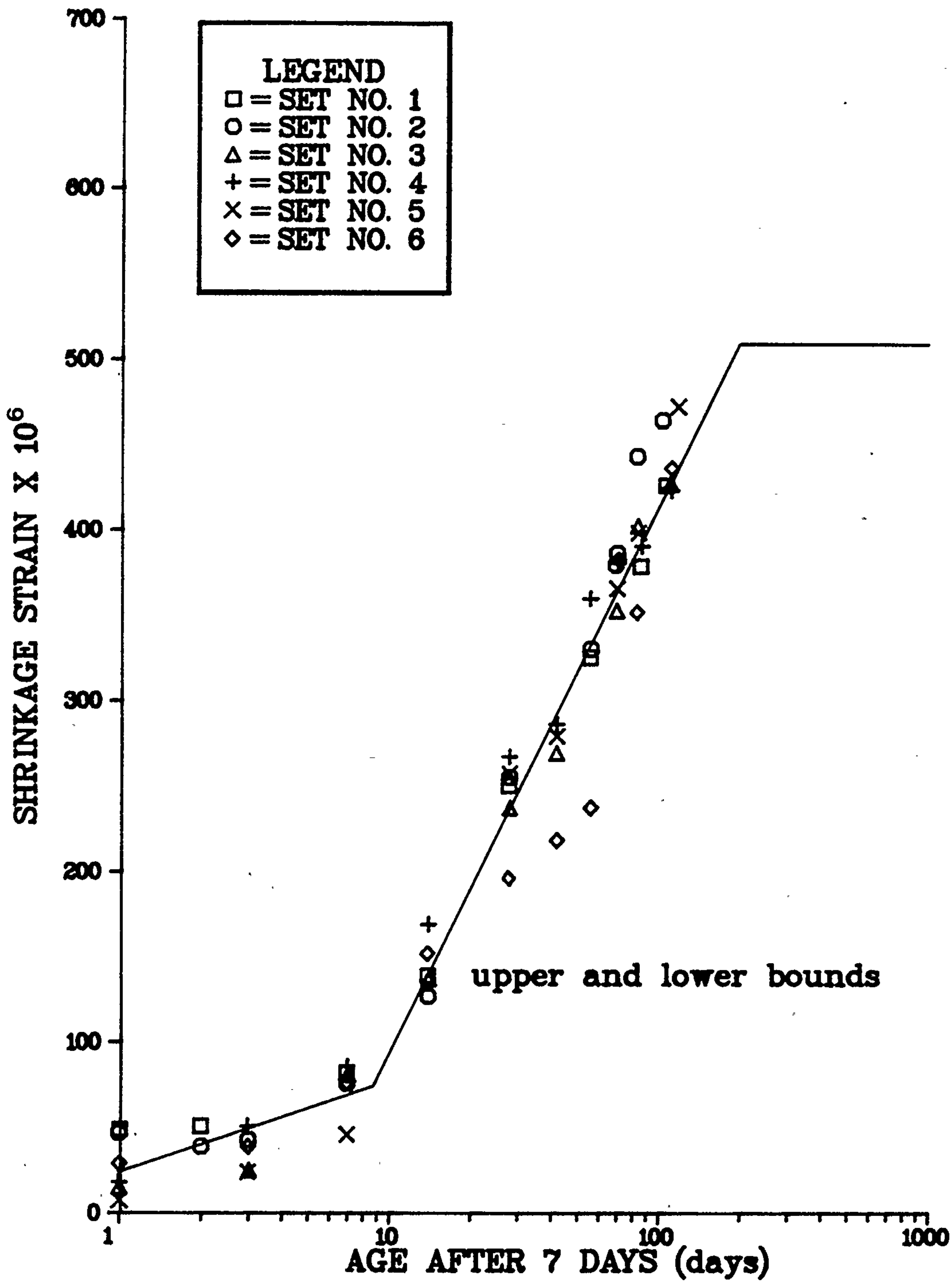

FIG. 4.6 SHRINKAGE STRAIN VERSUS TIME

FOR "N" MORTAR

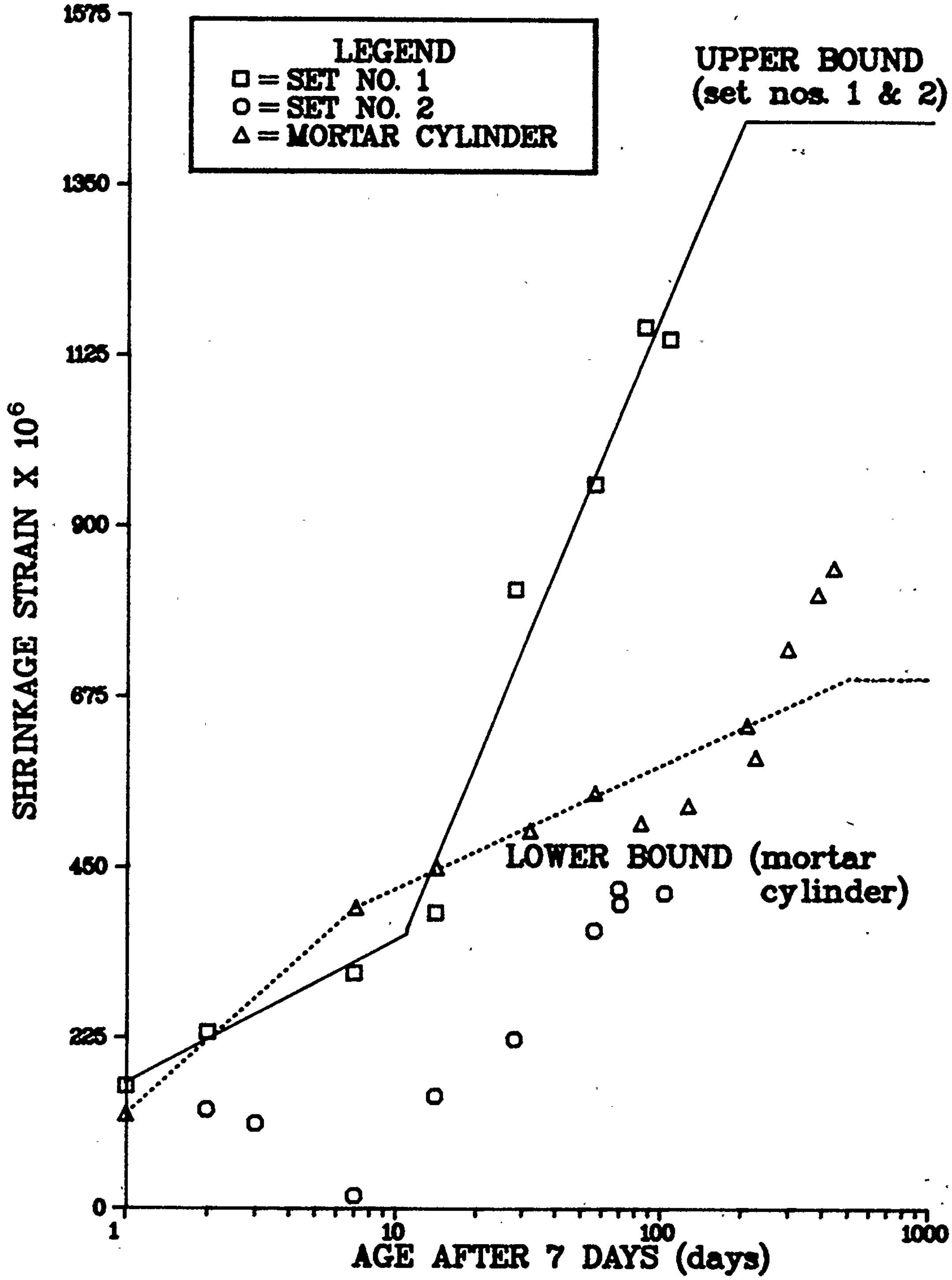

The best fitting line was extrapolated to 500 days and then a horizontal line was assumed.

The following expressions were obtained.

(1) Upper Bound

(i) for $(t-t_s) \leqq 11$ days

$$\varepsilon^s(t,t_s) = [82.413 \ \ln(t-t_s) + 164.75] \times 10^{-6} \tag{4.24}$$

(ii) for 11 days $< (t-t_s) \leqq 200$ days

$$\varepsilon^s(t,t_s) = [367.64 \ \ln(t-t_s) - 512.73] \times 10^{-6} \tag{4.25}$$

(iii) and for $(t-t_s) > 200$ days

$$\varepsilon^s(t,t_s) = 1435.0 \times 10^{-6}. \tag{4.26}$$

(2) Lower Bound

(i) for $(t-t_s) \leqq 10$ days

$$\varepsilon^s(t,t_s) = [140.29 \ \ln(t-t_s) + 124.00] \times 10^{-6} \tag{4.27}$$

(ii) for 10 days $< (t-t_s) \leqq 500$ days

$$\varepsilon^s(t,t_s) = [70.696 \ \ln(t-t_s) + 259.57] \times 10^{-6} \tag{4.28}$$

(iii) and for $(t-t_s) > 500$ days

$$\varepsilon^s(t,t_s) = 700.0 \times 10^{-6}. \tag{4.29}$$

(c) <u>M-Mortar</u>

Similar to the N-mortar case, upper and lower bound expressions were obtained. The expressions are plotted in Figure 4.7 and are as follows.

FIG. 4.7 SHRINKAGE STRAIN VERSUS TIME

FOR "M" MORTAR

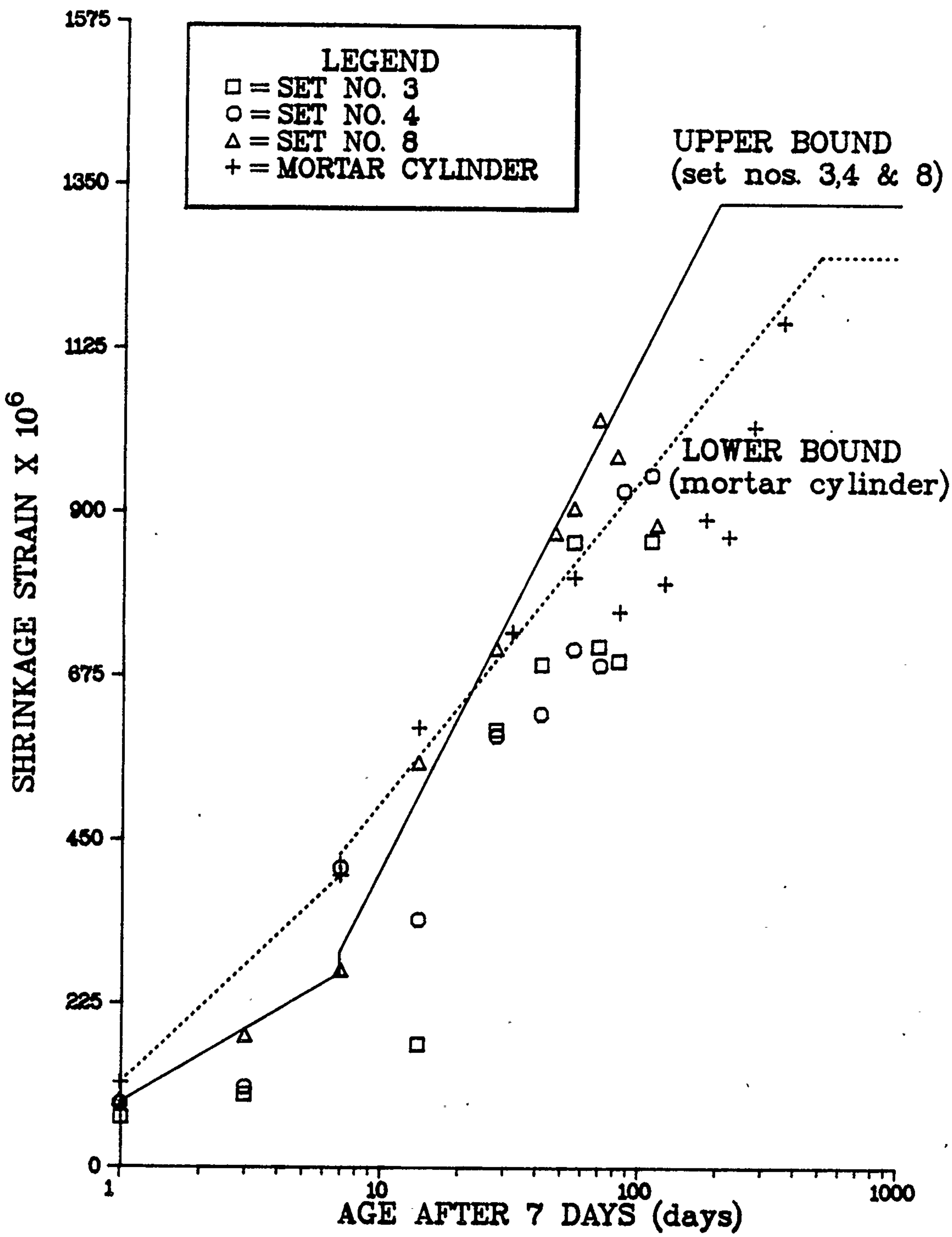

(1) Upper Bound

(i) for $(t-t_s) \leqq 10$ days

$$\varepsilon^s(t,t_s) = [91.457 \ \ln(t-t_s) + 88.519] \times 10^{-6} \tag{4.30}$$

(ii) for 10 days $< (t-t_s) \leqq 200$ days

$$\varepsilon^s(t,t_s) = [306.85 \ \ln(t-t_s) + 301.44] \times 10^{-6} \tag{4.31}$$

(iii) and for $(t-t_s) > 200$ days

$$\varepsilon^s(t,t_s) = 1325.0 \times 10^{-6}. \tag{4.32}$$

(2) Lower Bound

(i) for $(t-t_s) \leqq 10$ days

$$\varepsilon^s(t,t_s) = [146.46 \ \ln(t-t_s) + 116.00] \times 10^{-6} \tag{4.33}$$

(ii) for 10 days $< (t-t_s) \leqq 500$ days

$$\varepsilon^s(t,t_s) = [192.41 \ \ln(t-t_s) + 55.872] \times 10^{-6} \tag{4.34}$$

(iii) and for $(t-t_s) > 500$ days

$$\varepsilon^s(t,t_s) = 1252.0 \times 10^{-6}. \tag{4.35}$$

(d) Brick Units

Ameny (1982) observed very low shrinkage strain in the brick units and concluded that the strain could be neglected. A similar conclusion was made by Lenczner (1971). For this study, shrinkage strain in the brick units has also been neglected.

Ameny (1982) reported little reversible expansion strain in the brickwork as the brick units used were old and thoroughly presoaked in water. Lenczner et al (1976) observed a maximum expansion strain of 30 x 10^{-6} in the individual bricks. CMHC (1981) recommends an average expansion strain of 200×10^{-6} in clay brick masonry. Moisture expansion of brickwork reduces the loss of prestress. To be on the conservative side, moisture expansion has been neglected for the present study.

4.3 Stress Relaxation Input Data

Stress-time functions for different types of steel were described in Section 3.2.6. For the input data of normal relaxation steel, Equation (3.21) was used while for low relaxation steel, Equation (3.22) was employed. During any time interval, the loss of prestress in steel due to stress relaxation was found by Equation (3.32). In finite element analysis, the prestress loss due to relaxation was represented by an equivalent thermal load. A temperature rise was obtained from Equation (3.54) wherein the inverse of multiplication factors matrix, [M], discussed in Sections (3.3.3.2) and (3.3.4.2), was used as input data.

4.4 Efficient Computer Storage

In the shrinkage analysis, incremental shrinkage strain calculations by Equation (3.20) requires the knowledge of shrinkage strains at different times. Logarithmic expressions developed in Section (4.2.3.2) can easily be incorporated in the computer program with no additional storage requirement. Similarly, for relaxation analysis, stress-time functions of prestressing steel (Equations in Sections 3.2.6 and 3.2.7) are easily inserted in the computer program. On the other hand in the case of creep analysis, for incremental creep strain calculations by Equation (3.19), creep strains at different times for different ages at loading and the stress increments applied at all the previous time steps are needed. The analysis procedure was discussed in detail in Section (3.2.3.2). Although creep strains can be found from the expressions developed in Sections (4.2.3.1), storage of the stress history becomes a limitation on the size of the problem and on the number of time steps to be considered in the computations. To overcome the storage problem, Equation (3.19) was modified such that only a few stress histories need be stored. In the field of concrete structures, it has been reported that a certain type of mathematical expressions for the creep function can overcome the problem of stress history storage while representing the step-by-step solution technique (Equation 3.19) accurately. A similar creep function, chosen for the present study, is discussed in the following sections.

4.4.1 Creep Function to Avoid Stress History Storage

The creep function proposed by Kabir (1976) has been selected for the present study.

The function is of the form:

$$C(t,t_o,T) = \sum_{i=1}^{m} a_i(t_o)[1 - e^{-b_i \phi(T)(t-t_o)}] \qquad (4.36)$$

where m is the number of terms to be considered, $a_i(t_o)$ is a scale factor dependent on t_o (the age at loading), b_i is the exponential constant determining the shape of the logarithmically decaying creep curve and $\phi(T)$ is a shift function dependent on temperature T.

In the present study, the effect of temperature variation is not considered. Thus, Equation (4.36) reduced to:

$$C(t,t_o) = \sum_{i=1}^{m} a_i(t_o)[1 - e^{-b_i(t-t_o)}] \qquad (4.37)$$

To develop an expression similar to Equation (3.19), Equations (3.10) and (3.11) are rewritten here.

$$\varepsilon^c(t_n) = \sigma_o C(t_n,t_o) + \sum_{i=1}^{n-1} \Delta\sigma_i \; C(t_n,t_i) \tag{4.38}$$

and $\Delta\sigma_i = \sigma_i - \sigma_{i-1}$ (4.39)

Substituting the values of C from equation (4.37) into Equation (4.38), we get:

$$\begin{aligned}\varepsilon^c(t_n) &= \sigma_o \sum_{i=1}^{m} a_i(t_o)[1 - e^{-b_i(t_n-t_o)}] \\ &+ \Delta\sigma_1 \sum_{i=1}^{m} a_i(t_1)[1 - e^{-b_i(t_n-t_1)}] \\ &+ \\ &\cdot \\ &\cdot \\ &\cdot \\ &+ \Delta\sigma_{n-1} \sum_{i=1}^{m} a_i(t_{n-1})[1 - e^{-b_i(t_n-t_{n-1})}]\end{aligned} \tag{4.40}$$

and

$$\begin{aligned}\varepsilon^c(t_{n-1}) &= \sigma_o \sum_{i=1}^{m} a_i(t_o)[1 - e^{-b_i(t_{n-1}-t_o)}] \\ &+ \Delta\sigma_1 \sum_{i=1}^{m} a_i(t_1)[1 - e^{-b_i(t_{n-1}-t_1)}] \\ &+ \\ &\cdot \\ &\cdot \\ &\cdot \\ &+ \Delta\sigma_{n-2} \sum_{i=1}^{m} a_i(t_{n-2})[1 - e^{-b_i(t_{n-1}-t_{n-2})}]\end{aligned} \tag{4.41}$$

Then

$$\Delta\varepsilon^c_{n-1,n} = \varepsilon^c_n - \varepsilon^c_{n-1} \tag{4.42}$$

where $\Delta\varepsilon^c_{n-1,n}$ is the incremental creep strain in the n^{th} time interval. From Equations (4.40), (4.41) and (4.42) we obtain:

$$\begin{aligned}
\Delta\varepsilon^c_{n-1,n} = {} & \sum_{i=1}^{m} \sigma_o\, a_i(t_o)\,[e^{-b_i(t_{n-1}-t_o)} - e^{-b_i(t_n-t_o)}] \\
& + \sum_{i=1}^{m} \Delta\sigma_1\, a_i(t_1)\,[e^{-b_i(t_{n-1}-t_1)} - e^{-b_i(t_n-t_1)}] \\
& + \\
& \cdot \\
& \cdot \\
& \cdot \\
& + \sum_{i=1}^{m} \Delta\sigma_{n-2}\, a_i(t_{n-2})\,[e^{-b_i(t_{n-1}-t_{n-2})} - e^{-b_i(t_n-t_{n-2})}] \\
& + \sum_{i=1}^{m} \Delta\sigma_{n-1}\, a_i(t_{n-1})\,[1 - e^{-b_i(t_n-t_{n-1})}]
\end{aligned} \tag{4.43}$$

$$\begin{aligned}
\text{i.e. } \Delta\varepsilon^c_{n-1,n} = {} & \sum_{i=1}^{m} \sigma_o\, a_i(t_o)\,e^{-b_i(t_{n-1}-t_o)}[1 - e^{-b_i(t_n-t_{n-1})}] \\
& + \sum_{i=1}^{m} \Delta\sigma_1\, a_i(t_1)\,e^{-b_i(t_{n-1}-t_1)}[1 - e^{-b_i(t_n-t_{n-1})}] \\
& + \\
& \cdot \\
& \cdot \\
& \cdot \\
& + \sum_{i=1}^{m} \Delta\sigma_{n-2}\, a_i(t_{n-2})\,e^{-b_i(t_{n-1}-t_{n-2})}[1 - e^{-b_i(t_n-t_{n-1})}] \\
& + \sum_{i=1}^{m} \Delta\sigma_{n-1}\, a_i(t_{n-1})\,[1 - e^{-b_i(t_n-t_{n-1})}]
\end{aligned} \tag{4.44}$$

or

$$\Delta\varepsilon^c_{n-1,n} = \sum_{i=1}^{m} A_{i,n-1}[1 - e^{-b_i(t_n-t_{n-1})}] \tag{4.45a}$$

where

$$A_{i,n-1} = A_{i,n-2}\, e^{-b_i(t_{n-1}-t_{n-2})} + \Delta\sigma_{n-1}\, a_i(t_{n-1}) \qquad (4.45b)$$

and

$$A_{i,o} = a_i(t_o)\, \sigma_o \qquad (4.45c)$$

Equation (4.45a) resembles Equation (3.19) but does not require the storage of all previous stress increments. The previous stress history is stored in the factor A which can be calculated from Equations (4.45b) and (4.45c). Thus, Equation (4.45a) requires the storage of stress history of only one time-step previous to the one under consideration reducing the storage and computation time to a great extent. This makes the creep analysis of large structural problems possible.

4.4.2 Determination of Creep Function Coefficients

In the present study, only partial experimental data were available. The data have been smoothed and extrapolated by fitting to a linear logarithmic expression form. To incorporate accurately the formulation described in the previous section, creep functions of the logarithmic form are to be converted to a form described by Equation (4.37).

$$\text{i.e. } C(t,t_o) = \sum_{i=1}^{m} a_i(t_o)\,[1 - e^{-b_i(t-t_o)}]$$

The method used is as follows:

(1) A particular age at loading, t_o, is chosen. For the present case t_o = 7 days, is selected, as experimental observations were made on specimens loaded at the age of seven days.

(2) Using expressions developed in Section (4.2.3.1), specific creep

strains for all different cases were generated for 24 age durations, i.e. for $(t-t_o)$ equal to 0.3, 0.4, 0.5, 1, 2, 5, 10, 15, 22, 30, 40, 60, 90, 120, 160, 200, 250, 320, 400, 500, 1000, 2000, 3500, and 6000 days.

(3) Then the following equations are developed.

$$\begin{bmatrix} 1 - e^{-b_1(t_1-t_o)} & \cdots & 1-e^{-b_m(t_1-t_o)} \\ \cdot & & \\ \cdot & & \\ \cdot & & \\ 1 - e^{-b_1(t_n-t_o)} & \cdots & 1-e^{-b_m(t_n-t_o)} \end{bmatrix}_{nxm} \begin{Bmatrix} a_1(t_o) \\ a_2(t_o) \\ \cdot \\ \cdot \\ a_m(t_o) \end{Bmatrix}_{mx1} = \begin{Bmatrix} C(t_1,t_o) \\ C(t_2,t_o) \\ \cdot \\ \cdot \\ C(t_n,t_o) \end{Bmatrix}_{nx1} \quad (4.46)$$

or $\quad [b]_{nxm}\{a\}_{mx1} = \{s\}_{nx1}$ (4.47)

For the present case, $n = 24$ and $t_o = 7$ days. For $n > m$, Equation (4.47) is a system of overdeterminate set of equations. Equation (4.47) is solved by the least square method.

i.e. $[b]^T[b]\{a\} = [b]^T\{s\}$

and $\{a\} = [[b]^T[b]]^{-1}[b]^T\{s\}$ (4.48)

Thus, the coefficients, a_i, are evaluated. The values of m and b_i are to be chosen such that the least square error, X, is minimized where

$$X = \sum_{i=1}^{m} [([b]\{a\})_i - \{s\}_i]^2 \quad (4.49)$$

Kabir (1976) selected the number of terms, m, equal to 3. Using $b_1 = 0.1$, $b_2 = 0.01$ and $b_3 = 0.001$, experimental creep data for a particular age at loading were fitted to the creep function and the values of a_1, a_2 and a_3 were evaluated.

For the present study, the effect of m value on accuracy was investigated. Three values of m (3, 4 and 6) were tried. With different b_i values, values of a_i were calculated and evaluated. Finally, m = 6 was selected because it gave the minimum least square error. Values of b_i and a_i (for i=1,...,6) for different cases are tabulated in Table 4.1. To check the acceptability of the creep function chosen, the specific creep strains generated by Equation (4.37) are compared to the specific creep strains generated by logarithmic expressions and short-term experimental data in Figures 4.8 to 4.10. The theoretical curves generated by Equation (4.37) are plotted and the experimental and log plot specific creep strain values are superimposed on the plot. As shown in Figures 4.8 to 4.10, log values fit exactly on the curves generated by the creep function of the form of Equation (4.37). The derived specific creep curves for the specimens loaded at seven days were acceptable for the present study. To obtain the specific creep curves for specimens loaded at different ages, Equation (4.16) with the age coefficient recommended by the CEB-FIP (1970) model, was used.

4.5 Computer Programming

Before the computer programming steps are described, the two basic assumptions made in the present study are reviewed.

(1) It has been assumed that elastic strain remains constant during the entire time analysis. Thus, structural stiffness based on the initial elastic properties has been used throughout the analysis. Elastic properties of the different components used in the present analysis are taken from Ameny (1979 and 1982) and are listed in Table 4.2.

(2) It has been assumed that the age at application of initial loading, or prestressing in the present case, t_o, and the age at start of drying, t_s, are the same and are equal to seven days.

The program SMAC was modified to perform non-linear time dependent

	Concrete Block Unit		N-Mortar		M-Motar	
	Upper Bound	Lower Bound	Upper Bound	Lower Bound	Upper Bound	Lower Bound
a_1	0.1667×10^{-4}	0.1046×10^{-4}	0.6540×10^{-3}	0.2185×10^{-3}	0.3960×10^{-3}	0.1338×10^{-3}
a_2	0.3669×10^{-4}	0.2357×10^{-4}	0.5585×10^{-3}	0.3800×10^{-3}	0.3728×10^{-3}	0.1304×10^{-3}
a_3	0.1164×10^{-3}	0.6186×10^{-4}	0.5663×10^{-3}	0.6654×10^{-4}	0.3781×10^{-3}	0.1253×10^{-3}
a_4	0.2471×10^{-4}	0.1598×10^{-4}	0.6765×10^{-3}	0.1250×10^{-3}	0.3706×10^{-3}	0.1568×10^{-3}
a_5	0.8055×10^{-4}	0.3756×10^{-4}	-0.2329×10^{-2}	-0.6413×10^{-4}	0.3954×10^{-3}	-0.5311×10^{-3}
a_6	-0.2356×10^{-3}	-0.7103×10^{-4}	0.2267×10^{-1}	0.1028×10^{-2}	0.3357×10^{-3}	0.5062×10^{-2}
b_1	1.0	1.0	0.5	1.6	4.8	0.7
b_2	0.1	0.1	0.05	0.16	0.48	0.07
b_3	0.01	0.01	0.005	0.016	0.048	0.007
b_4	0.001	0.001	0.0005	0.0016	0.0048	0.0007
b_5	0.0001	0.0001	0.00005	0.00016	0.00048	0.00007
b_6	0.00001	0.00001	0.000005	0.000016	0.000048	0.000007

Table 4.1 Creep Function Coefficients

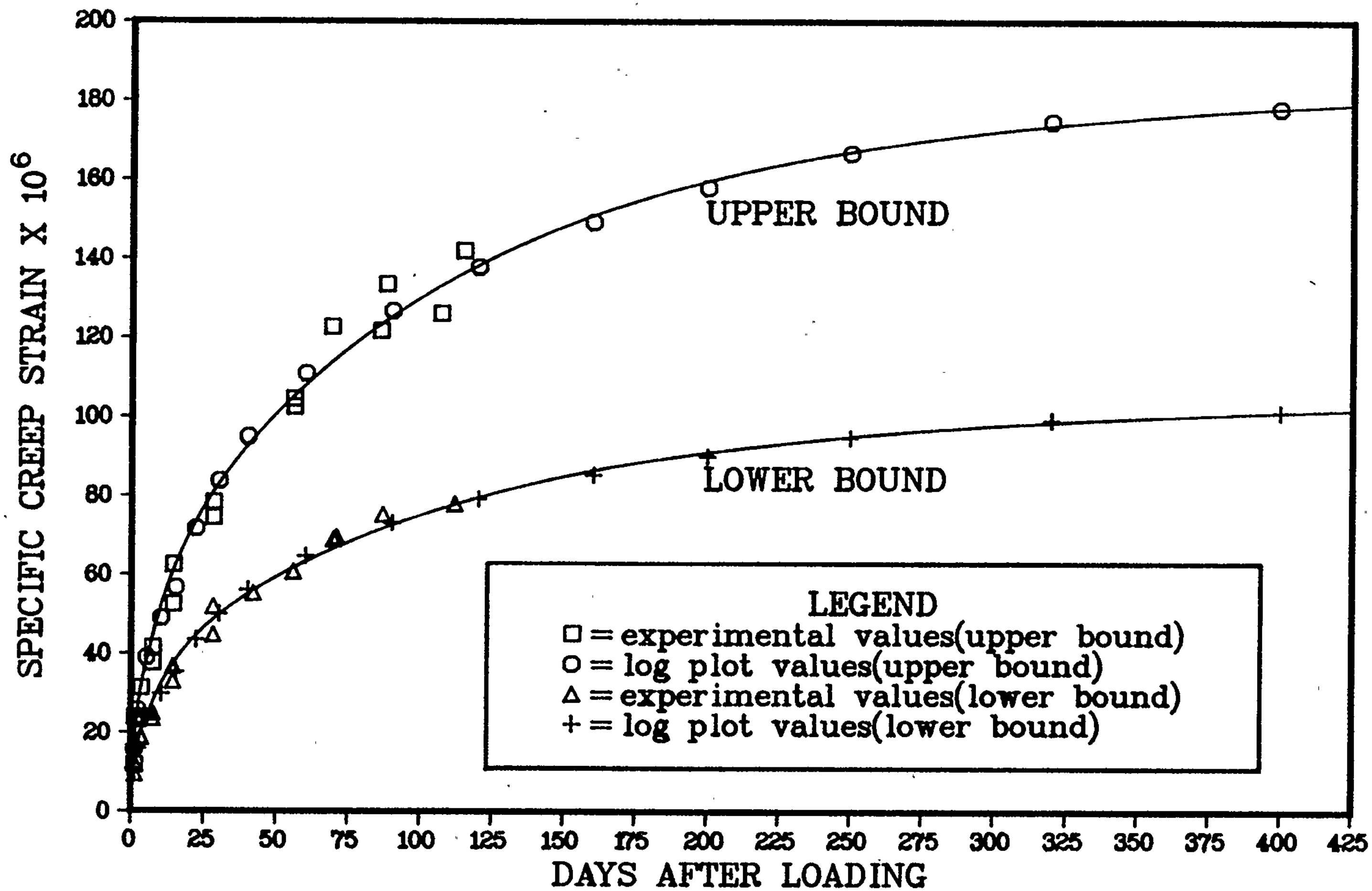

FIG. 4.8 SPECIFIC CREEP STRAIN VERSUS TIME

FOR CONCRETE BLOCK UNITS

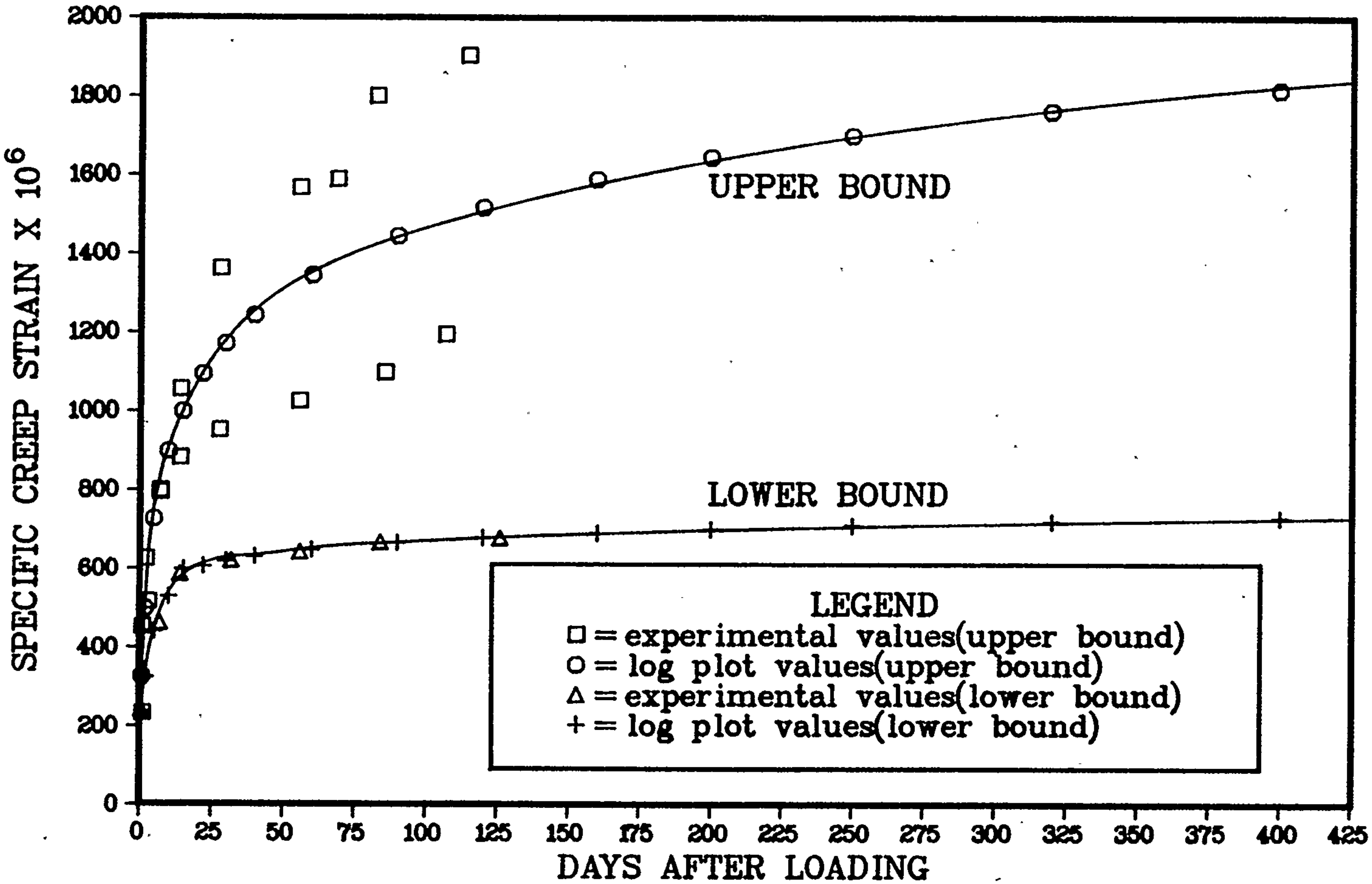

FIG. 4.9 SPECIFIC CREEP STRAIN VERSUS TIME

FOR "N" MORTAR

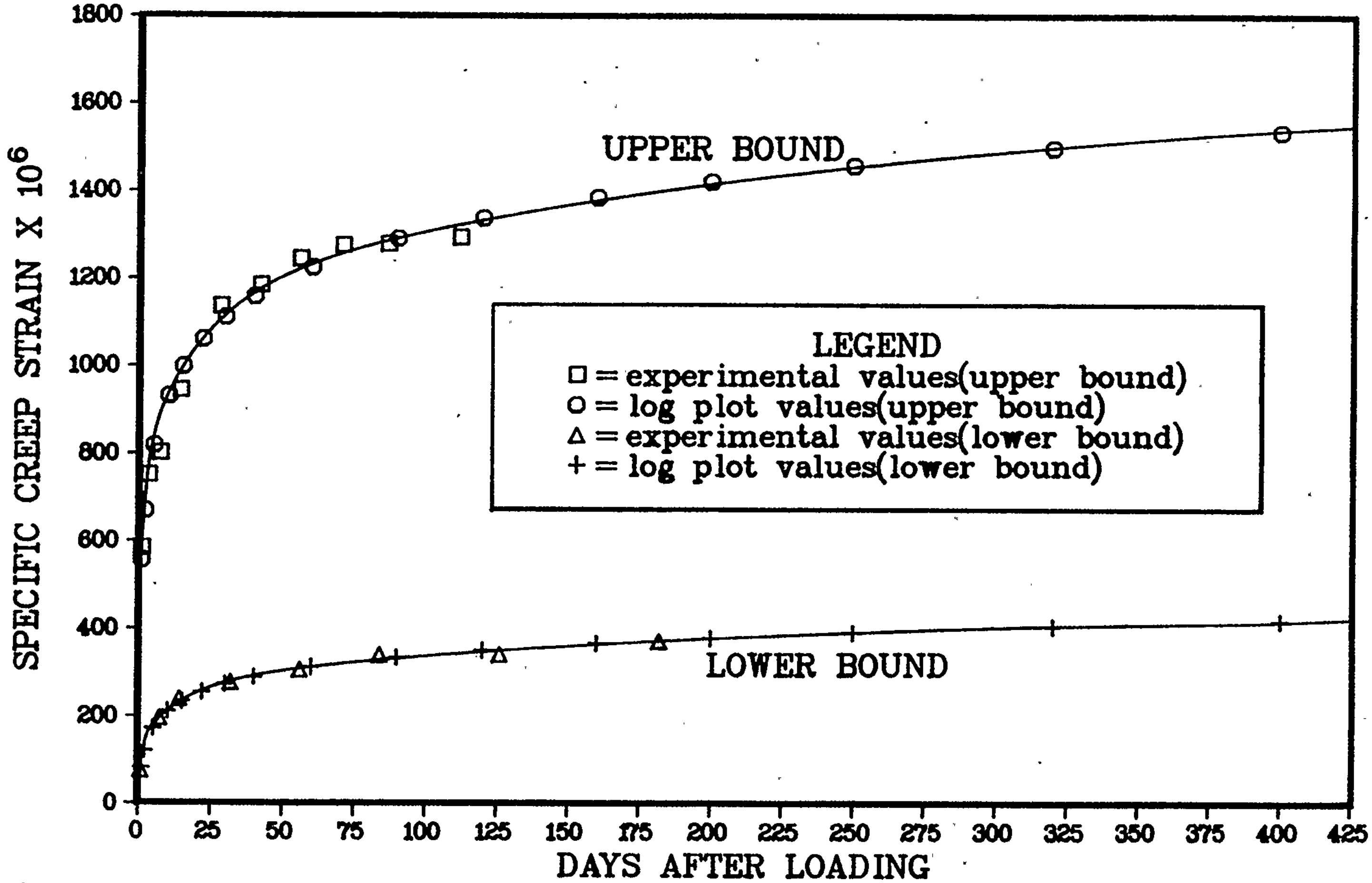

FIG. 4.10 SPECIFIC CREEP STRAIN VERSUS TIME

FOR "M" MORTAR

analysis by a step-by-step numerical solution technique for creep, shrinkage and relaxation properties of masonry components. The solid element subroutine was modified to include the effects of creep and shrinkage in mortar and concrete block units while the truss subroutine was developed further to incorporate the stress relaxation property of prestressing steel. In the modified SMAC program, the user has the option to perform any of the following analysis procedures.

(1) Elastic Analysis,

(2) Creep Analysis,

(3) Shrinkage Analysis,

(4) Creep and Shrinkage Analyses Together.

There is a choice of including relaxation analysis with any of the above mentioned time dependent analyses. Both normal as well as low relaxation steel properties have been included. With creep and/or shrinkage analyses either upper or lower bound results may be sought. A flow chart, describing the various steps of the analysis procedure, is presented in Figure 4.11.

	Concrete Block Unit	Brick Unit	N-Mortar	M-Mortar	Steel Plate
Modulus of Elasticity E(N/mm²)	8000	8000	8000	8000	2×10^5
Poisson's Ratio ν	0.2	0.2	0.2	0.2	0.3

Table 4.2 Elastic Properties

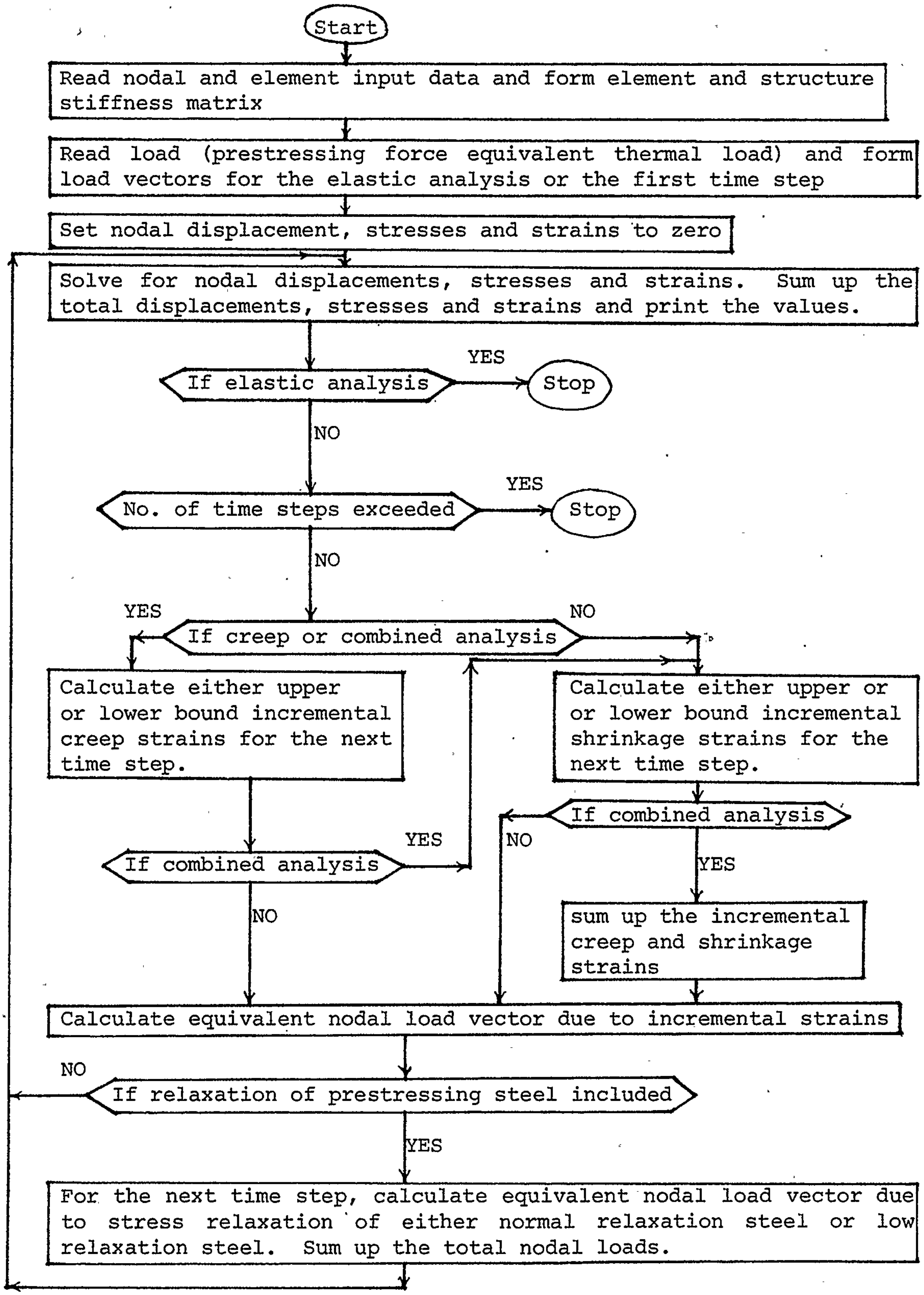

Figure 4.11 Flow Chart

CHAPTER 5

MODELS FOR POST-TENSIONED HOLLOW MASONRY WALLS

5.1 Introduction

The modified program was used to analyse models for several cases of concrete block and brick walls. Different parts of the masonry unit and the mortar joint locations are defined in Figure 5.1. A typical vertically post-tensioned masonry wall specimen is shown in Figure 3.5. Several bonding patterns of the masonry units and the mortar joints are possible. Two typical cases of running bond and stack bond patterns are shown in Figures 5.2 and 5.3. For details and other definitions, the reader may review CSA Standard CAN3-A370-M84 (1984). As shown in Figure 5.1, the prestressing steel passes through the hollow core of the unit. With a stack bond pattern, the construction of masonry walls result in vertically aligned cores so that the prestressing steel bars can be placed in the walls. On the other hand, with a running bond pattern, the shape of the standard units may not permit any vertically aligned core. In the present study, only the stack bond pattern case has been considered.

Prestressing is the only load which was considered in the present analysis. Self weight of the walls or any other external load has been ignored for all the wall models. As illustrated in Figure 3.5, the prestressing force is transmitted to the wall through the end steel plates.

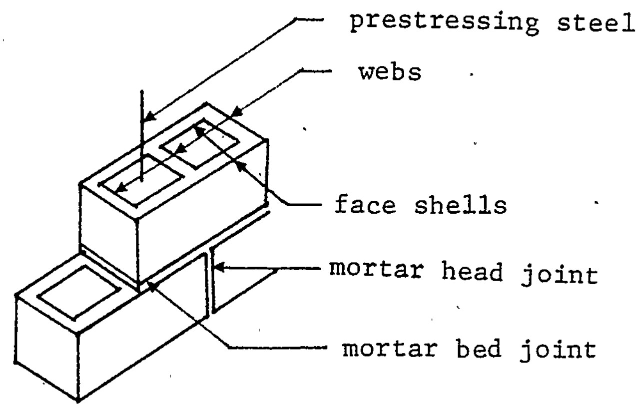

Figure 5.1 Detail Showing Mortar Joints

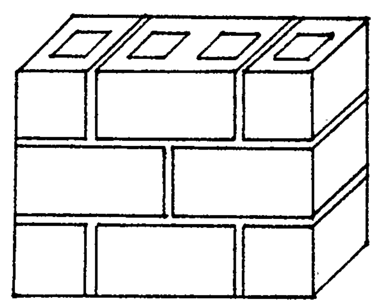

Figure 5.2 Running Bond Patern

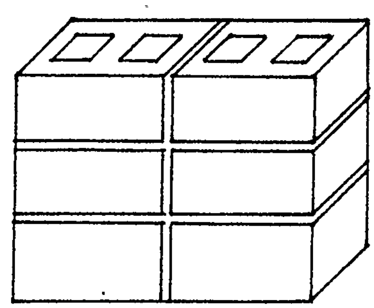

Figure 5.3 Stack Bond Patern

5.2 Types of Specimens

5.2.1 Unit Geometry

A typical concrete block unit is shown in Figure 5.4a. To avoid complexity in the finite element mesh, the simpler unit geometry, shown in Figure 5.4b, was adopted. Regarding brick units, the same cross-sectional configuration was assumed. Figure 5.4c shows the brick unit dimensions which were used in the present analysis.

5.2.2 Mortar Bed Types

The masonry units are joined together either by full mortar bedding or by face-shell bedding. In the case of full bedding, mortar is applied to the whole bed face of the unit while in face-shell bedding, only the face shells of the unit are mortared. A comparison between the two has been made in Figure 5.5. For the present study, both full bedded and face-shell bedded specimens have been modelled.

5.2.3 Different Cases to be Analysed

The following options were included in the wall models.

(1) Concrete block units or brick units;

(2) N-mortar or M-mortar;

(3) Full mortar bedding or face-shell mortar bedding;

(4) Upper bound or lower bound limits;

(5) Creep and shrinkage analyses or creep, shrinkage and relaxation analyses.

With these options thirty-two different cases could be analysed. Since there were practical limitations of time and cost of execution, the total number of cases to be analysed was reduced to sixteen. In Chapter 4, creep and shrinkage strains of N-mortar were observed to be

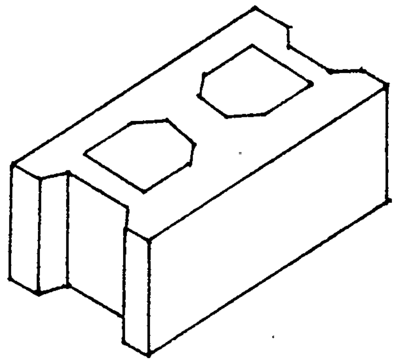

(a) Typical Concrete Block Unit

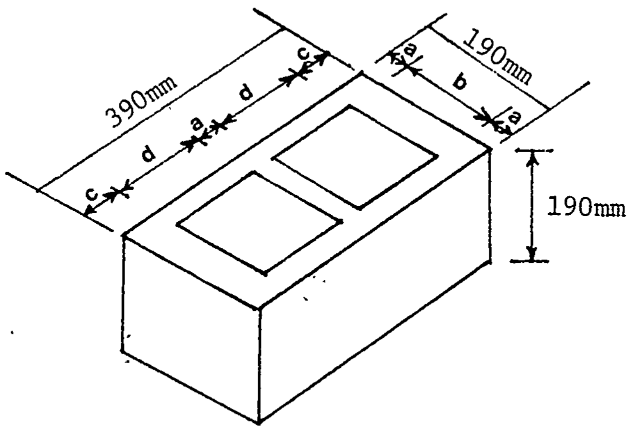

(b) Concrete Block Unit Selected

a=35mm

b=120mm

c=50mm

d=127.5mm

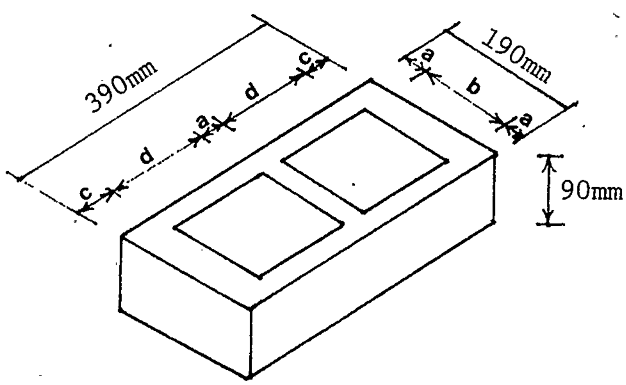

(c) Brick Unit Selected

Figure 5.4 Unit Configuration

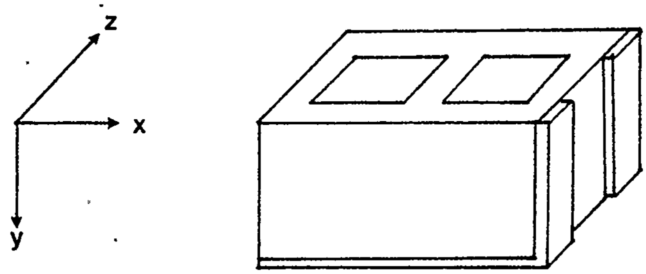

(a)

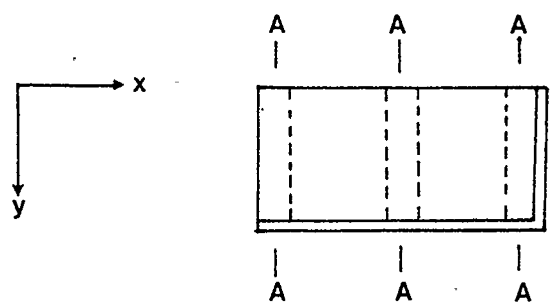

(b)

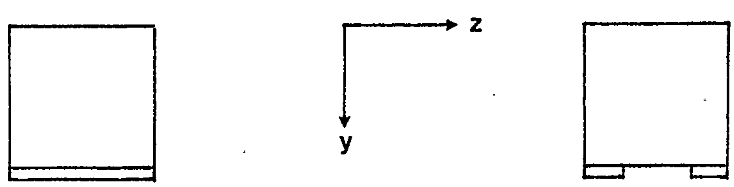

(c) Full Bed Mortar (d) Face Shell Mortar

A - Plane

Figure 5.5 Mortar Bed Types

more than those of M-mortar. As the main objective was to find upper and lower bound limits to loss of prestress, N-mortar wall model specimens were analysed for upper bound values while M-mortar specimens were investigated for lower bound results. Thus, (1) creep and shrinkage analyses, and (2) creep, shrinkage and relaxation analyses were performed for both concrete block walls and brick walls for the following combinations.

(1) N-mortar, full mortar bedding and upper bound case

(2) N-mortar, face-shell mortar bedding and upper bound case

(3) M-mortar, full mortar bedding and lower bound case

(4) M-mortar, face-shell mortar bedding and lower bound case.

5.3 Wall Models

Time and cost of computation were the main limiting factors in selecting the size of the wall models. On the other hand, the models had to simulate actual wall behaviour. The models selected for concrete block walls and brick walls are shown in Figures 5.6 and 5.7 respectively. Although of the same height, 1190 mm, the concrete block wall model was six blocks high while the brick wall was twelve units tall. Both wall models were single wythe and four blocks long (1590 mm) where a wythe is defined as a continuous vertical section of masonry wall, one unit in thickness. All mortar joints were 10 mm thick. The height to length ratio of the model was selected from the range of values used for actual masonry walls. Two steel bars were used to prestress the wall models. The steel bearing plates, used for the model specimens, were 212.5 mm long, 190 mm wide and 20 mm thick. The plates spanned the hollow core and the adjoining webs of the unit in order to transmit the prestressing force evenly.

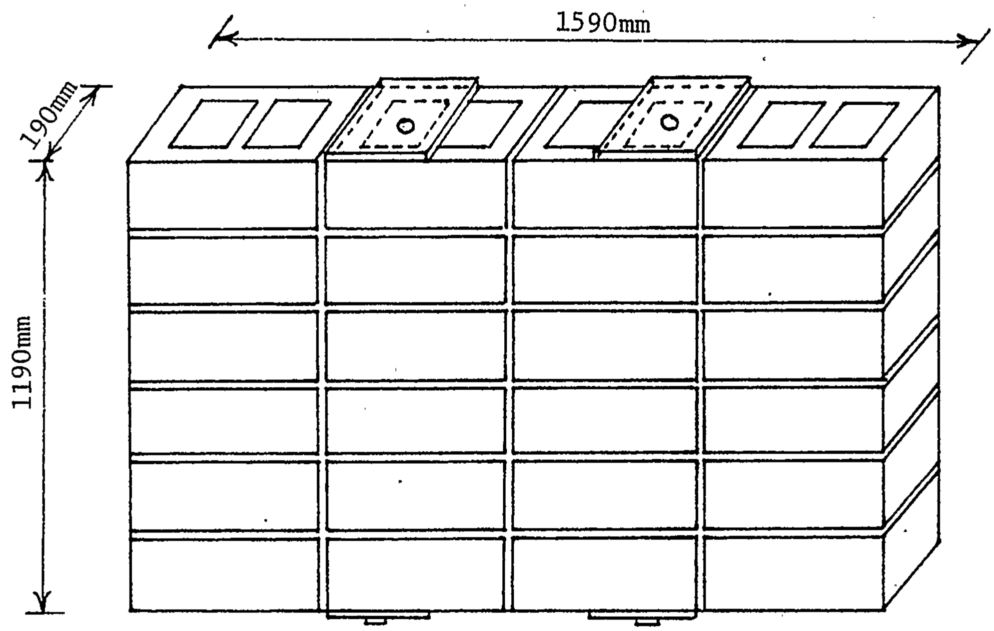

Figure 5.6 Concrete Block wall Model

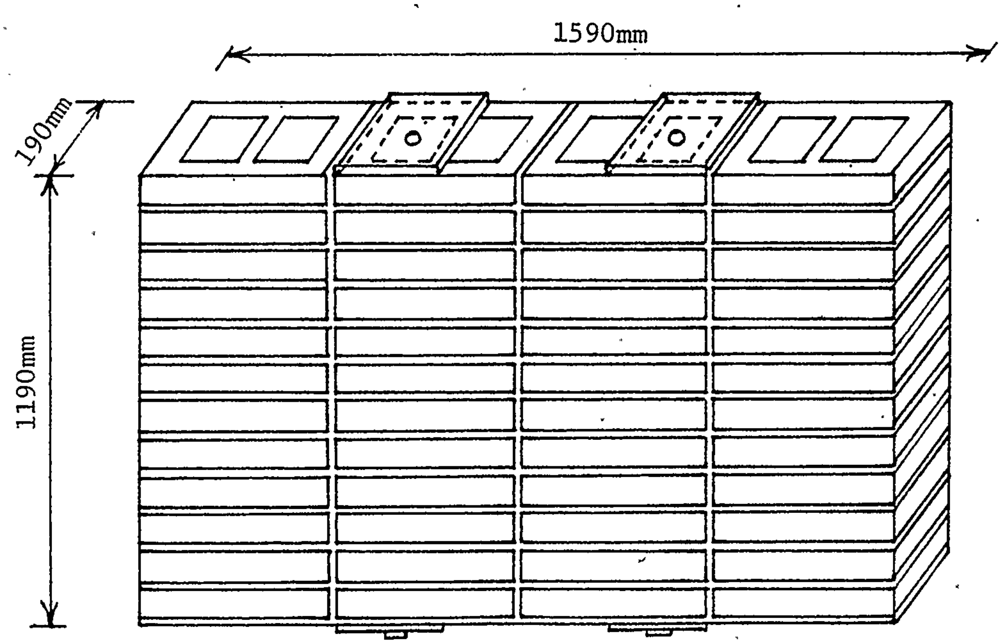

Figure 5.7 Brick Wall Model

In finite element modelling of wall specimens, the masonry units, mortar and steel plates were represented by 3-dimensional 8-node solid hybrid elements while uniaxial truss elements were used for the prestressing steel bars. Both units and mortar were assumed homogeneous, isotropic and linearly elastic. Perfect bond was assumed between units and mortar, and unit, mortar and steel plates. The elastic properties of the masonry components and the steel plates are tabulated in Table 4.2.

Wall models were prestressed to a stress of 25% of the ultimate compressive strength of the masonry. The initial prestressing force was designed to meet requirements of CSA, Code of Practice, CAN3-S304-M84 (1984).

In Figure 5.8a, b is the length, t is the thickness, h is the height of the wall model and A_{ps} is the area of the prestressing steel. For the present case:

$h = 1190$ mm, $b = 1590$ mm and $t = 190$ mm

For masonry walls $b > 3t$ and for axial compressive loading $h < 30\ t$.

Wall models selected for the present study satisfy both the criteria. The allowable vertical compressive load, P, is given as:

$$P = C_e C_s f_m A_m$$

where C_e is the eccentricity coefficient, C_s is the slenderness coefficient, f_m is the allowable compressive stress and A_m is the mortar bedded area.

For vertical compressive loading,

$$f_m = 0.25\ f'_m$$

where f'_m is the ultimate compressive strength. The average value obtained by Ameny (1979 and 1982) for the prism test specimens for f'_m

was $8 N/mm^2$.

Thus $f_m = 0.25 \times 8 = 2 N/mm^2$

For full mortar bedded area,

$A_m = 1.59 \times 0.19 - 8 \times 0.12 \times 0.1275$

$= 0.1797\ m^2$.

For the selected models, $C_e = 1$ and $C_s = 1$.

Then $P = 2 \times 0.1797 \times 10^6$

$= 0.3594 \times 10^6\ N$

$P_b = 0.3594 \times 10^6/2$

$= 1.797 \times 10^5\ N$

$= 179.7\ kN$

where P_b is the force in each prestressing bar.

In order to prestress the bars to 70% of the ultimate tensile strength, a seven wire strand with the following properties was selected.

Size Designation	- 15
Nominal Diameter	- 15.24 mm
Nominal Area (A_{ps})	- 140 mm^2
f_{pu}	- 1860 N/mm^2
$0.7\ f_{pu}A_{ps}$	- 182 kN
$f_{pu}A_{ps}$	- 261 kN

where f_{pu} is the ultimate tensile strength.

The same prestressing bar was used for both full bedded and face-shell bedded specimen models.

Both the geometry of the models and the loading were symmetrical about the three directional axes. Making use of the symmetry, only one-eighth of the wall model was analysed and is shown by the shaded area in

Figure 5.8a. The area of the prestressing steel and the loading to be considered for the symmetrical portion are shown in Figure 5.8b.

5.4 Finite Element Mesh

Figure 5.9a shows a typical 3-dimensional 8-node solid element while a uniaxial truss element is shown in Figure 5.9b. For each element the stresses, strains and displacements at all the nodal points were obtained in the output. A separate mesh generation program was developed for the preparation of input of the nodal coordinates and element topologies of the models.

For the finite element analysis of masonry walls, several mesh schemes were investigated by Simbeya (1985). A mesh scheme similar to one adopted by Simbeya was selected for the present analysis. Various meshes for the different models are illustrated in the following sections.

5.4.1 Cross-Sectional Mesh

Cross-sectional meshes were the same for both concrete block and brick wall models as the same cross-sectional dimensions were used.

(a) Full Mortar Bedding Specimens

Since the mortar covered the whole bed face of the unit, cross-sections through the unit layer and the mortar layer had the same configuration which is shown in Figure 5.10a. The cross-sectional mesh through the steel bearing plate is shown in Figure 5.10b.

(b) Face-Shell Mortar Bedding Specimens

The unit layer and steel plate layer cross-sectional meshes were identical to those of the full mortar bedding specimens and are shown in Figures 5.10a and 5.10b respectively. The cross-sectional mesh through

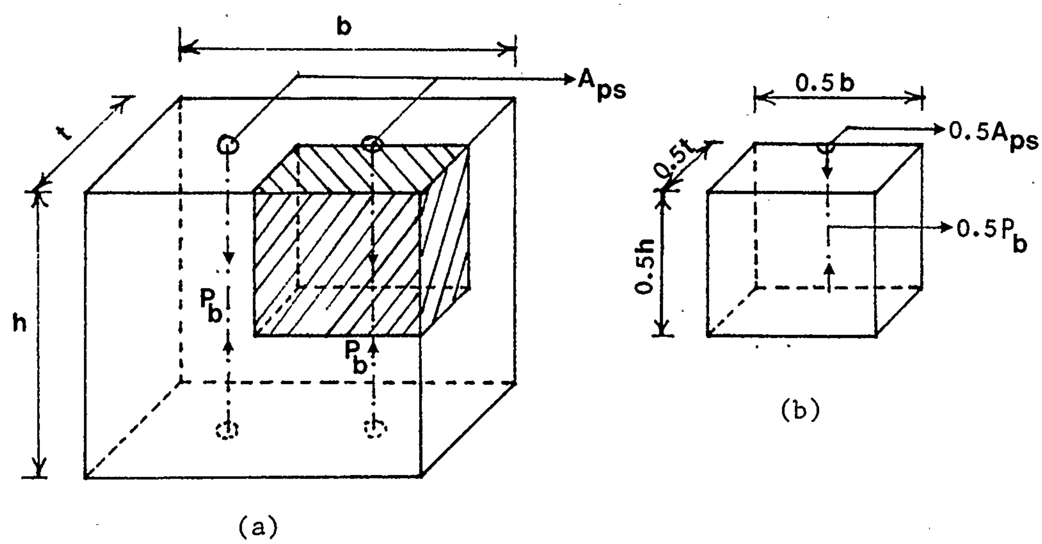

Figure 5.8 Wall Model and Symmetry

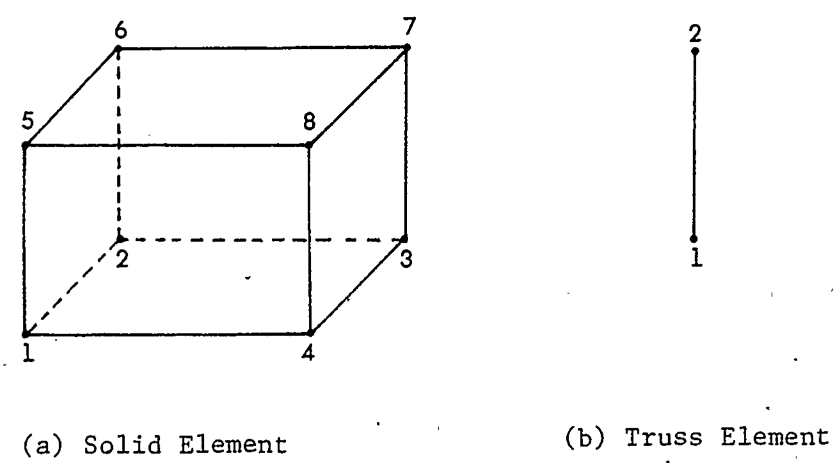

Figure 5.9 Element Types and Nodal Points

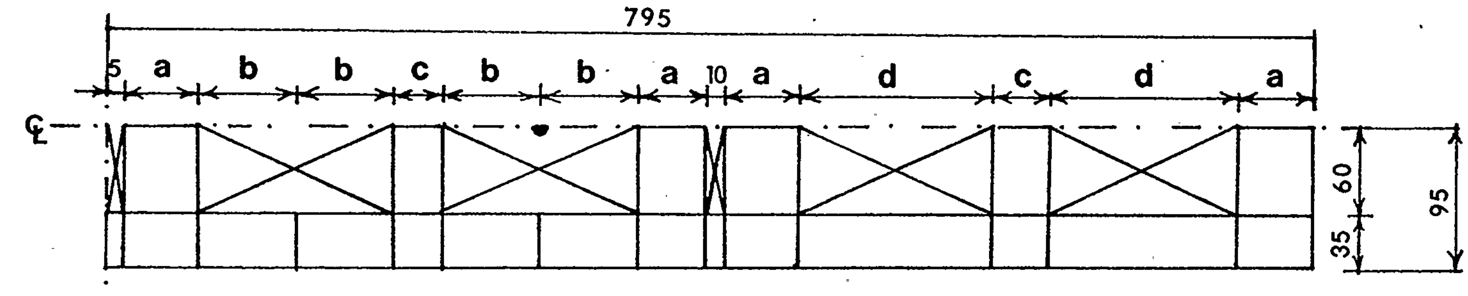

a=50 , b=63.75 , c=35 , d=127.5

(a) Mortar Layer (Full Bedded) and Unit Layer

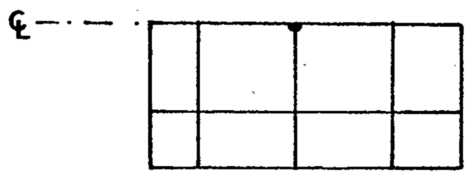

(all dimensions are in mm)

(b) Steel Plate Layer

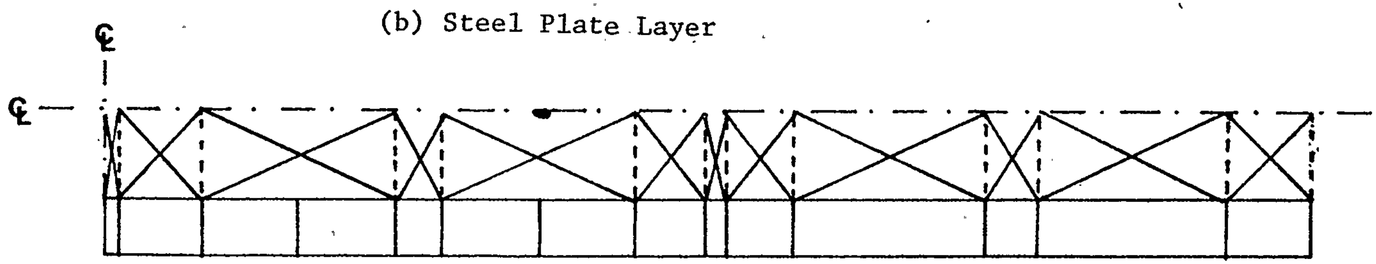

(c) Mortar Layer (Face-Shell Bedded)

Figure 5.10 Cross-Sectional Meshes

the mortar layer is illustrated in Figure 5.10c.

5.4.2 Elevational Mesh

Elevational meshes are the same for full mortar bedding and face-shell mortar bedding specimens. The elevational mesh of the concrete block wall models is shown in Figure 5.11 whereas the details of the elevational mesh of the brick wall specimens are illustrated in Figure 5.12.

5.4.3 Boundary Conditions

The boundary conditions of the wall models are described using the symmetrical portion of the model which is shown in Figure 5.13a. The corresponding planes of symmetry and their boundary conditions are illustrated in Figure 5.13b. In Figure 5.13b, u, v and w are the displacements in the directions x, y and z, respectively.

5.5 Summary

In this chapter, post-tensioned hollow masonry walls were modelled. Only stack-bond pattern specimens were considered. Computer time was the principal factor which controlled the size of the models and the number of cases analysed in this study. Taking advantage of the symmetry, only one-eighth of the wall models were analysed.

In the later sections, finite element meshes were developed for both concrete block wall and brick wall models with full mortar bedding as well as face-shell mortar bedding options included. Finally, the boundary conditions were evolved for the finite element models chosen for the present study.

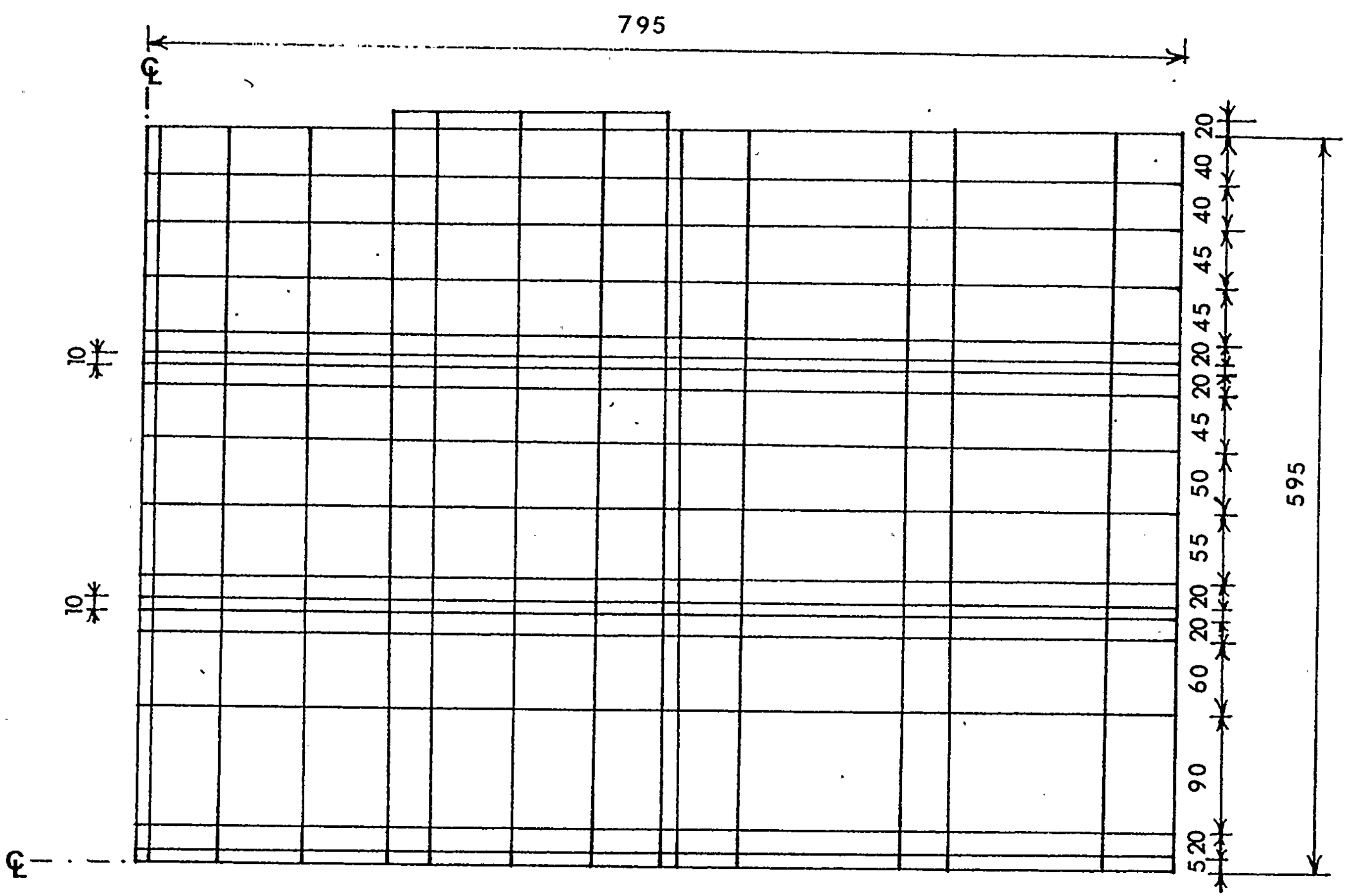

(all dimensions are in mm)

Figure 5.11 Elevational Mesh for Concrete Block Wall Models

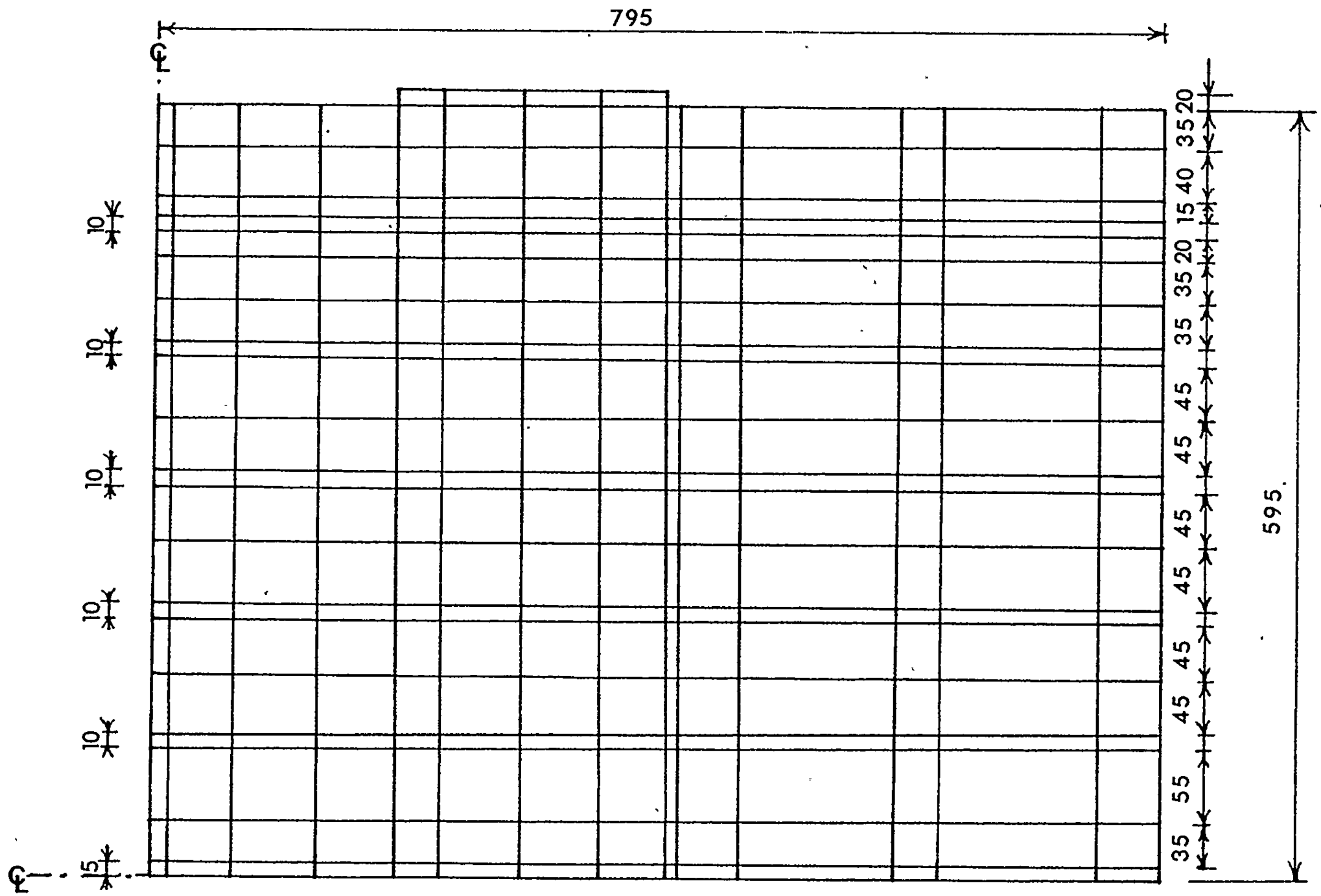

(all dimensions are in mm)

Figure 5.12 Elevational Mesh for Brick Wall Models

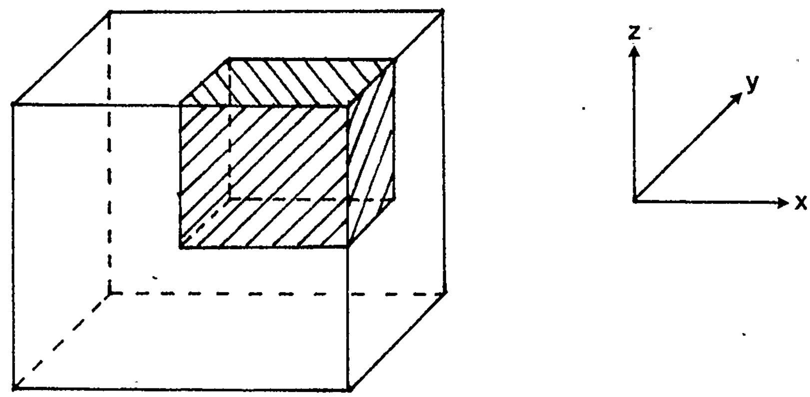

(a)

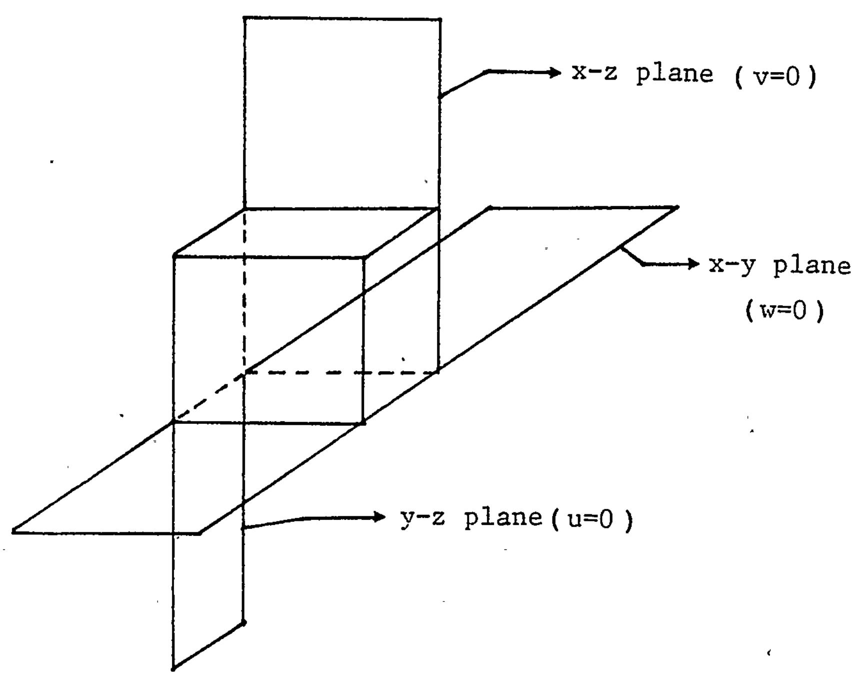

(b)

Figure 5.13 Boundary Conditions

CHAPTER 6

RESULTS AND DISCUSSIONS

6.1 Introduction

Using the input data and methodology described, results were obtained for the time-dependent changes in the masonry wall models.

Upper and lower bound values of prestress losses are computed and short-term prestress losses are compared with experimental values reported in the literature. Finally, the redistribution of stresses between masonry units and mortar due to creep and shrinkage are discussed and compared with the initial elastic distributions.

It is interesting to note that, although the numerical solution technique was developed on a CDC-CYBER 175 computer, a CDC-CYBER 205 supercomputer was used to obtain the final results. For the same problem, the CYBER 205 was found to be 5-6 times faster than the CYBER 175 (without vectorization of the computer program). Furthermore, the CYBER 175 was observed to be 6-7 times faster than the Honeywell Multics computer, also available to the author.

In the last section, an approximate analytical solution to prestress losses was obtained for a simple wall model and was compared with the results of the step-by-step solution technique method.

6.2 Presentation of Results

Material interaction between units and mortar is one of the factors which influence the stress distributions in masonry. The main results were obtained with an elastic modulus of the mortar equal to that of the masonry units. In a few cases the stiffness of the mortar was reduced to half the initial value and the results are compared and discussed in a later section.

As described in Section (3.2.3.2), the numerical solution of creep problems using a time incremental procedure requires the selection of appropriate time intervals so that numerically stable as well as accurate results are obtained. The time-step length selection criteria are discussed in the next section.

6.2.1 Selection of Time-Step Length

In the field of concrete structures, Bazant (1975) reported that to achieve the best results under steady loading, the time intervals should be chosen in the form of a geometric progression. The lengths of the time intervals should be approximately equal in log (time) plot. He proposed the following relationship:

$$(t_{i+1} - t_o) = 1.333\ (t_i - t_o) \tag{6.1}$$

or

$$\Delta t_{i+1} = t_{i+1} - t_i = 0.333\ (t_i - t_o) \tag{6.2}$$

where t_o is the age at initial loading and t_i, t_{i+1} are the two successive times. Bazant suggested that with $\Delta t_1 = 0.01$ day a high accuracy could be achieved.

The basic assumption in the step-by-step procedure is that the stresses remain constant during any time interval. The solution diverges and becomes unstable when large time-step lengths are chosen. Sutherland (1970) proposed that for stable numerical solutions, the maximum incremental creep strain should not exceed the maximum elastic strain during any time interval. Thus, the maximum time increment which can be used is restricted.

In the present study, upper bound results from the creep analysis did not converge even though Bazant's expression and Sutherland's criterion were satisfied. As stated in Chapter 4, for the case of upper bound limits, the ratio of the specific creep strains in the mortar joint to those of the concrete block units was in the order of 10-12. The creep strains of individual concrete block units were of the same order as those of conventional concrete. Thus, the probable reasons for the instability of the numerical solution were (1) the high magnitudes of the creep strains in mortar joints and (2) the difference of creep strain magnitudes of concrete block units and mortar joints. These reasons were confirmed by the fact that lower bound solutions converged with the time intervals chosen as per Equation (6.1). For lower bound limits, the ratio of the specific creep strains in the mortar joints to those of the concrete block units was in the range of 4-5. For a period of twelve years, adequate lower bound solutions were obtained with 125 time steps. However, upper bound solutions did not converge even after selecting time intervals equal to one-tenth of those chosen for the lower bound limits, i.e. for a period of twelve years, even 1250 time steps were not sufficient to acquire upper bound solutions. In terms of computer time and money, it became impractical to increase the number of time steps any further. At this level, it was decided to make an approximation in the case of upper bound results. The detailed step is discussed in the next section.

6.2.2 Loss of Prestress

As discussed in the previous section, it was not feasible to obtain long-term upper bound results for a period of twelve years. It was decided to reduce the mortar's upper bound creep property so that numerical instability could be avoided. All the model specimens were analysed with the reduced creep property and the approximate upper bound results were obtained. A few specimens were analysed with 100% mortar creep property and short-term upper bound results were attained. Then long-term approximate results were calculated by multiplying by a correction factor in proportions to the corresponding short-term results obtained with 100% and reduced mortar creep property. With 100% creep property, 2500 time steps were used to obtain short-term results. Although, as discussed in Section (3.2.3.2), numerical stability does not necessarily mean that the final results are correct, the upper bound short-term prestress loss results were concluded to have converged due to the following reasons. (1) 2500 time steps (a large number) were used to obtain short-term results which compared very well with the experimental results reported in the literature. (2) The shape of prestress loss curves in the time domain matched the curves obtained for lower bound results.

6.2.2.1 Concrete Block Walls

Both short-term and long-term prestress losses for lower bound and upper bound solutions of the concrete block wall models are summarized in Table 6.1.

Although face-shell bedded specimens sustained more prestress loss than full-bedded specimens, the difference was insignificant. Overall upper and lower bound prestress losses versus time are plotted in Figures 6.1 and 6.2 for creep and shrinkage analyses, and creep, shrinkage and relaxation analyses respectively. Fifty percent of the ultimate loss at twelve years occurred during the first 25-40 days. In general, post-tension losses due to creep and shrinkage effects were obtained between 15% and 24% where lower and upper limits reflect the different

		Upper Bound Solutions (with N-Mortar)		Lower Bound Solutions (with M-Mortar)	
		Full Mortar Bedded Models	Face-Shell Mortar Bedded Models	Full Mortar Bedded Models	Face-Shell Mortar Bedded Models
Prestress Loss due to Creep and Shrinkage Analyses (%)	After 200 Days	18.3	19.6	12.4	13.0
	After 1 Year	19.3	20.6	13.1	13.9
	After 12 Years	21.9	23.6	14.6	15.5
Prestress Loss due to Creep, Shrinkage and Relaxation Analyses (%)	After 200 Days	25.6	26.7	20.4	21.0
	After 1 Year	26.6	27.8	21.3	21.9
	After 12 Years	30.0	31.5	23.8	24.4

Table 6.1 Loss of Prestress for Concrete Block Wall Models

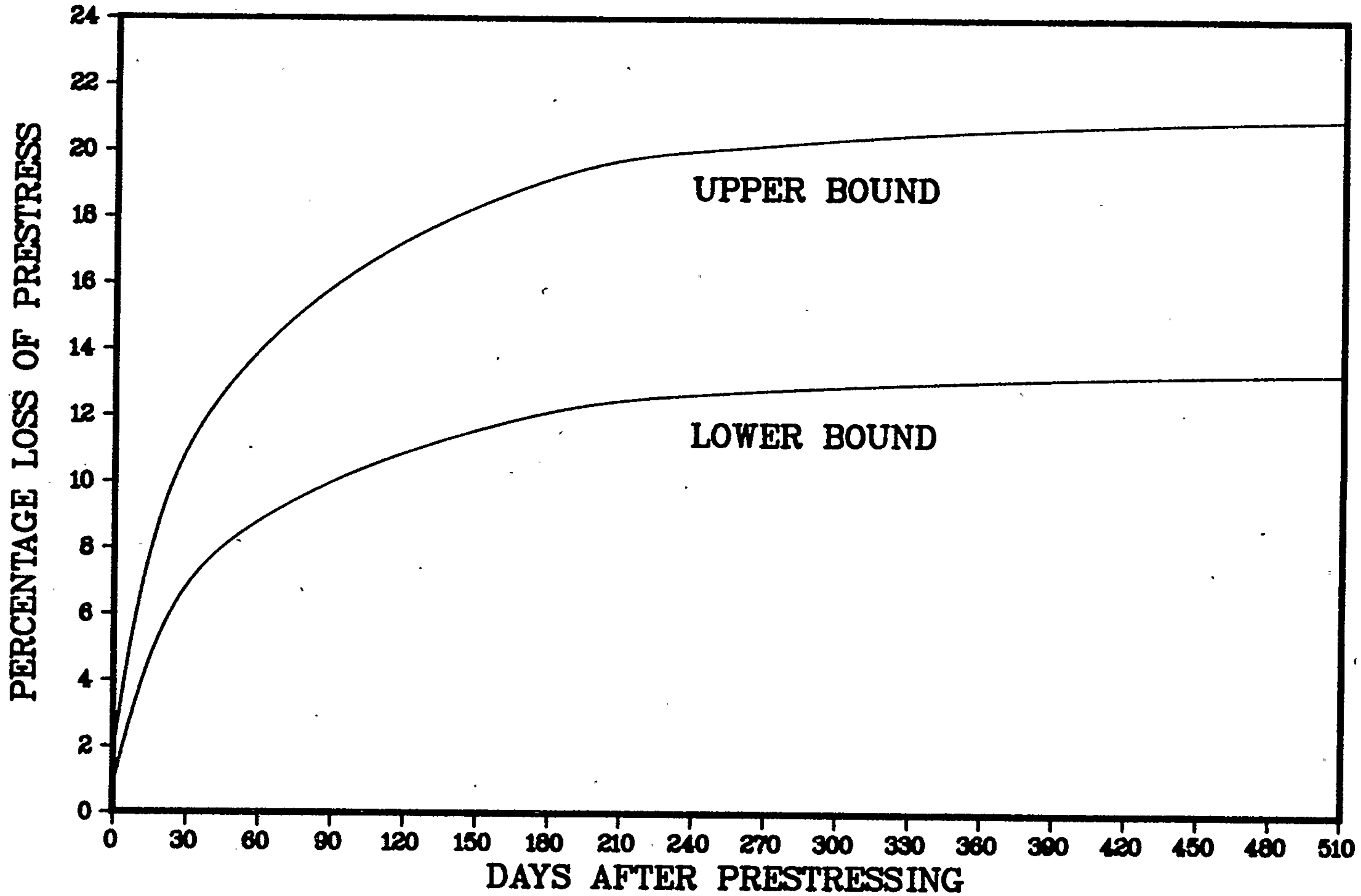

FIGURE 6.1 PRESTRESS LOSS IN CONCRETE BLOCK WALLS

(CREEP AND SHRINKAGE ANALYSES)

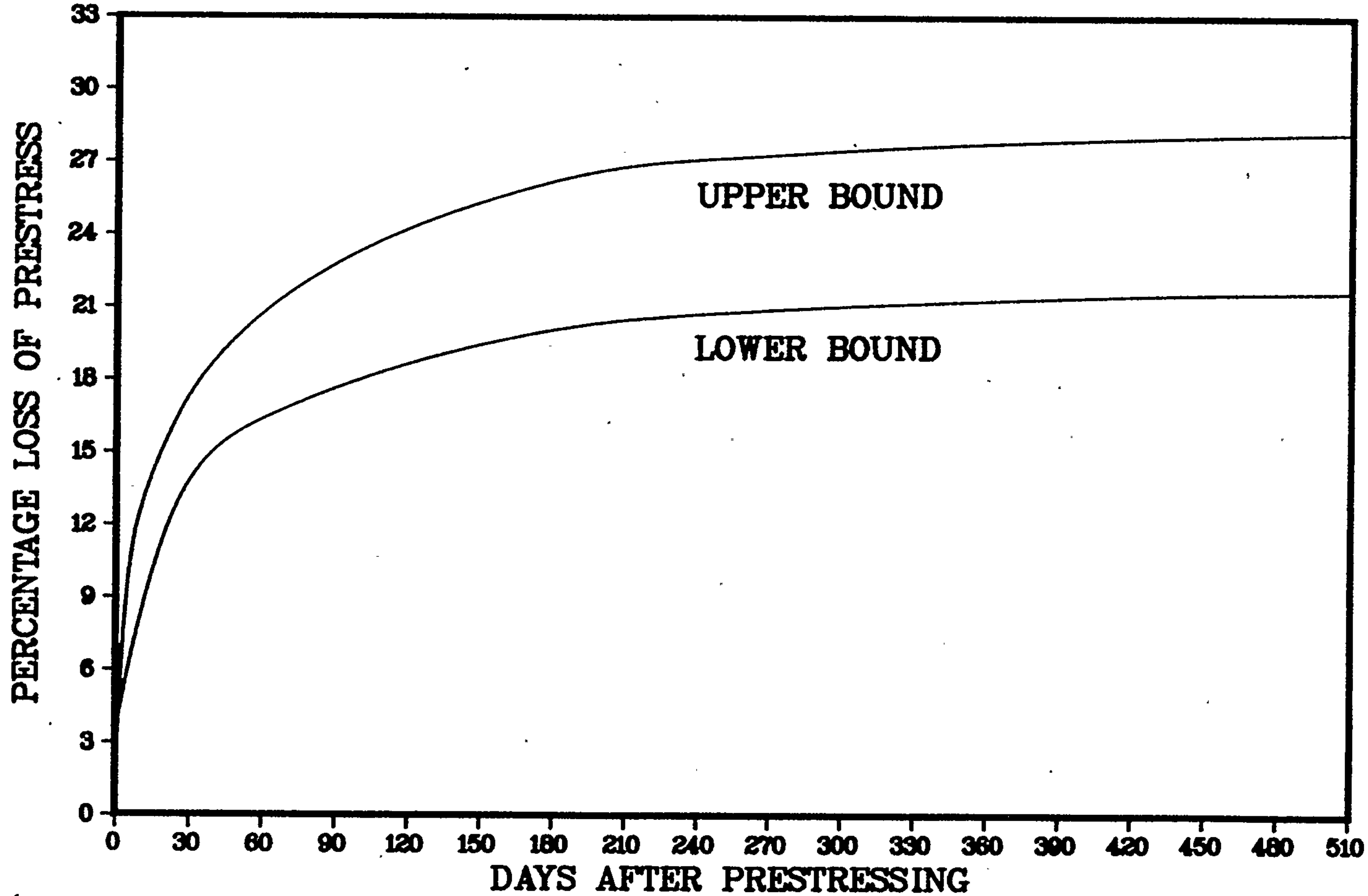

FIGURE 6.2 PRESTRESS LOSS IN CONCRETE BLOCK WALLS

(CREEP , SHRINKAGE AND RELAXTION ANALYSES) creep and shrinkage properties of the masonry units and mortars adopted for the present study. Similarly, losses due to creep, shrinkage and stress relaxation effects were acquired in the range of 24-31%. The post-tensioned steel bars were of high tensile strength and were stressed to 70% of the ultimate strength.

6.2.2.2 Brick Walls

The summary of short-term and long-term prestress losses for the brick wall models is given in Table 6.2. Prestress losses in face-shell bedded and full-bedded specimens were of the same order. The computed upper and lower bound prestress losses are plotted in Figures 6.3 and 6.4 for creep and shrinkage effects, and creep, shrinkage and relaxation effects respectively. Fifty percent of the ultimate loss at twelve years occurred during the first 25-30 days. Prestress losses due to creep and shrinkage were obtained between 5% and 10% where the two limits correspond to the upper and lower bounds of the creep and shrinkage properties of the mortar. It is recalled that the brick units were assumed to have no creep and shrinkage strains. Further, moisture expansion strains in the brick units were also neglected. The prestress loss will be reduced if the moisture expansion of the brick units is included in the analysis. The computed losses from creep, shrinkage and relaxation analyses were in the range of 17-22%. The steel bars were of high tensile strength and were prestressed to 70% of the ultimate tensile strength.

In the present study, the effect of different lengths of steel wires on prestress losses was not studied. But, the wall models were designed to meet requirements of CSA, Code of Practice, CAN3-S304-M84 (1984) and the height to length ratio of the models was selected from

		Upper Bound Solutions (with N-Mortar)		Lower Bound Solutions (with M-Mortar)	
		Full Mortar Bedded Models	Face-Shell Mortar Bedded Models	Full Mortar Bedded Models	Face-Shell Mortar Bedded Models
Prestress Loss due to Creep and Shrinkage Analyses (%)	After 200 Days	7.7	8.5	3.7	4.1
	After 1 Year	8.1	8.9	4.0	4.5
	After 12 Years	9.1	10.1	4.7	5.2
Prestress Loss due to Creep, Shrinkage and Relaxation Analyses (%)	After 200 Days	17.2	17.8	13.1	13.4
	After 1 Year	18.0	18.7	13.9	14.3
	After 12 Years	21.3	22.1	16.8	17.2

Table 6.2 Loss of Prestress for Brick Wall Models

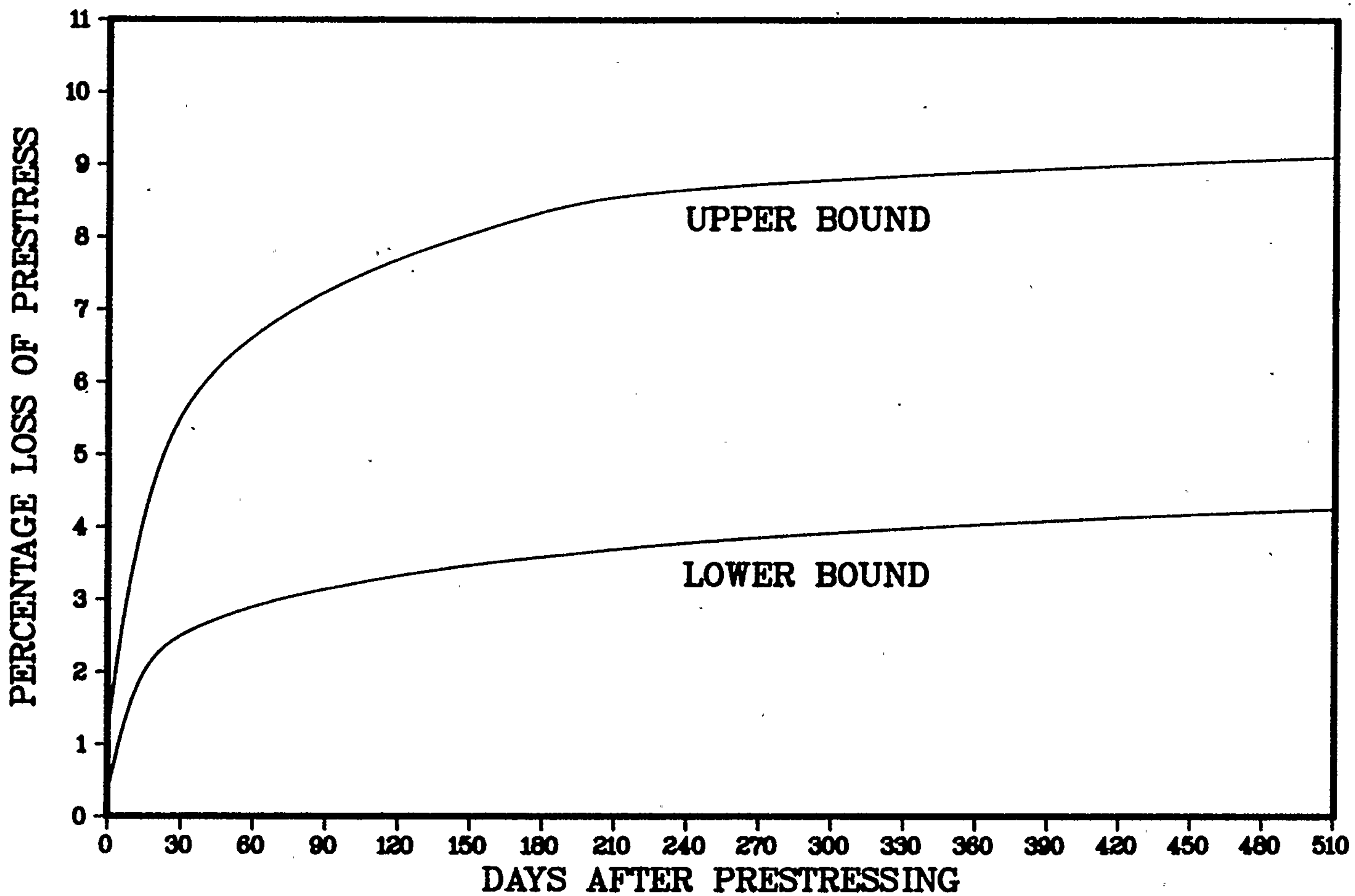

FIGURE 6.3 PRESTRESS LOSS IN BRICK WALLS

(CREEP AND SHRINKAGE ANALYSES)

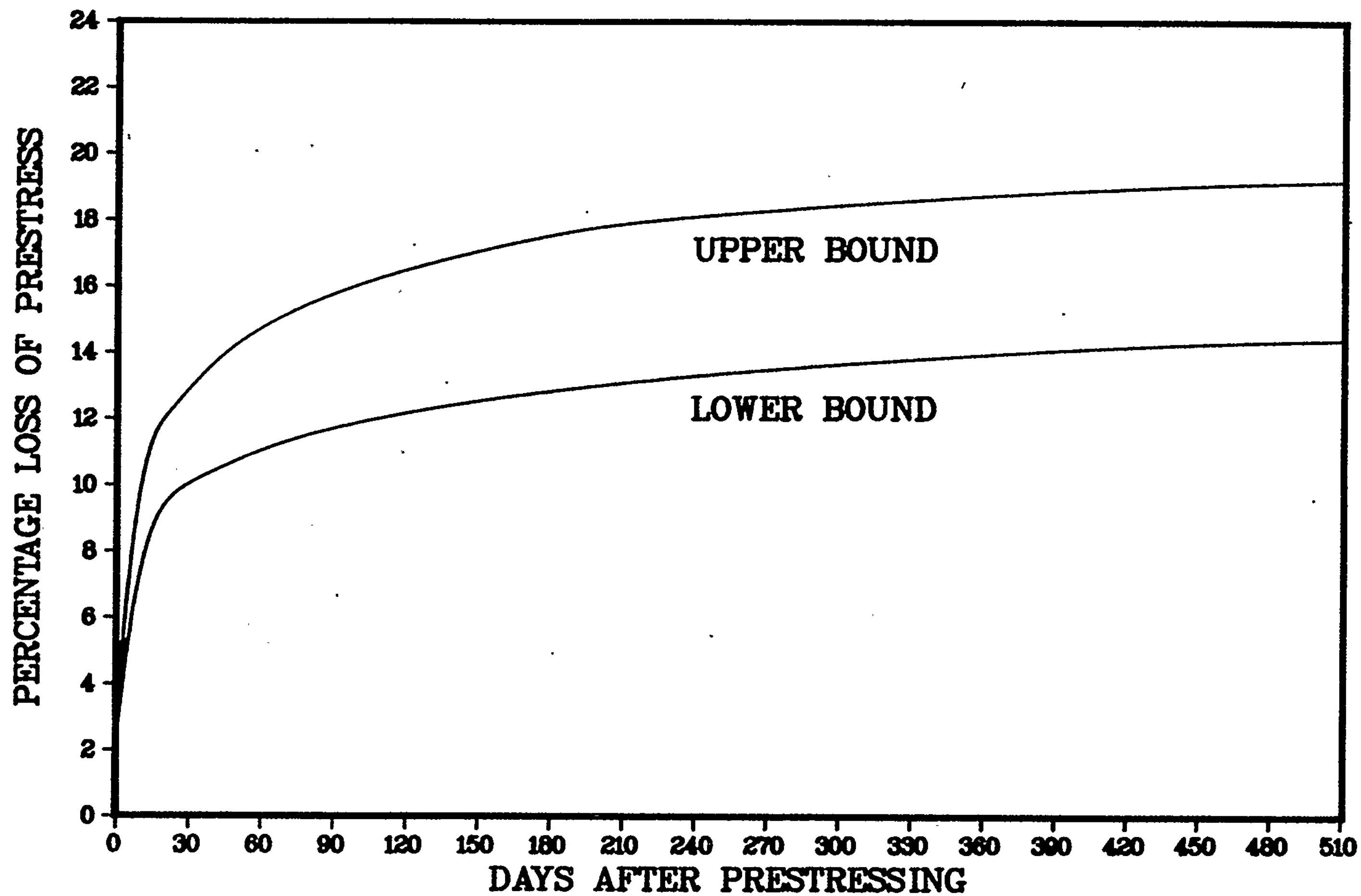

FIGURE 6.4 PRESTRESS LOSS IN BRICK WALLS

(CREEP , SHRINKAGE AND RELAXTION ANALYSES) the range of values used for actual masonry walls.

6.2.2.3 Comparison with Previous Results

Tatsa et al (1973) reported a few experimental observations of the prestress losses in concrete block walls. With a ratio of creep strains in the mortar joints to those in the block units of 4.4, the observed prestress loss due to creep, shrinkage and relaxation after 180 days was in the order of 20% wherein the losses due to creep and shrinkage were 12.5%. A creep ratio (creep in joint/creep in block) of 4.4 corresponds to the lower bound limits of the present model. From the present analysis, after 180 days the lower bound prestress losses due to creep and shrinkage were in the order of 12% whereas the overall lower bound losses were 20%. These figures match the numbers reported by Tatsa et al (1973).

Huizer and Shrive (1984) reported short-term losses in a post-tensioned concrete block wall. The block units used were over three years old and were not expected to contribute much creep and shrinkage. Thus, their wall panel is similar to the brick wall model of the present investigation as the creep and shrinkage strains in the brick units were neglected. After 200 days, the overall observed prestress loss by Huizer and Shrive was 16% or less. In their test, the post-tensioning steel wires were of high tensile strength and were prestressed to 70% of the ultimate strength. As shown in Table 6.2, the present analysis resulted in 13.1% prestress loss in the lower bound case and 17.8% loss in the upper bound case. The results compare favourably.

Lenczner and Davis (1984) reported short-term prestress losses in post-tensioned brick walls. After about a year 9-11% prestress loss was observed. In their tests, the prestressing bars were not stressed more than 50% of the ultimate strength. Thus, the overall loss was because of creep and shrinkage only. It was observed that 50% of the loss occurred during the first 25-40 days. From the present analysis, due to creep and shrinkage upper bound loss after a year was in the order of 9%. Further, 50% of the loss occurred during the first 25-30 days.

Thus, the short-term results obtained from the present analysis relate very well with the experimental results reported in the literature.

In "Masonry Designer's Manual" by Curtin et al (1982), 20% ultimate prestress loss is suggested for designing post-tensioned brickwork masonry. In the present study, the computed losses from creep, shrinkage and relaxation analyses were in the range of 17-22%. These results also compare very well.

6.2.3 Stress Distributions

The study of elastic stress distributions in masonry walls due to concentrated axial load was done in detail by Simbeya (1985). In general, lateral tensile stresses are induced due to an axial compressive load on hollow masonry work. In the present study, similar tensile stresses were obtained from the elastic analysis of post-tensioned hollow masonry walls. In the following sections, the redistribution of lateral tensile stresses due to creep and shrinkage are compared with the initial elastic stress distributions. The basic definitions of lateral tensile stresses are reviewed in the next section. In one wall model case, the redistribution of vertical compressive stresses is also shown.

6.2.3.1 Definitions

Two types of face-shell lateral tensile stresses are induced due to axial loading. These are named as (1) Tearing Stresses and (2) Splitting Stresses. Another type of lateral tensile stress is induced in the cross-webs in the case of face-shell bedded specimens and is termed a Web Splitting Stress.

The origin and coordinate system, chosen for the present study, is shown in Figure 6.5.

Figure 6.6, an elevational view of the wall model subjected to concentrated loads, has been taken from Simbeya (1985) and illustrates the different zones in which the two types of face-shell tensile stresses occur. Both splitting and tearing stresses are represented by σ_x in the face-shells. A typical distribution of the splitting stress along the height of the wall is shown in Figure 6.7.

The web splitting stress is represented by σ_y in the webs and a typical vertical distribution through the web centre-line is depicted in Figure 6.8.

6.2.3.2 Redistribution of Tensile Stresses due to Creep and Shrinkage

The lateral tensile stresses may change with time due to the effects of creep and shrinkage. Redistribution is assessed from the long-term lower bound results of the creep and shrinkage analyses for the masonry wall models.

The stresses are identified with the coordinate system shown in Figure 6.5. Tensile stresses have been considered to be positive and compressive stresses negative.

To show the locations of reference points for the plotting of tensile stress distributions, a cross-sectional mesh is redrawn in

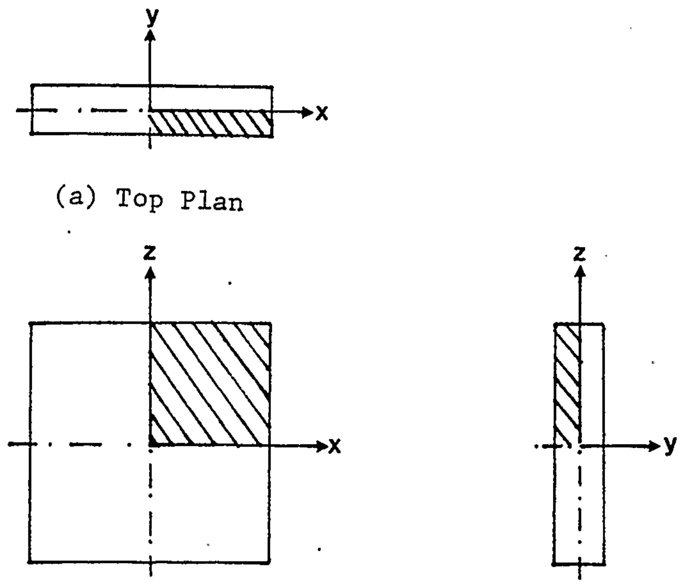

(a) Top Plan

(b) Front Elevation

(c) Side Elevation

Figure 6.5 Coordinate System

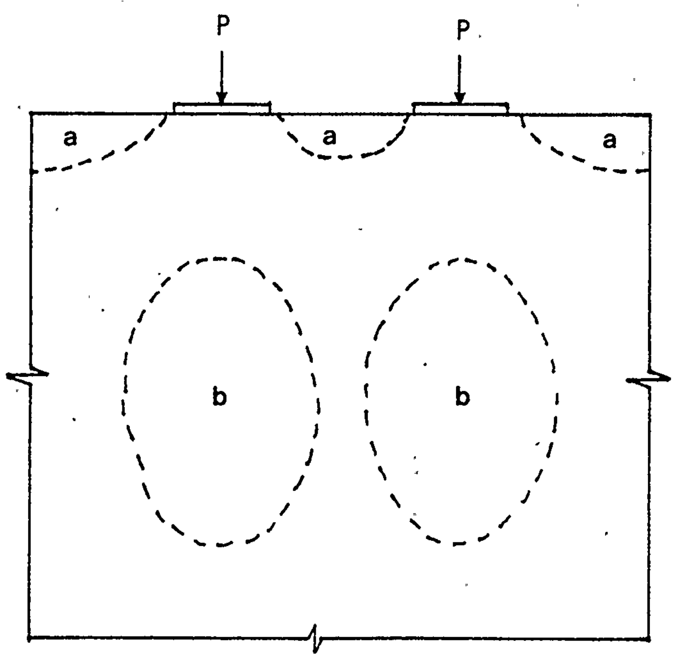

a - Tearing Stresses b - Splitting Stresses

Figure 6.6 Tensile Zones in a Wall

due to Concentrated Loading

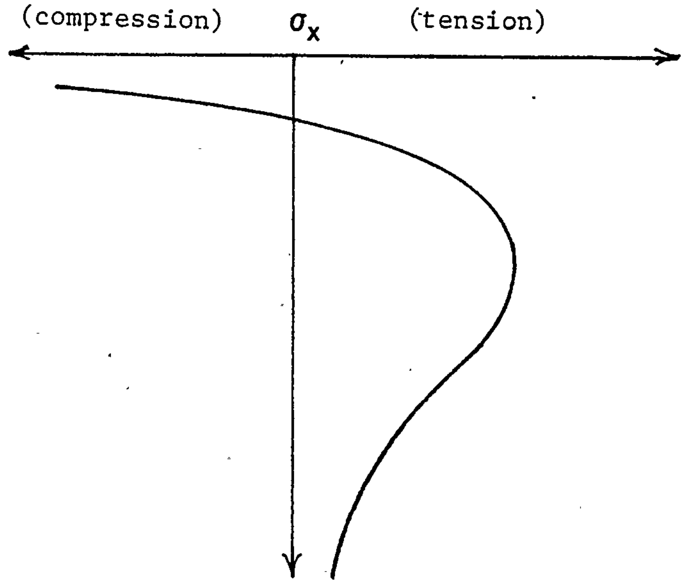

Figure 6.7 Vertical Distribution of Face-Shell Splitting Stresses

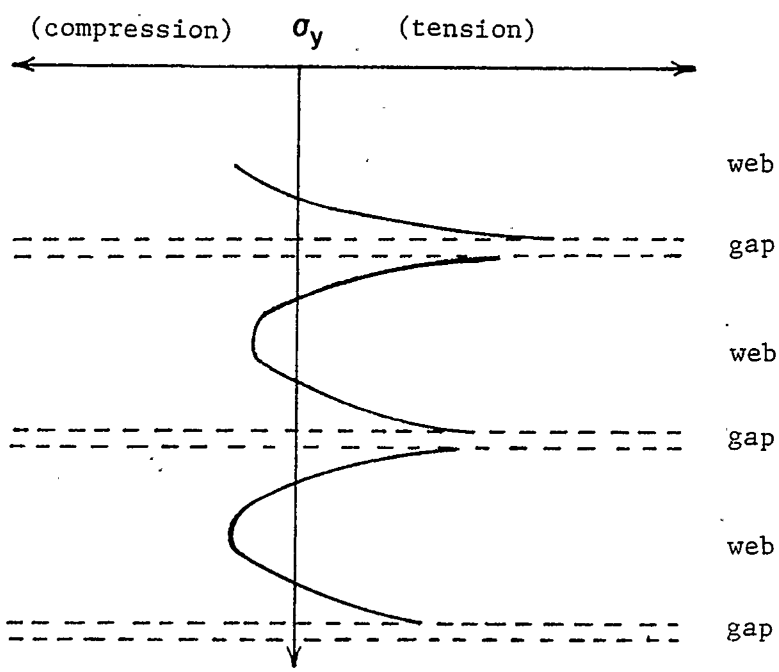

Figure 6.8 Vertical Distribution of Web Splitting Stresses

Figure 6.9. The stress distributions for the tearing stresses (σ_x) are plotted along the horizontal line A-A at the top of the wall model. The face-shell splitting stress (σ_x) distributions are plotted along a vertical line passing through point '1' and the web splitting stresses (σ_y) are plotted along a vertical line passing through point '2'.

For each element, the stresses at the corner nodal points were obtained in the output. The stress values plotted are the averages of the stresses from all the elements meeting at the nodal points.

(a) Tearing Stresses

The tearing stresses for full-bedded and face-shell bedded specimens of the concrete block wall models are plotted in Figures 6.10 and 6.11 respectively. The elastic stress distributions are compared with the stresses obtained from the creep and shrinkage analyses.

There was a significant reduction of the tensile stress in the mortar joint at x = 0 while the unit next to the mortar joint (at x = 5 mm) incurred an increase in tensile stress. This change can be explained due to the difference in creep behaviour of the mortar and masonry units. It is recalled that creep strains of the mortar joint were much higher than those of the concrete block unit. Under a compressive loading, the walls expand laterally in the x-direction. Due to creep, the lateral expansion of the walls increases with time. The mortar joint tends to expand more than the adjoining units because of the higher creep property. Thus, the expansion of mortar is restrained, resulting in compressive stress in the mortar joint and tensile stress in the adjacent units. A similar effect was observed at the other mortar joint at x = 400 mm. The compressive stress in the mortar joint was increased while the adjoining units had a decrease in the compres-

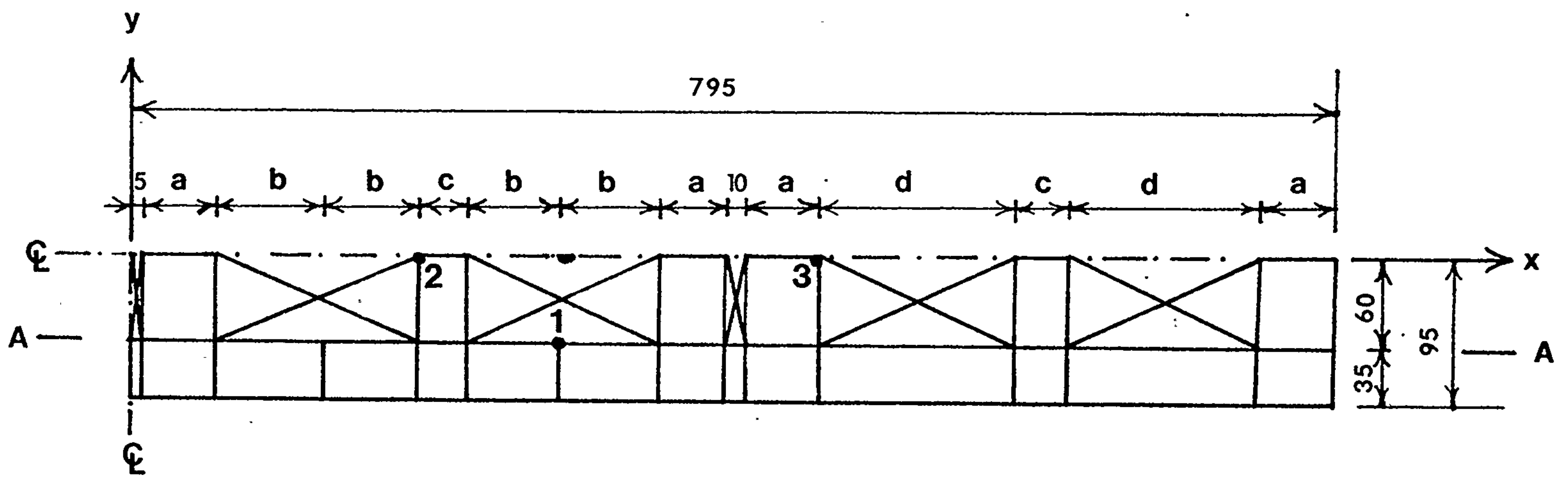

a=50 , b=63.75 , c=50 , d=127.5

(all dimensions are in mm)

Figure 6.9 Cross-Sectional Mesh and Locations of

Reference Points for Stress Distributions

FIGURE 6.10 TEARING STRESSES

CONCRETE BLOCK WALL (FULL BEDDED)

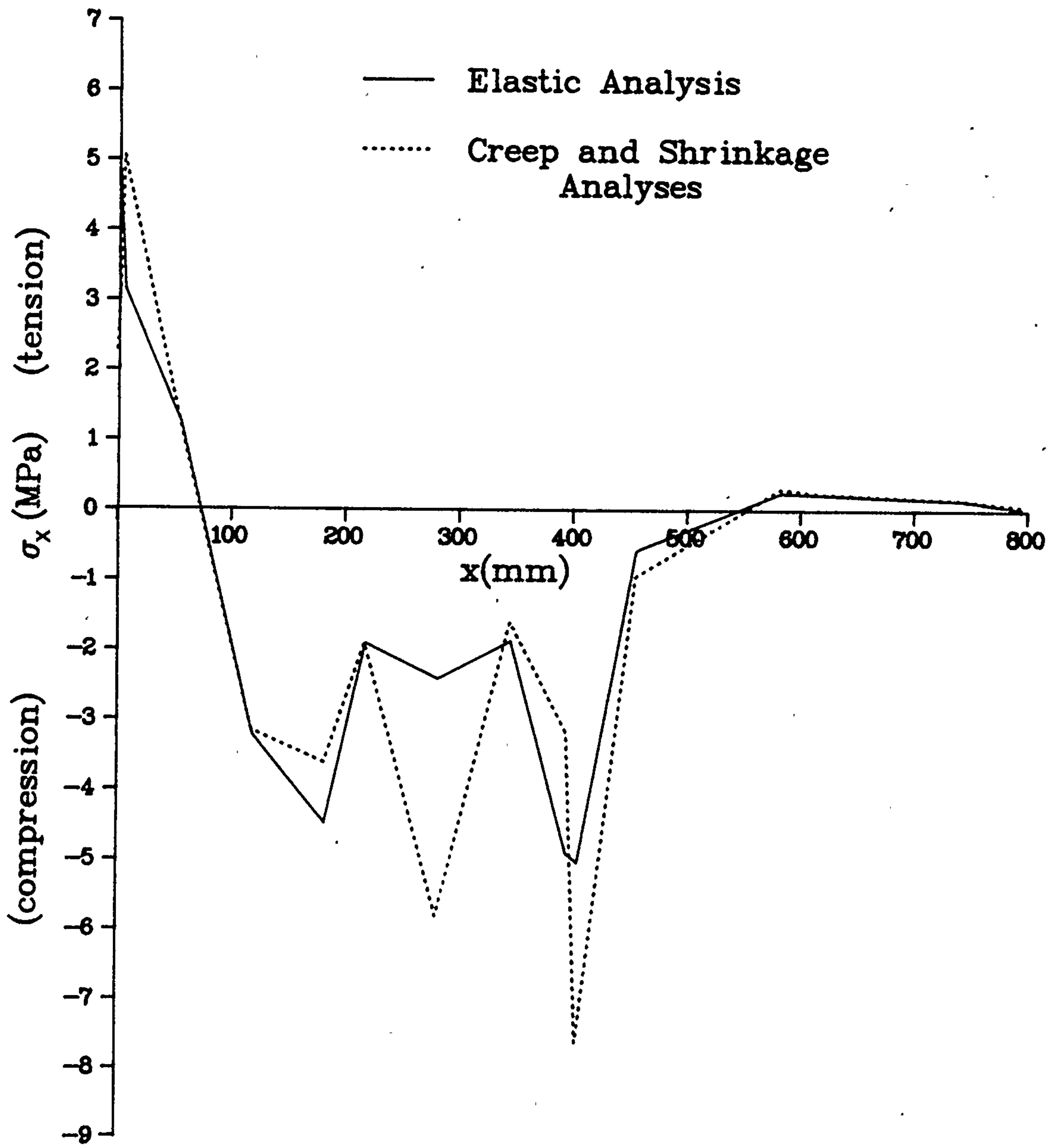

FIGURE 6.11 TEARING STRESSES

CONCRETE BLOCK WALL (FACE-SHELL BEDDED)

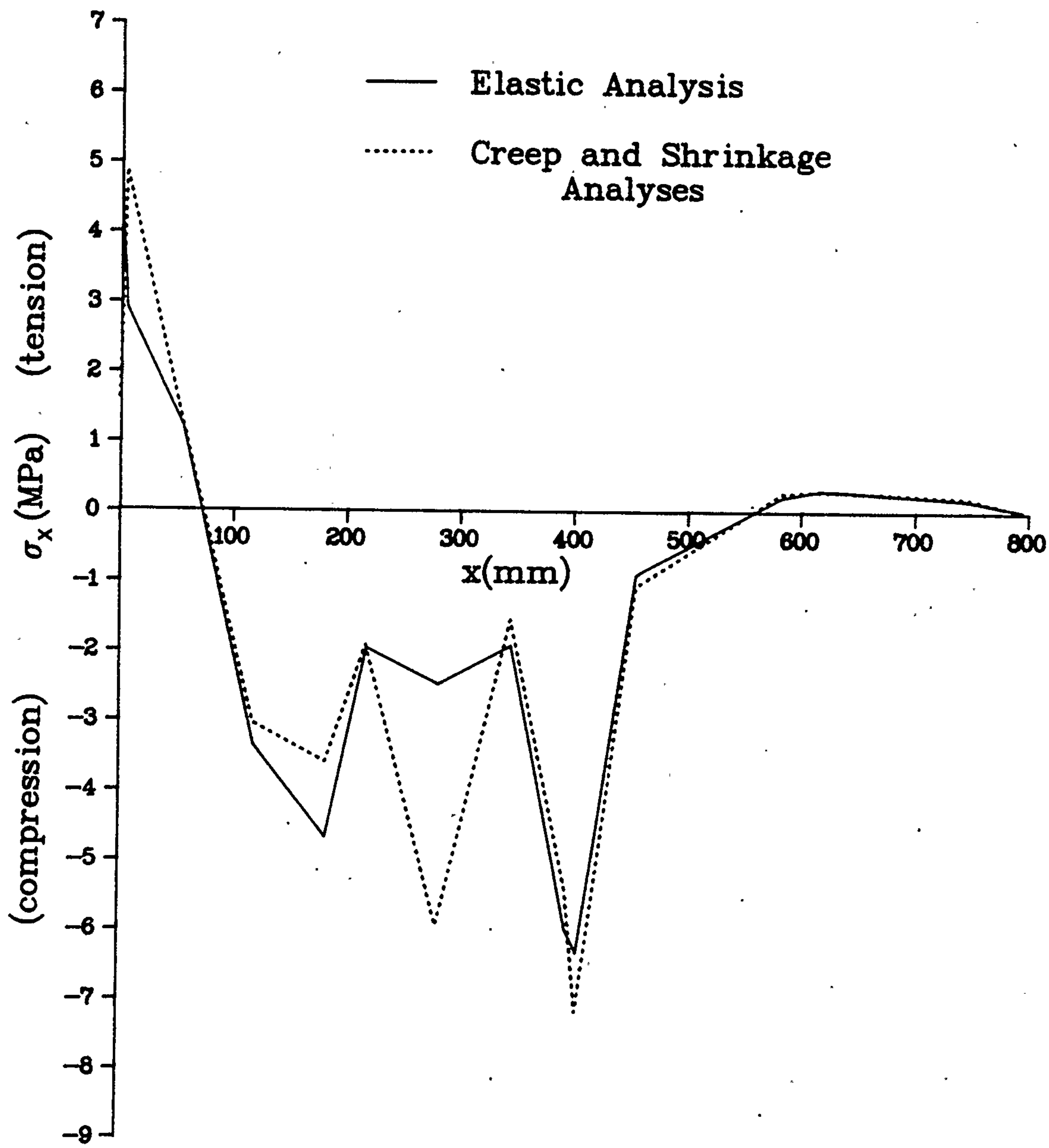

sive stress.

The stress distribution results for the brick wall models, shown in Figures 6.12 and 6.13, display the same results in the mortar joint. The reader will recall that the brick units were assumed not to creep.

For lateral stresses, the shrinkage effect is opposite to the creep effect. Since the difference between the creep strains of mortar and units is more than their shrinkage strain difference, the creep effect is dominating.

As depicted in Figures 6.10 and 6.11, at $x = 281.25$ mm there was a noticeable increase of the compressive stress in the concrete block wall models while this effect was missing in the case of brick wall models. At $x = 281.25$ mm, the units are in contact with the steel plate. Due to creep, the concrete block units tend to expand laterally. The expansion is restrained by the steel plate and a higher compressive stress in the block units results. As the brick units did not creep, such a change was not observed in the brick wall model results.

For the concrete block as well as the brick wall model, the maximum tearing (tensile) stress due to creep and shrinkage was of the same order as that obtained from the elastic analysis.

(b) Splitting Stresses

The splitting stress distributions for the full-bedded specimens of the concrete block and the brick wall models are illustrated in Figures 6.14 and 6.15 respectively. Two main aspects may be observed. (1) In both wall models, the tensile splitting stress decreased all along the height except at one place. In the case of the brick wall model, there was an increase in the tensile stress in the topmost unit layer. (2) In the mortar joints, there was a conspicuously large reduction in the

FIGURE 6.12 TEARING STRESSES

BRICK WALL (FULL BEDDED)

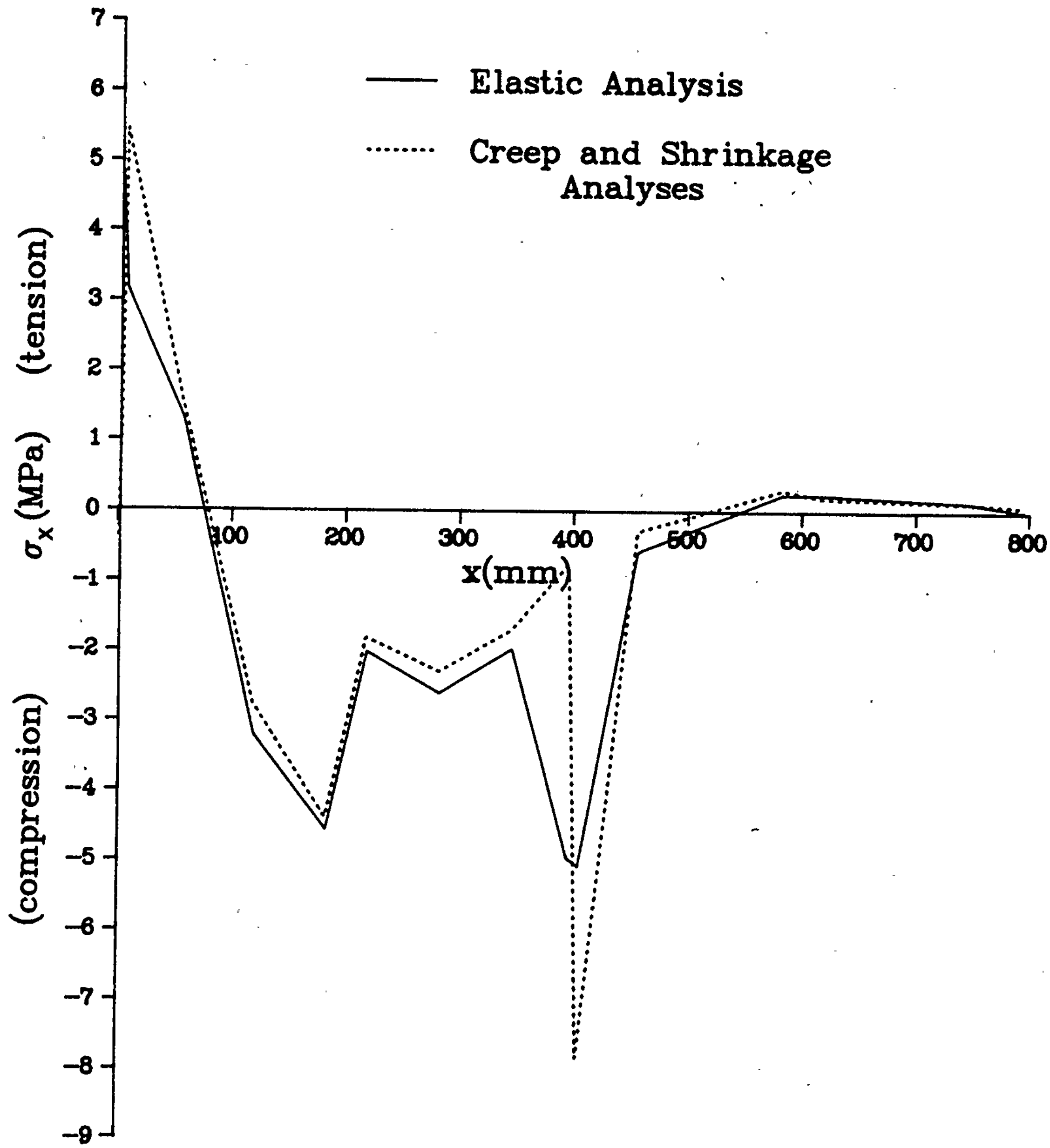

FIGURE 6.13 TEARING STRESSES

BRICK WALL (FACE–SHELL BEDDED)

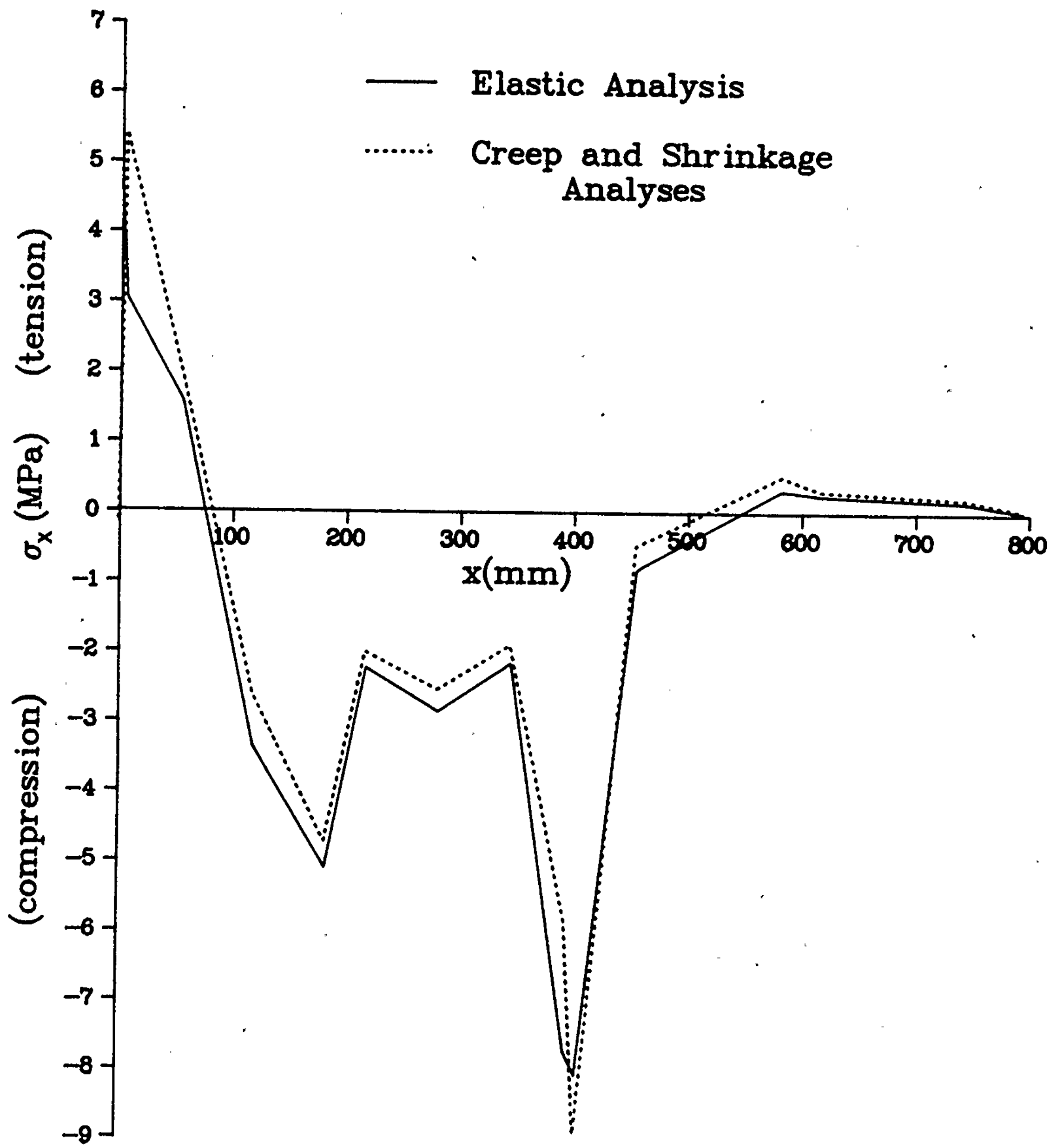

FIGURE 6.14 SPLITTING STRESSES

CONCRETE BLOCK WALL (FULL BEDDED)

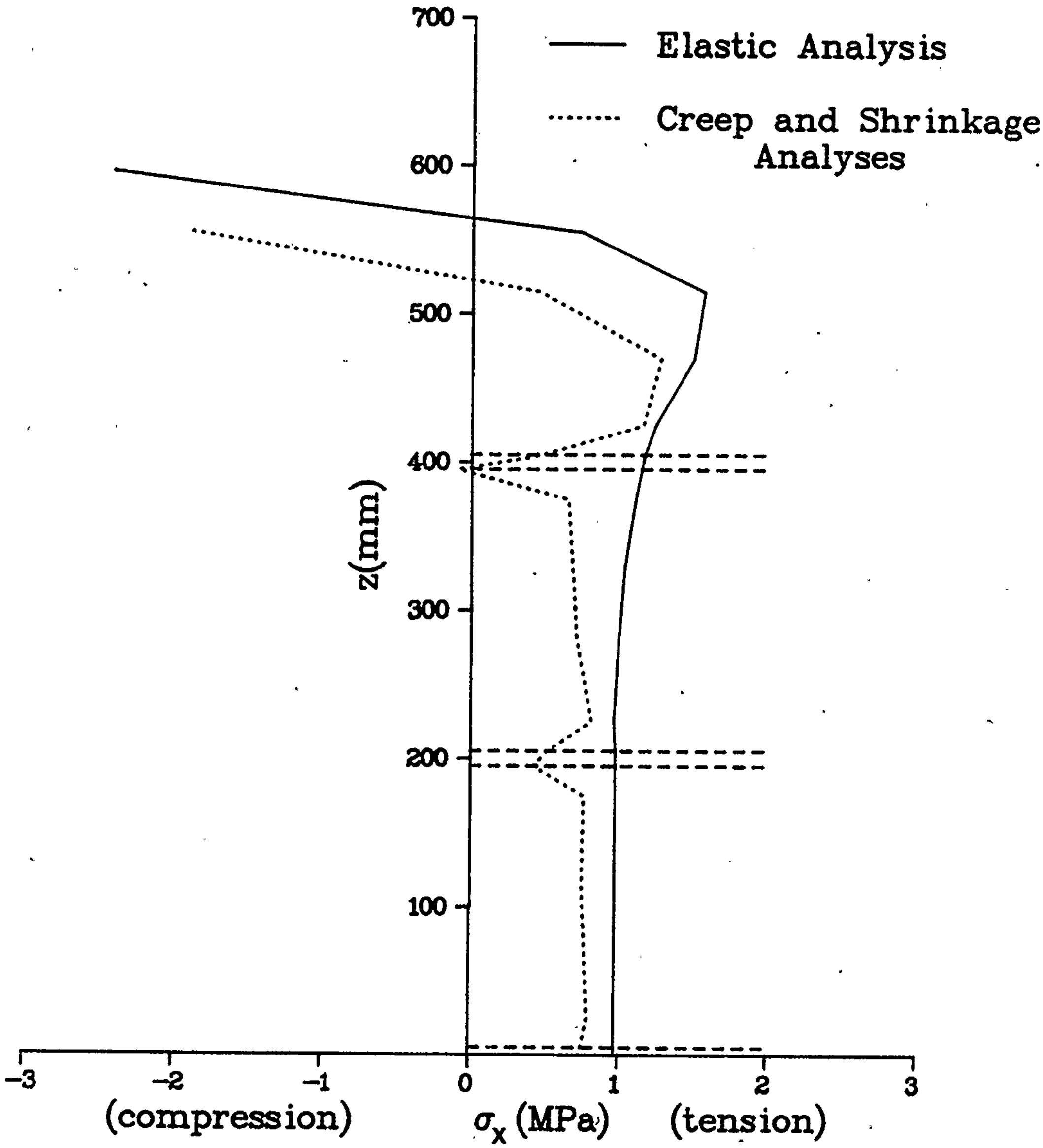

FIGURE 6.15 SPLITTING STRESSES

BRICK WALL (FULL BEDDED)

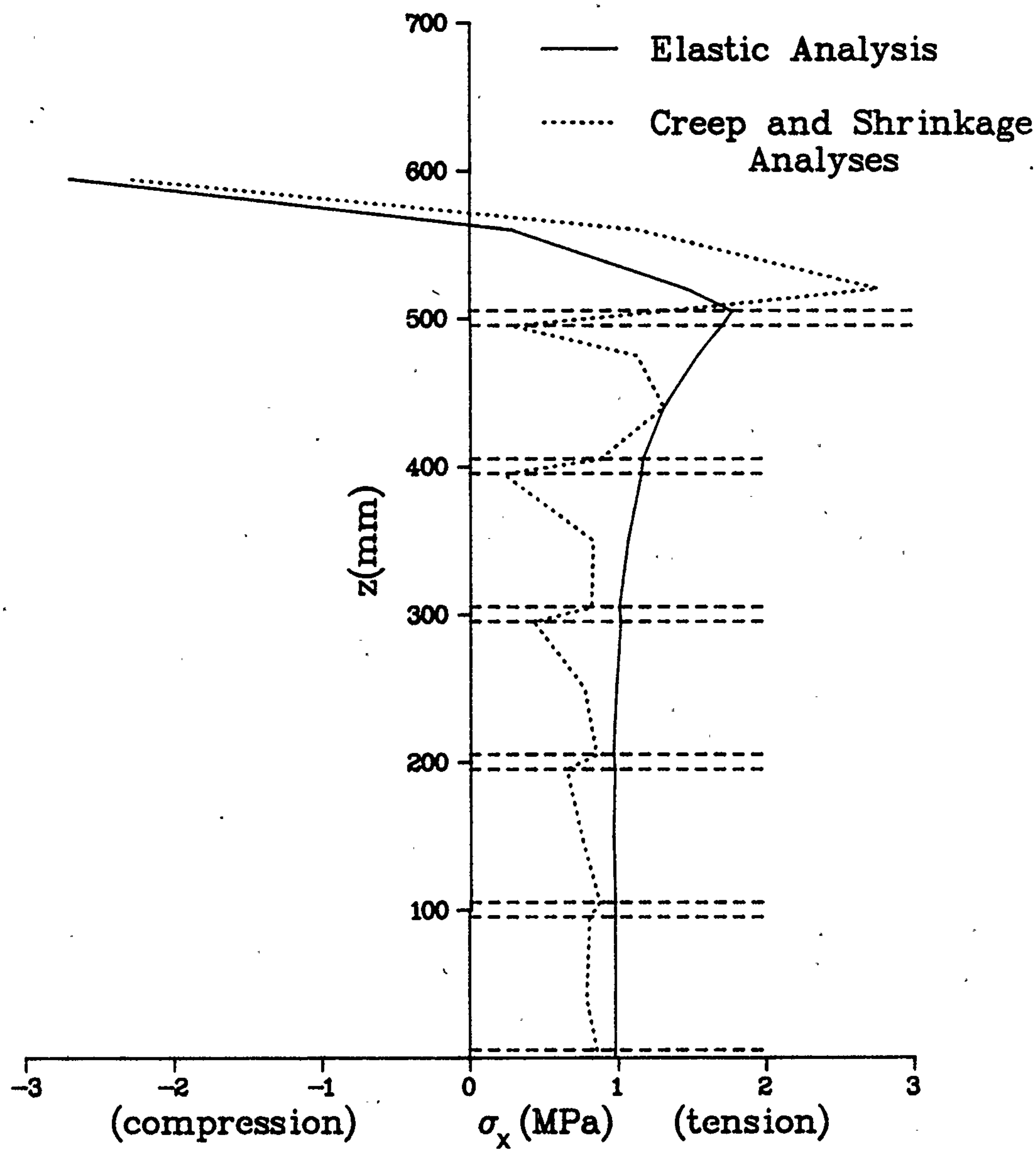

lateral tensile stress.

Due to creep and shrinkage phenomena, there was a loss of the prestress which resulted in an overall reduction of the splitting stress with time. In the mortar joint, the lateral expansion due to creep was restrained by the adjoining units which resulted in a compressive stress in the mortar joint and a tensile stress in the adjacent units. Thus, the tensile stress in the mortar joint decreases significantly. In the case of the brick wall model, the increase of tension near the top horizontal mortar joint caused an overall increase of the tensile stress in the top unit layer. In the concrete block wall model, the lateral expansion of the top unit due to creep was restrained by the steel plate which contributed towards the reduction of the tensile stress in the top unit layer.

The splitting stresses for face-shell bedded specimens of the concrete block and the brick wall models are plotted in Figures 6.16 and 6.17. There was a reduction in the elastic tensile stress in the mortar joints for both concrete block and brick wall models. Simbeya (1985) described the changes in the elastic tensile stress in the mortar joint due to a horizontal joint rotation mechanism which is discussed below. In the face-shell bedded specimens the continuity of the cross-webs along the height is broken at the horizontal mortar joint level as mortar is applied to the face-shells only. In Figure 6.18a, the webs of two horizontal unit layers with the intermediate face-shell mortar joint are shown in side elevation. Due to the discontinuity, the webs are subjected to concentrations of vertical compressive stresses at the mortar joint intersections as shown in Figure 6.18b. The deformation of web under face-shell loading of Figure 6.18b is depicted in Figure

FIGURE 6.16 SPLITTING STRESSES

CONCRETE BLOCK WALL (FACE–SHELL BEDDED)

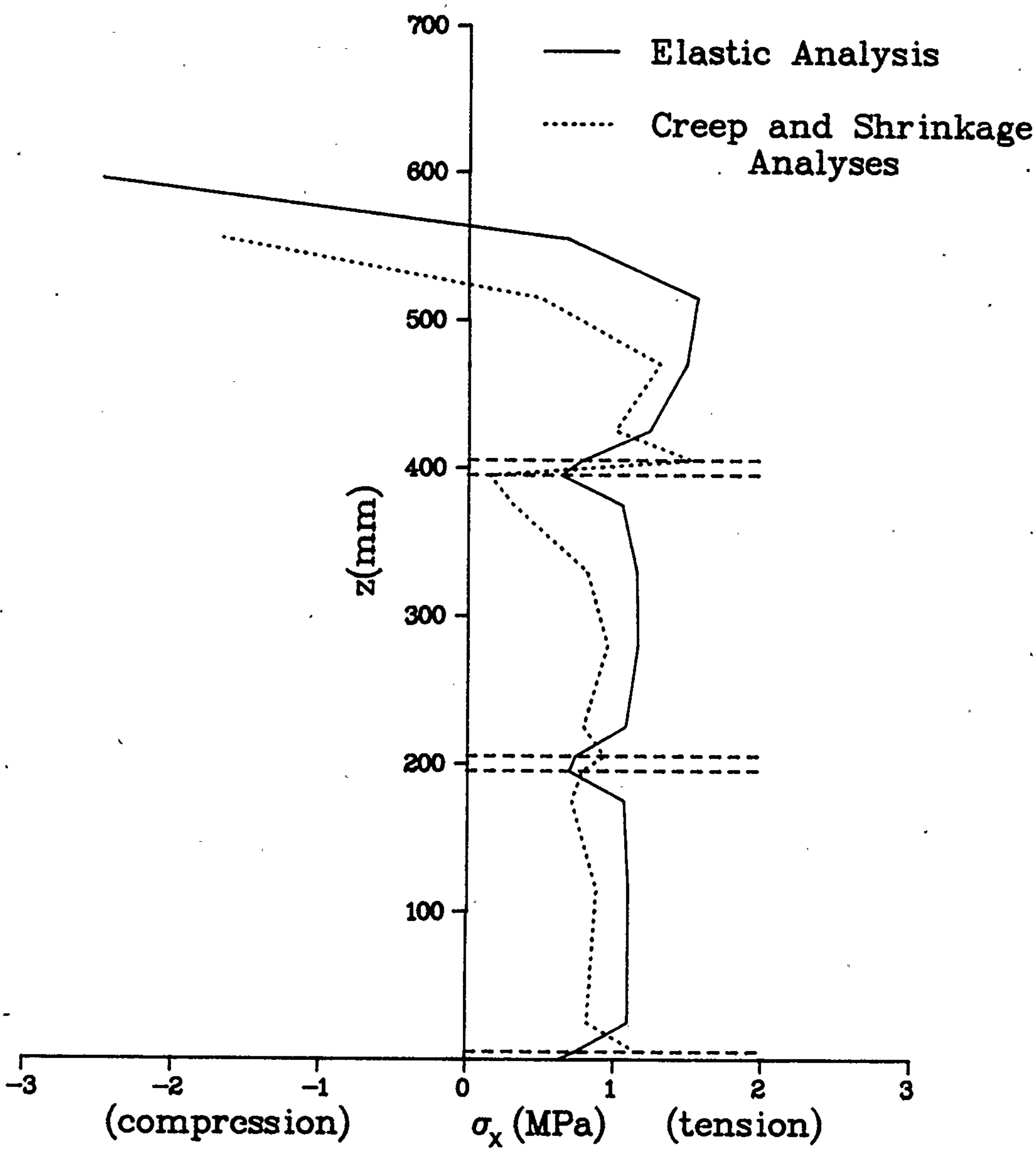

FIGURE 6.17 SPLITTING STRESSES

BRICK WALL (FACE–SHELL BEDDED)

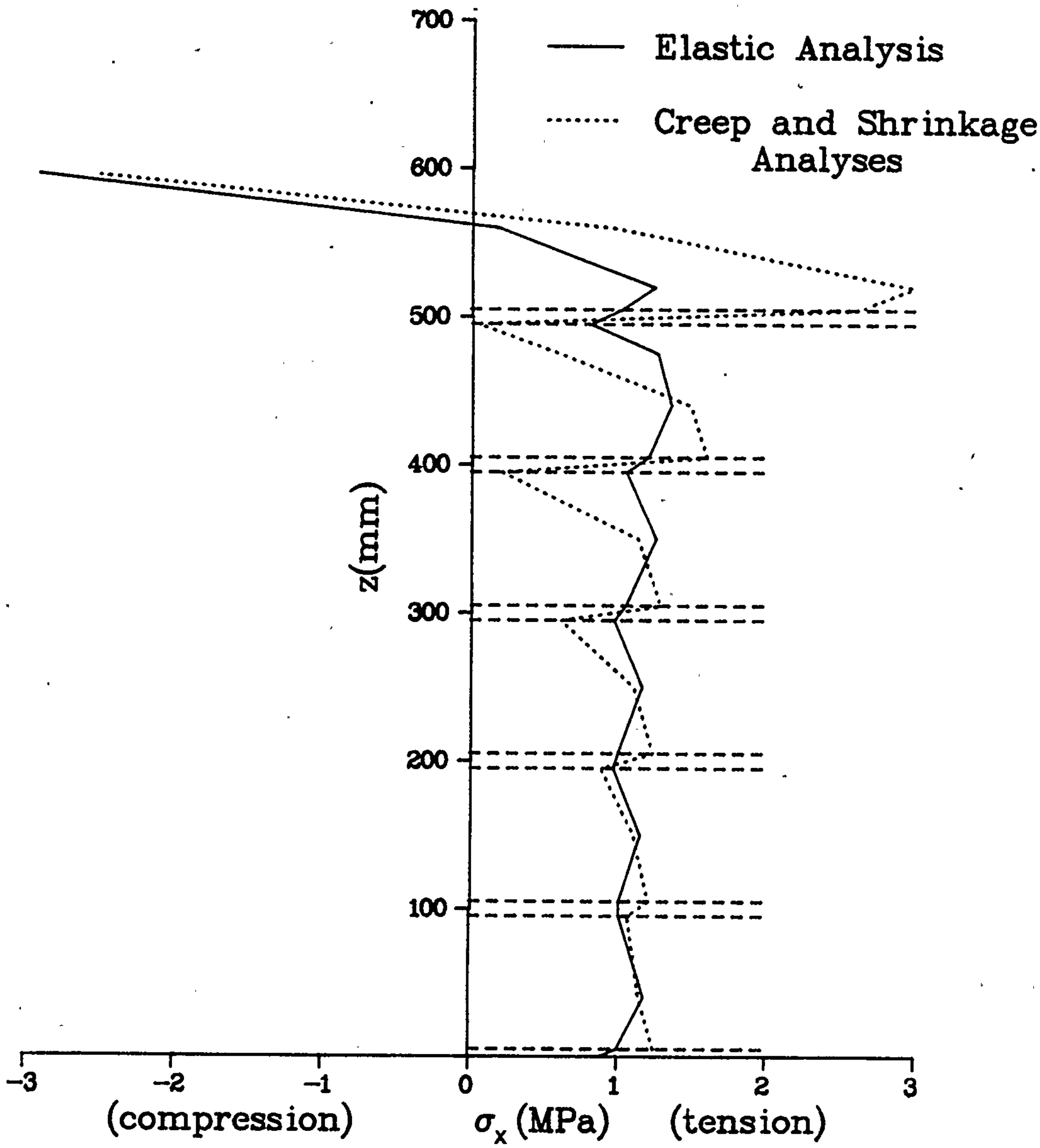

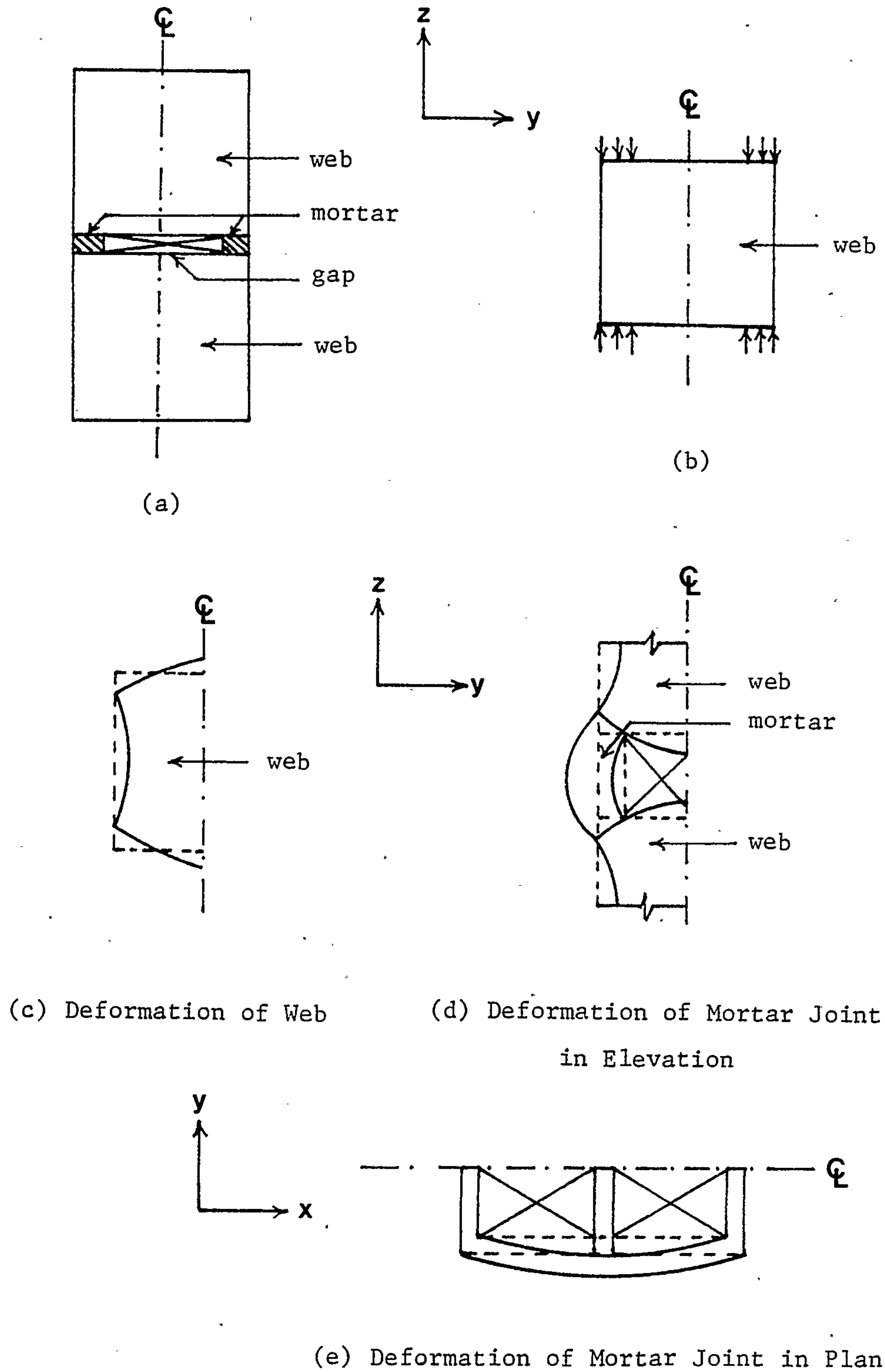

Figure 6.18 Horizontal Joint Rotation Mechanism

6.18c. The face-shell mortar joint is rotated vertically due to the deformations of the webs from above and below the mortar joint as illustrated in Figure 6.18d. The outward vertical rotation of the mortar joint causes a horizontal deformation of the joint as shown in Figure 6.18e. This implies that horizontal flexure stresses are induced in the mortar joint causing tension to the outside face and compression to the inside face. Thus, the flexure compressive stresses are added to the tensile splitting stresses on the inside face resulting in a reduction of the tensile stress at the horizontal mortar joint level.

As shown in Figures 6.16 and 6.17, the redistribution of stresses due to creep and shrinkage causes an increase in the tensile stress in the mortar joint. The effect of the horizontal joint rotation mechanism appears to dominate. Due to creep, the mortar joint tends to increase rotation. The rotation is restrained by the units causing a tensile stress on the inner face of the mortar joint and a compressive stress in the adjoining units. Thus, Figures 6.16 and 6.17 show an increase of the tensile stress in the mortar joint.

Due to creep and shrinkage, full-bedded specimens of the concrete block walls had an overall reduction of the elastic tensile stress whereas in face-shell bedded specimens, the maximum tensile stress obtained from the creep and shrinkage analyses was of the same order as that acquired from the elastic analysis. On the other hand, in the case of brick wall models, creep and shrinkage induced an increase in the maximum elastic tensile stress by 60% in full-bedded specimens and by 125% in face-shell bedded specimens. In both cases, the increase was observed near the top horizontal mortar joint. Since these results are from lower bound solutions, the increase in the lateral tensile stresses will be more in the upper bound solutions.

(c) Web Splitting Stresses

The web splitting stress distributions for the concrete block and the brick wall models are sketched in Figures 6.19 and 6.20 respectively.

For a uniform axially loaded face-shell bedded specimen, the elastic web splitting stress distribution theory was suggested by Shrive (1982). For a concentrated axial load, Shrive's web bending theory was modified by Simbeya (1985). To illustrate the effects of creep and shrinkage on redistribution of web splitting stresses, both theories are summarized here.

A concentrated axial load disperses to the whole cross-section of the wall as the depth increases. Since prestressing is a form of concentrated load, the intensity of web loading decreases towards the bottom in the upper half of the wall model. The equivalent of the web loading of Figure 6.18b is shown in Figure 6.21a, where (P+V) is the total vertical load at the top, V is the load which is distributed to the face-shells inducing shear stresses in the face-shell portion of the webs. The web loading of Figure 6.21a can be divided into two separate cases as shown in Figures 6.21b and 6.21c. The analytical theory for web loading of Figure 6.21b was given by Shrive (1982) and is discussed below. Since the loading is symmetrical in both horizontal and vertical directions, one quarter (ABCD) of the web is analysed. Because of the symmetry, no shear acts on the faces AD and DC. For vertical equilibrium, only normal forces act on face DC and in order to have a continuous deformation, the normal stress on face DC should be distributed as shown in Figure 6.21d. The vertical stress distribution on face DC can be replaced by a single equivalent force 'P', shown in Figure 6.21e,

FIGURE 6.19 WEB SPLITTING STRESSES

CONCRETE BLOCK WALL (FACE–SHELL BEDDED)

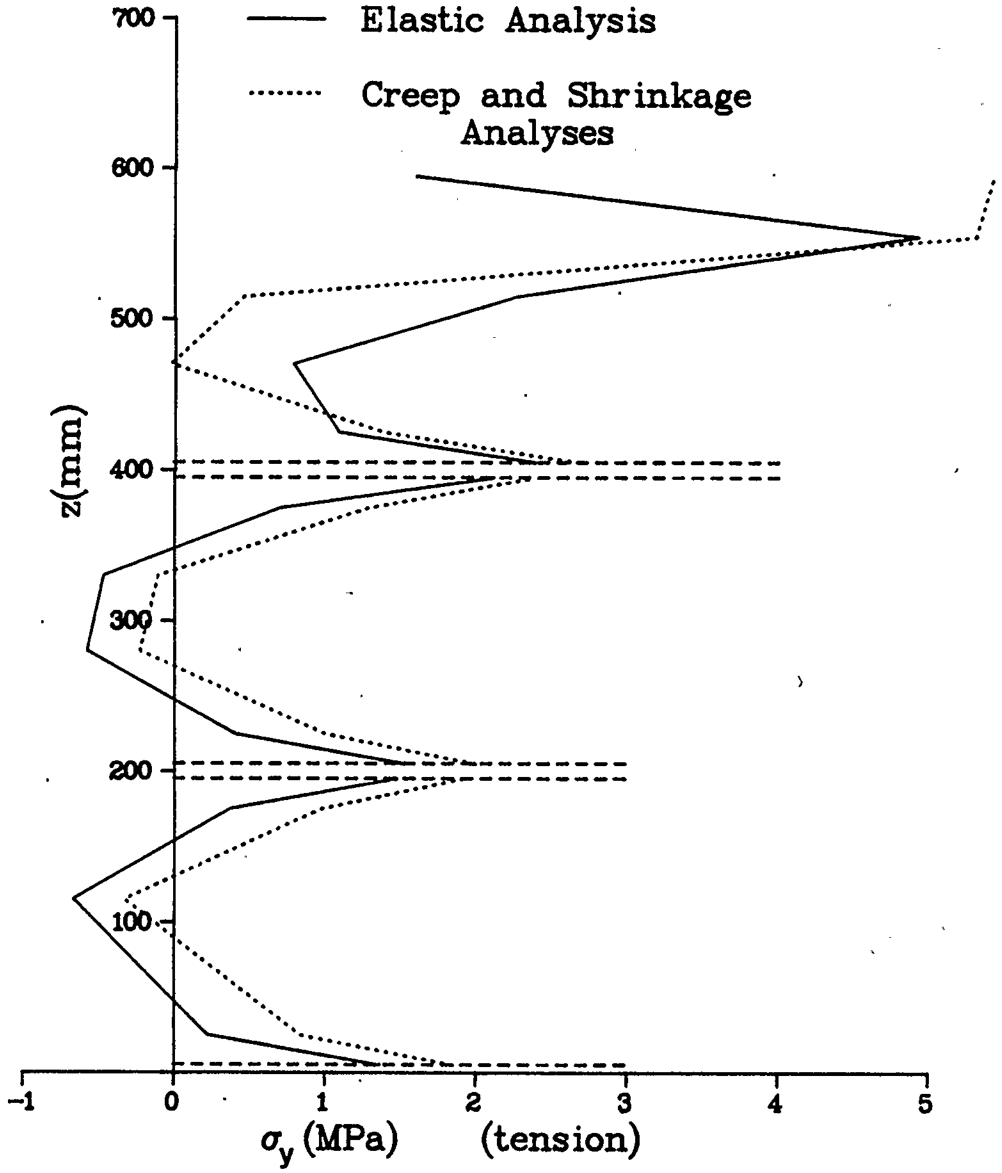

FIGURE 6.20 WEB SPLITTING STRESSES

BRICK WALL (FACE–SHELL BEDDED)

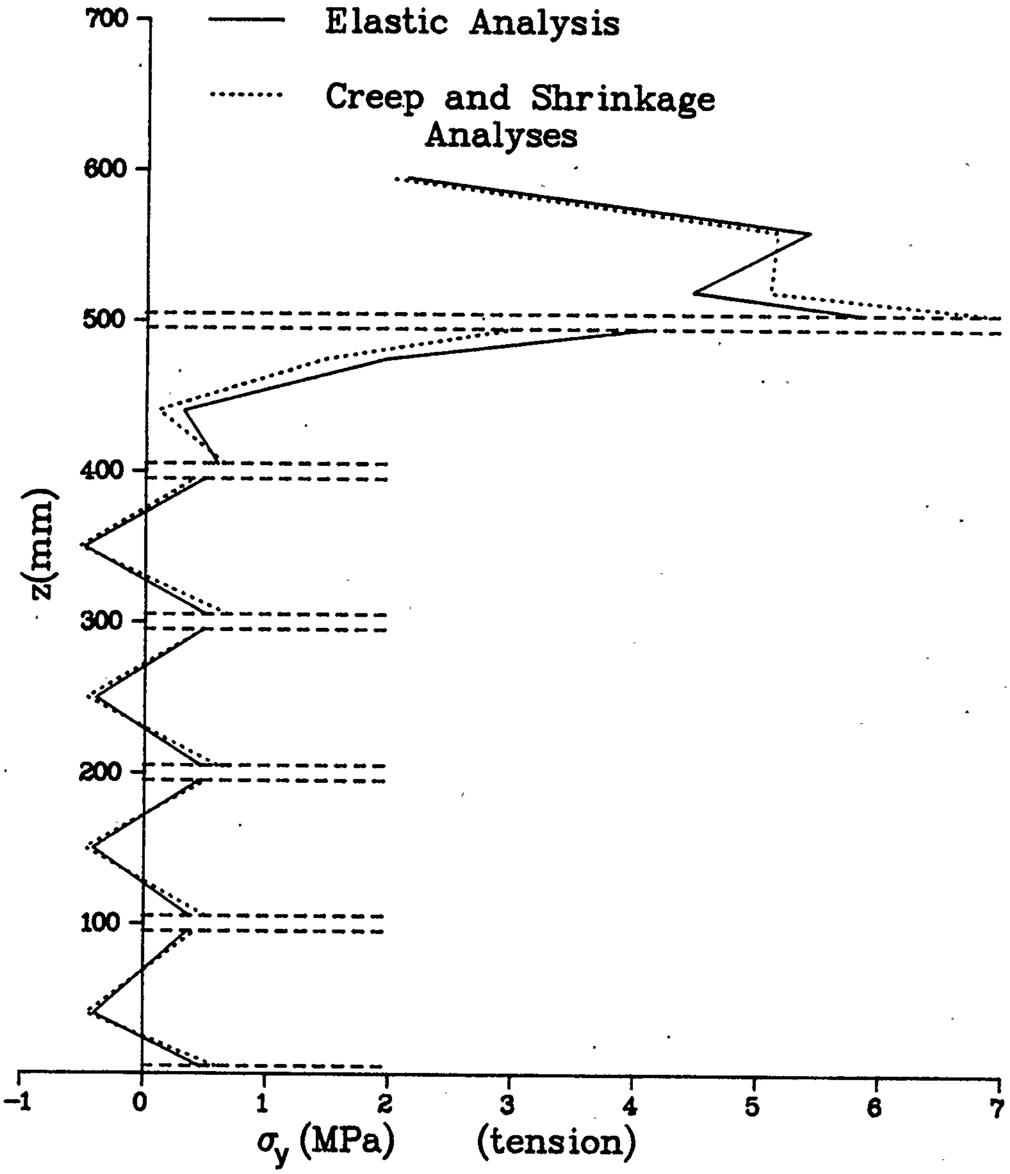

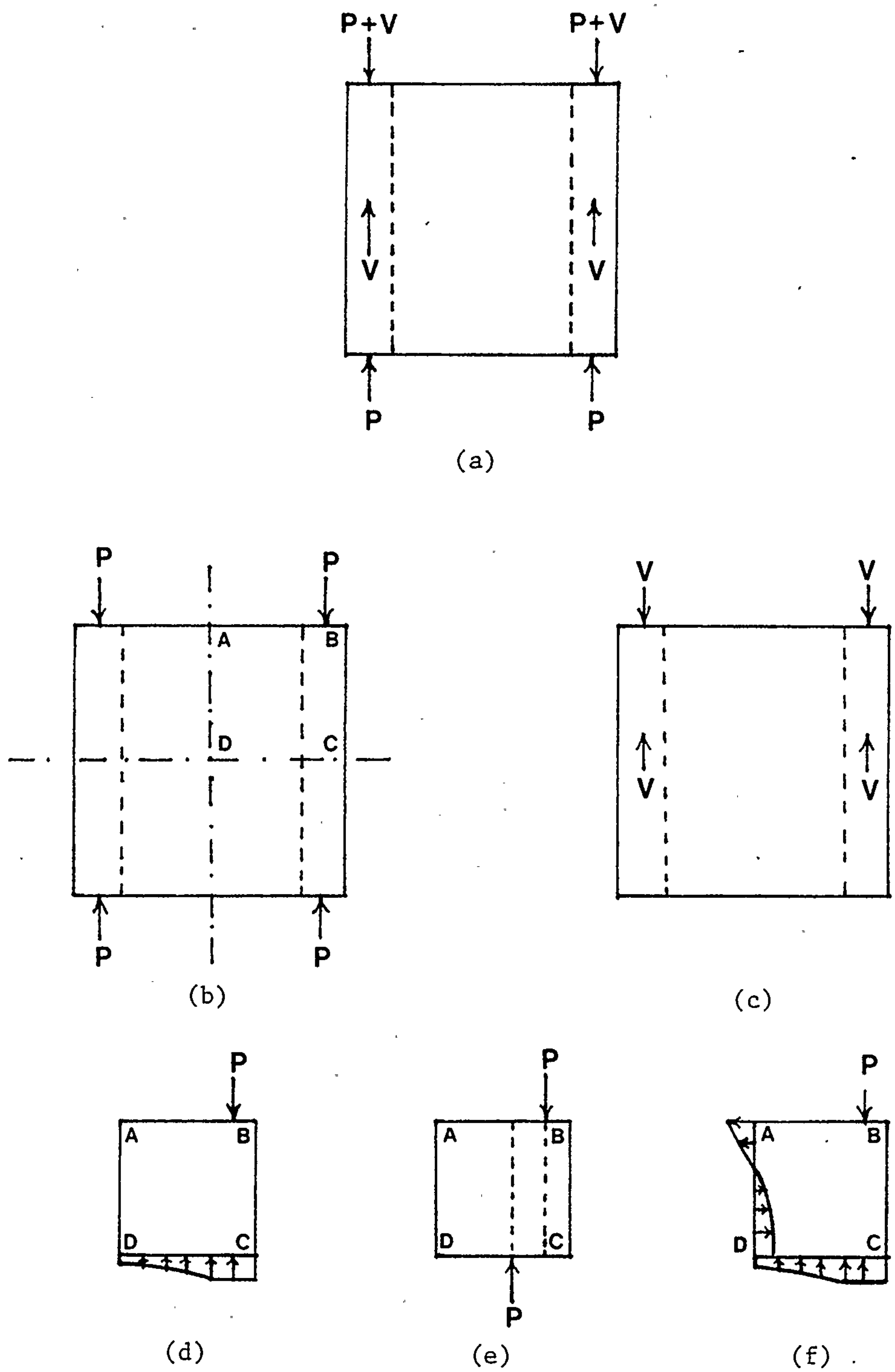

Figure 6.21 Web Bending Theory

resulting in a clockwise moment about D due to external load 'P'. To balance the clockwise moment, an anti-clockwise moment due to internal stresses must be produced. As only normal stresses can occur on face AD and the horizontal stress resultant should be zero there, a tensile stress near A and a compressive stress near D is required on face AD as shown in Figure 6.21f. For web loading of Figure 6.21c, Simbeya (1985) suggested that web bulging mechanism introduces higher tensile stresses at the top of the web and lower tensile stresses at the bottom of the web.

As depicted in Figure 6.19, creep and shrinkage in the concrete block wall model resulted in a shift of the web splitting stresses to the right indicating that the tensile stress was introduced all along the depth of the web. The increase in the maximum tensile stress was in the order of 10%. Due to creep in the concrete block unit, the web under compressive loading bulges more with time, thus inducing higher tensile stresses. The tensile stress on the web faces are balanced by compressive stresses (σ_y) on the middle of the face-shells as shown in Figure 6.22. Thus, creep results in a twisting action on the face-shells of the block unit. The twisting action was confirmed by verifying the variation of σ_y along the length of the wall model, on the face-shells. In the case of upper bound solutions, the increase in the web splitting stresses will be more due to higher creep strains in the concrete block units.

On the other hand in the case of the brick wall model results, the web bulging action of the elastic analysis did not result in any further increase in the tensile stress and can be justified since the brick units did not creep. As shown in Figure 6.20, the web splitting stress-

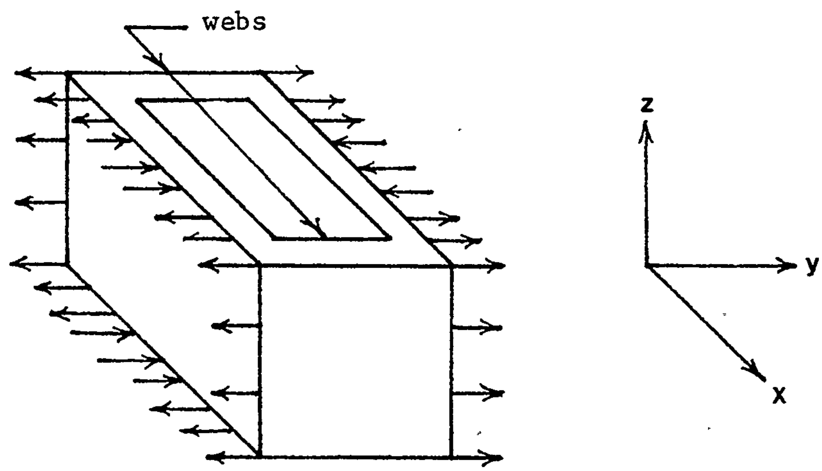

Figure 6.22 Twisting Action due to Creep

es due to creep and shrinkage remained more or less the same as that obtained from the elastic analysis. Even though the compressive load was decreasing with time, the web splitting stress did not decline. Thus, it can be concluded that with redistribution of stresses due to creep and shrinkage, the webs shared more vertical load.

6.2.3.3 Redistribution of Vertical Compressive Stress due to Creep and Shrinkage

It was observed that there was an overall decrease in the vertical compressive stress (σ_z) with time. Due to creep and shrinkage, there was a loss of the prestress which caused a reduction of the vertical compressive force. Since there was an overall reduction of the vertical compressive stress, only the results from full bedded concrete block wall models are illustrated. In Figure 6.23, the stress distribution is plotted along the vertical line passing through point '3' and in Figure 6.24, the vertical stress is plotted along the horizontal line A-A at about mid height (z = 280 mm) of the symmetrical wall model (locations are shown in Figure 6.9). The elastic stresses are compared with the stresses obtained from the long-term lower bound results of the creep and shrinkage analyses. As shown in Figure 6.24, there was a noticeable decrease of the compressive stress in the vertical mortar joints. Due to creep, the mortar joint tends to compress more. The compression is restrained by the adjacent units and a lower compressive stress in the mortar joint results.

Because of symmetry, only one-eighth of the wall models were analysed. Thus, the stress distributions obtained for the symmetrical proportion are applicable for other parts of the wall models as well.

FIGURE 6.23 VERTICAL COMPRESSIVE STRESS CONCRETE BLOCK WALL (IN VERTICAL PLANE)

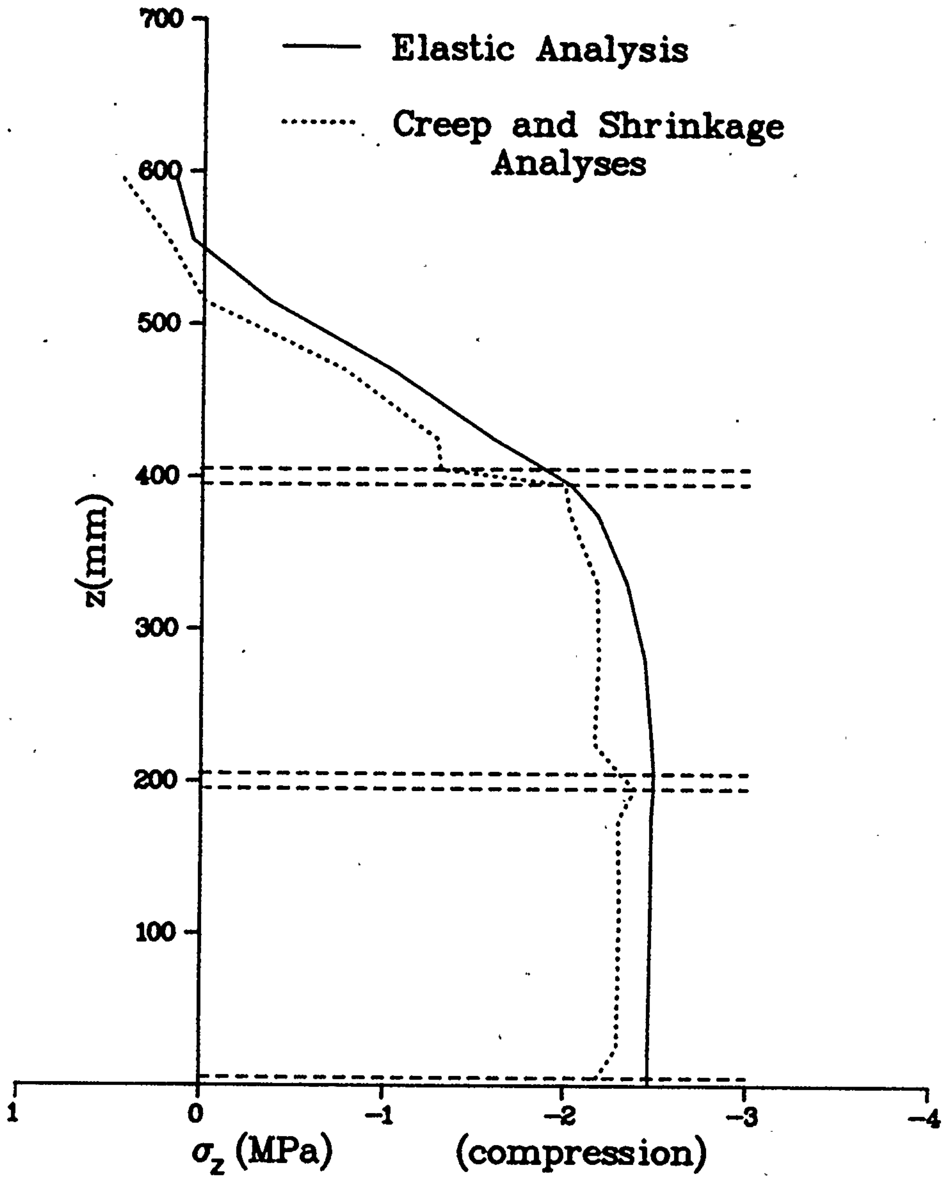

FIGURE 6.24 VERTICAL COMPRESSIVE STRESS

CONCRETE BLOCK WALL (IN HORIZONTAL PLANE)

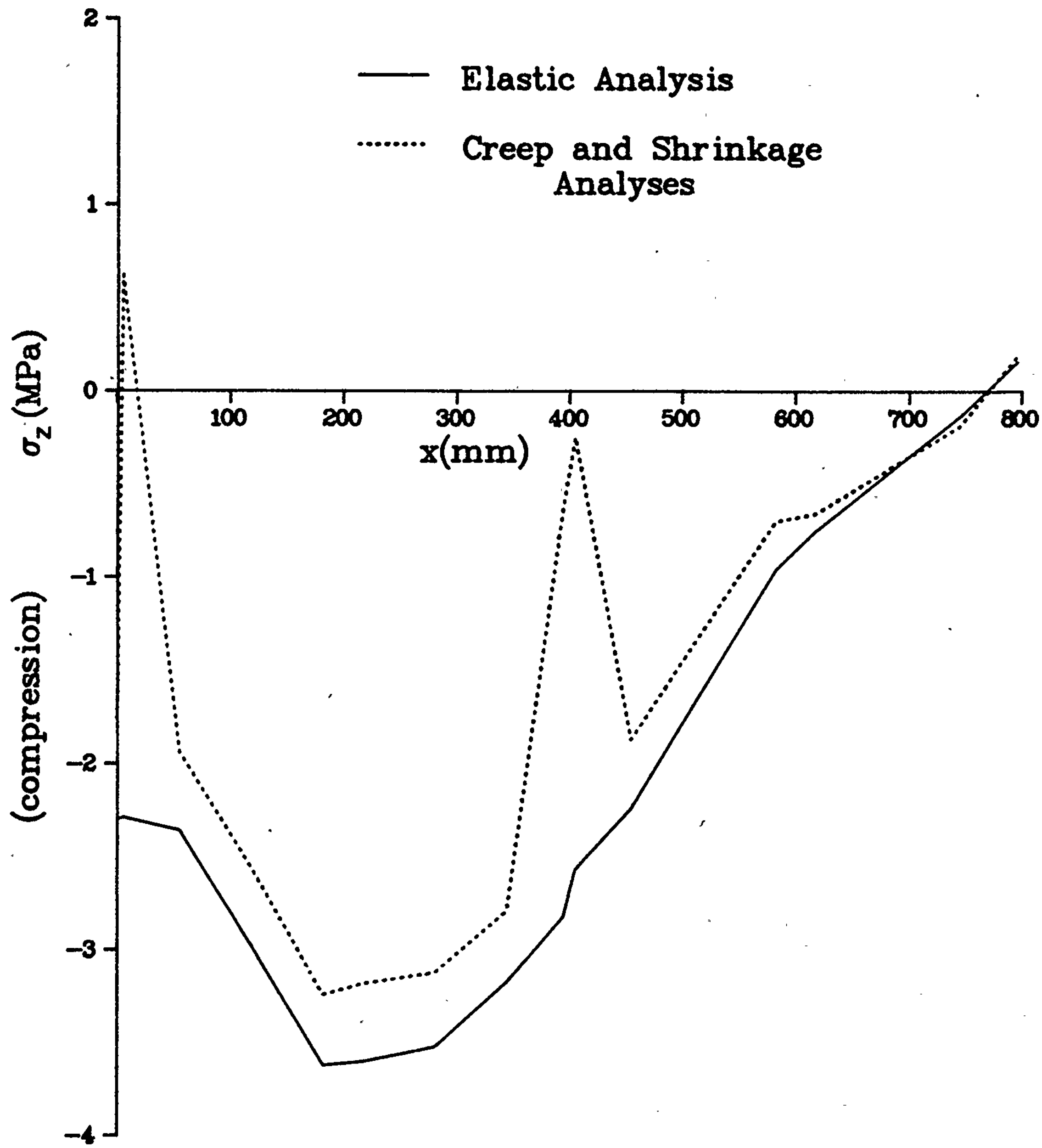

6.2.4 Effects of Material Interaction

The main results were obtained with an elastic modulus of the mortar taken equal to that of the masonry units. In general, the modulus of elasticity of mortar is less than that of masonry units. Lack of quality control or workmanship may reduce the mortar stiffness further. Reduced mortar stiffness induces higher stresses in the units and lower stresses in the mortar joints. In the present analysis, the main aim was to obtain an overall upper and lower bound to loss of prestress. Since the creep and shrinkage strains of mortar are more than those of the units, the reduced stiffness of mortar was expected to result less prestress loss because of the lower lateral stresses in mortar. This was confirmed by analysing two wall models with the stiffness of mortar reduced to half the initial value. The results are compared in Table 6.3, where n is the modular ratio and is equal to (E of unit)/(E of mortar) and E is the modulus of elasticity.

	Concrete Block Wall Models Lower Bound Solution (with M-Mortar)			
	Full Bedded Specimens		Face-Shell Bedded Specimens	
	n = 1	n = 2	n = 1	n = 2
Ultimate Prestress Loss after 12 Years due to Creep and Shrinkage Analyses (%)	14.6	13.6	15.5	14.3

Table 6.3 Comparison of Prestress Losses due to Material Interaction

6.2.5 Summary of Results

A good correlation was found between short-term prestress losses obtained from the present analysis and short-term experimental values reported in the literature. The overall long-term prestress losses due to creep, shrinkage and relaxation effects were in the range of 24-31% for the concrete block and 17-22% for the brick wall models.

The redistribution of lateral tensile stresses due to creep and shrinkage were studies in detail. The tearing stress for both concrete block and brick wall models remained in the same order as that obtained from the elastic analysis. In the case of the brick wall specimens, the face-shell splitting stresses increased quite significantly in the top brick unit layer. On the other hand in concrete block wall specimens, there was an increase in the web splitting stresses which were maximum in the top unit layer. To increase the lateral tensile strength capacity, a horizontal steel tie member spanning both x and y directions may be provided near the end steel plates, in both post-tensioned concrete block and brick wall specimens. The steel tie member is illustrated in Figure 6.25 and may be placed in the top and bottom horizontal mortar joints.

The overall results indicate that post-tensioning is a potential method of increasing long-term flexure capacity in masonry walls.

6.3 Approximate Analytical Solution Method for Simplified Wall Models

To predict elastic, creep and shrinkage behaviour of masonry, approximate and simplified models have been suggested by Shrive and England (1981) and Ameny et al (1984). In this section, the concrete block and brick wall models of Figures 5.6 and 5.7 are replaced by a very simple wall model and the solution to prestress losses is obtained by

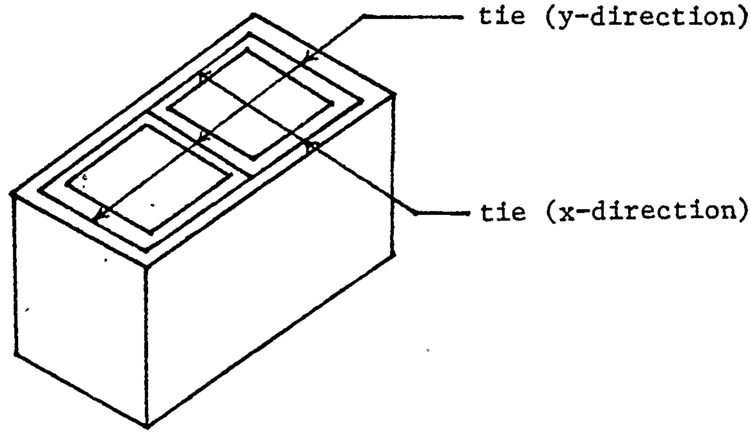

Figure 6.25 Steel Tie Member

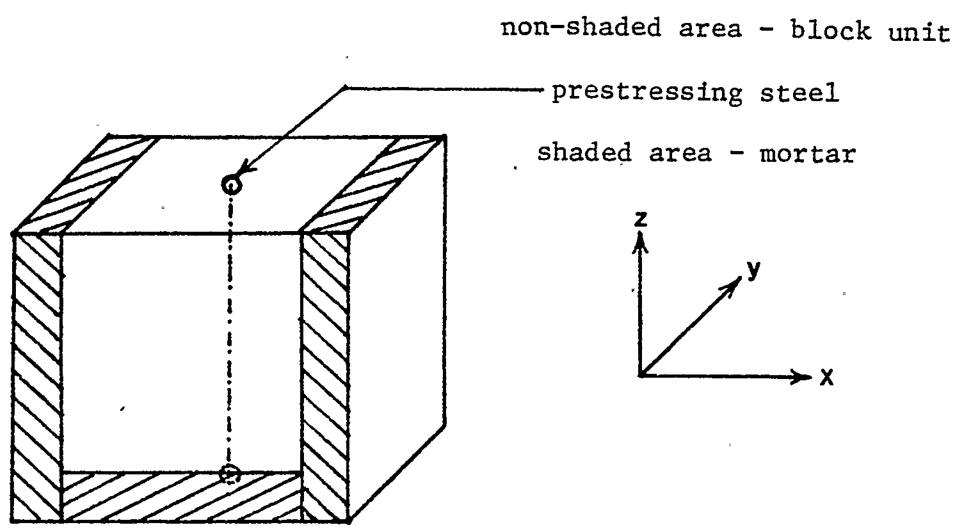

Figure 6.26 Simplified Wall Model

an analytical method. In the present research, the purpose of performing this approximate analysis is to determine whether such analyses may be worth pursuing in the future.

The wall models of Figures 5.6 and 5.7 are approximated by the solid wall model, shown in Figure 6.26. Only full mortar bedded models are analysed. It is assumed that time dependent masonry deformation is related to the relative volumes of block and mortar, and to the specific geometry of the wall model. In Figure 6.26, the block portion is shown by the non-shaded area and the mortar is represented by the shaded one. Since the loading was symmetrical, the prestressing steel is represented by a single bar in the centre of the wall model.

To analyse the composite wall model of Figure 6.26, an analytical solution method, described in a text by Ghali and Favre (1986), has been used. Both upper and lower bounds to prestress losses were obtained and are compared with the results obtained by the step-by-step solution technique (analysed by computer) in Tables 6.4 and 6.5 for concrete block and brick wall models respectively. The detailed derivation to calculate prestress loss analytically is described in the Appendix. As shown in Tables 6.4 and 6.5, the prestress losses obtained by the approximate solution method were less by 4-5% for upper bound results and 1.5-2.5% for lower bound values. In the approximate solution method, values of aging coefficient (χ) and reduced relaxation of prestressed steel (χ_r) were taken from concrete literature (Ghali and Favre; 1986). The difference between the two methods may be because a very simple wall model was adopted for the approximate solution.

Thus, it is recommended that improved wall models, like those suggested by Shrive and England (1981) or Ameny et al (1984), should be reconsidered. Improved values of the aging coefficient and the reduced relaxation coefficient, to be used for masonry structures, should also be examined.

		Upper Bound Solutions (with N-Mortar)		Lower Bound Solutions (with M-Mortar)	
		Approximate Analytical Solution Method	Step-by-Step Solution Method	Approximate Analytical Solution Method	Step-by-Step Solution Method
Prestress Loss due to Creep, Shrinkage and Relaxation Analyses (%)	After 200 Days	21.3	25.6	18.5	20.4
	After 12 Years	25.7	30.0	22.4	23.8

Table 6.4 Comparison of Prestress Losses for Concrete Block Wall Model (Full Bedded)

		Upper Bound Solutions (with N-Mortar)		Lower Bound Solutions (with M-Mortar)	
		Approximate Analytical Solution Method	Step-by-Step Solution Method	Approximate Analytical Solution Method	Step-by-Step Solution Method
Prestress Loss due to Creep, Shrinkage and Relaxation Analyses (%)	After 200 Days	12.1	17.2	10.8	13.1
	After 12 Years	16.2	21.3	14.3	16.8

Table 6.5 Comparison of Prestress Losses for Brick Wall Model (Full Bedded)

CHAPTER 7

CONCLUSIONS AND RECOMMENDATIONS

7.1 Conclusions

7.1.1 Creep and Shrinkage Properties

In Chapter 4, mathematical expressions were fitted to short-term experimental data for creep and shrinkage properties of masonry components. The following conclusions may be drawn.

(1) Most of the specific creep strain data available in the literature can be fitted quite well by one or two straight lines using a log (time) scale. The linear relationship between the specific creep strains and the logarithm of the time under load could easily be extrapolated to the requisite long-term times.

(2) A linear logarithmic relationship, similar to the one for the creep data, was obtained for short-term shrinkage strain values and extrapolated for long-term behaviour. The logarithmic expressions developed could easily be incorporated in the computer program used with no additional storage requirements.

(3) In the creep analysis procedure using a step-by-step time incremental solution technique, storage of stress values at all the time steps becomes a major limitation in terms of computer time and storage space. To avoid stress history storage while simultaneously representing the time incremental solution technique accurately, certain creep functions were developed in the field of concrete structures. For masonry components also, all developed logarithmic expressions for the creep data could be transformed very efficiently to such a creep function, represented by a series of real exponentials.

7.1.2 Loss of Prestress

Based on the results discussed in Chapter 6, certain conclusions were reached and are as follows.

(1) A good correlation was observed between short-term prestress losses computed from the present analysis and short-term experimental values reported in the literature. Thus, creep and shrinkage properties used for the present analysis could be adopted satisfactorily.

(2) The prestress losses in face-shell bedded and full-bedded specimens are of the same order.

(3) Fifty percent of the ultimate prestress loss may occur during the first fifty days.

(4) In the case of concrete hollow block wall specimens, ultimate post-tension losses can be expected to be 15-24% due to creep and shrinkage effects and 24-31% when the stress relaxation effect is included. Upper bound of prestress loss reflects the worst case of creep and shrinkage in concrete block units and in mortar whereas lower bound represents the best case of creep and shrinkage strains.

(5) In hollow brick wall specimens, ultimate prestress losses may be in the range of 5-10% due to creep and shrinkage properties and 17-22% when the stress relaxation property of post-tensioned steel is included. The two limits correspond to the upper and lower bounds of the creep and shrinkage properties of the mortar.

In the present study, the average compressive stress in wall models was 0.25 of the ultimate strength of masonry. The post-tensioned steel bars were of high strength and were stressed to 70% of the ultimate strength. During the course of experimental measurements for creep and shrinkage properties of masonry components, the observed temperature was in the range of 17-22°C and the relative humidity varied from 20-50%.

7.1.3 Redistribution of Stresses

Under a compressive axial load, the following are the main conclusions regarding redistribution of lateral tensile stresses due to creep and shrinkage phenomena.

(1) The lateral expansion of the mortar joint is restrained by the adjoining units resulting in a reduction of tensile tearing stress in the mortar joints and an increase in the adjacent units.

(2) For both concrete block and brick wall specimens, the maximum tearing stress remains in the same order as that obtained from the elastic analysis.

(3) In the case of concrete block wall models, full-bedded specimens experience an overall reduction of lateral tensile splitting stress along the depth, whereas in face-shell bedded specimens the splitting stress increases in the horizontal mortar joints. The order of maximum tensile splitting stress remains the same as that acquired from the elastic analysis.

(4) In the case of full-bedded brick wall specimens, the splitting stress decreases along the depth of the model except in the top and bottom brick unit layers (near the horizontal mortar joints). In face-shell bedded brick wall specimens, the splitting stress increases in the horizontal mortar joints. This increase is quite significant in the top and bottom mortar joints.

(5) Creep and shrinkage cause an increase of the tensile web splitting stresses in concrete block wall specimens (web bulging action due to

creep in block units) whereas in brick wall specimens, the web splitting stresses remain more or less the same.

(6) With redistribution of stresses, the webs share more vertical load with time.

(7) To increase the lateral tensile strength of post-tensioned concrete block and brick wall specimens, a horizontal steel tie member spanning both the x and y directions may be provided near the end steel plates.

As a general conclusion, the overall results indicate that post-tensioning is a viable method of increasing long-term flexural capacity of masonry walls.

7.2 Recommendations

In the present research, prestressing was the only load which was considered in the analysis. Only vertical post-tensioned hollow masonry walls were modelled. Further, only one size of the model was selected. More general results could be obtained using the present model by analysing the following cases:

(1) Gravity loads,

(2) Lateral loads, i.e. Wind loads or Earthquake loads,

(3) Different sizes of models,

(4) Grouted masonry walls,

(5) Biaxially post-tensioned walls, i.e. walls post-tensioned in the horizontal direction as well,

(6) Different type of structures, e.g. a masonry column or a masonry beam.

Since it was concluded that post-tensioning is a viable way of increasing the flexural capacity of masonry walls, it would be desirable to study existing deteriorating masonry structures. It may be practical to prestress existing cracked masonry structures. If so, it may be more economical to use prestressing compared to the cost of replacing structures with new ones, in terms of long-term life.

In the present study, the age at loading reduction factor for creep strains was taken from the CEB-FIP (1970) model. To be more precise, a detailed experimental program studying the effects of age at loading on creep strains, should be undertaken. An attempt should be made to divide the creep of masonry into two parts, (1) irreversible creep (plastic flow) and (2) reversible creep (delayed elastic strain), similar to the CEB-FIP (1978) model's expression for creep in concrete.

In the upper bound solutions, the problem of numerical instability was encountered. As discussed in Chapter 3, this problem can be avoided by implementing an implicit scheme which requires the knowledge of creep flow rate criteria. To improve the present creep model, a theoretical investigation should be made to establish general creep-time flow equations for masonry structures.

Finally, it is recommended that approximate analytical solutions to masonry models should be tried. Improved masonry models should be analysed to verify or to improve the values of aging coefficient, to be used for masonry structures.

REFERENCES

Ameny, P., (1979), "Elastic and Creep Properties of Lightweight Concrete Masonry", M.Sc. Thesis, The University of Calgary, 1979.

Ameny, P., (1982), "Modelling the Deformation of Masonry", Ph.D. Thesis, The University of Calgary, 1982.

Ameny, P., Loov, R.E. and Jessop, E.L., (1980), "Strength, Elastic and Creep Properties of Concrete Masonry", The International Journal of Masonry Construction, Vol. 1, No. 1, 1980, pp. 33-39.

Ameny, P., Loov, R.E. and Shrive, N.G., (1984), "Models for Long-Term Deformation of Brickwork", Masonry International, No. 1, April 1984, pp. 27-36.

Anand, S.C., Dandawate, B. and Brown, R.H., (1984), "A Finite Element Model for creep in Composite Masonry", Dept. of Civil Engg., Clemson University, Clemson, S.C., Report No. 20S-84, 1984.

Anand, S.C., Ghandhi, A. and Brown, R.H., (1983), "A Finite Element Model to Compute Stresses in Composite Masonry due to Creep, Shrinkage and Temperature", Dept. of Civil Engg., Clemson University, Clemson, S.C., Report No 5S-83, 1983.

Bazant, Z.P., (1975), "Theory of Creep and Shrinkage in Concrete Structures: A Precis of Recent Developments", Mechanics Today, Vol. 2, Pergamon Press, 1975, pp. 1-93.

Bazant, Z.P., (1982), "Mathematical Models for Creep and Shrinkage of Concrete", Creep and Shrinkage in Concrete Structures, Edited by Bazant, Z.P. and Wittmann, F.H., John Wiley & Sons, 1982.

Bazant, Z.P. and Wu, S.T., (1973), "Dirichlet Series Creep Function for Aging Concrete", Journal of the Engineering Mechanics Division, Proceedings, ASCE, 99, 1973, pp. 367-387.

CEB-FIP (1970), "International Recommendations for the Design and Construction of Concrete Structures - Principles and Recommendations", Comite European du Beton-Federation Internationale de la Precontrainte, FIP Sixth Congress, Prague, June 1970.

CEB-FIP (1978), "Model Code for Concrete Structures", Comite Euro-International du Beton-Federation Internationale de la Precontrainte, Paris, 1978, 348 pp.

CMHC (1981), "Exterior Wall Construction in High-Rise Buildings", Advisory Document, Canada Mortgage and Housing Corporation, Canada, 1981.

Canadian Standards Association (1984), "CAN3-A371-M84, Masonry Construction for Buildings", Canada, 1984.

Canadian Standards Association (1984), "CAN3-S304-M84, Masonry Design For Buildings", Canada, 1984.

Chieslar, J.D., (1985a), "SMAC-A Finite Element Program for the Systematic Matrix Analysis of Continua", Research Report No. CE85-5, Dept. of Civil Engg., The University of Calgary, 1985.

Chieslar, J.D., (1985b), "Hybrid Finite Elements for Solids and Shells", Ph.D. Thesis, The University of Calgary, 1985.

Cook, R.D., (1981), "Concepts and Applications of Finite Element Analysis", John Wiley & Sons, 1981.

Crandall, S.H., Dahl, N.C. and Lardner, T.J., (1972), "An Introduction to the Mechanics of Solids", McGraw-Hill Book Company, 1972.

Curtin, W.G., Shaw, G., Beck, J.K. and Bray, W.A., (1982), "Structural Masonry Designer's Manual", Granada, 1982.

Dilger, W.H., (1982), "Methods of Structural Creep Analysis", Creep and Shrinkage in Concrete Structures, Edited by Bazant, Z.P. and

Wittmann, F.H., John Wiley & Sons, 1982.

Ghali, A. and Favre, R., (1986), "Concrete Structures: Stresses and Deformations", Chapman and Hall Ltd., London and New York, 1986.

Haque, M.N., Valliapan, S. and Cook, D.J., (1974), "Tensile Creep Analysis of Concrete Structures", Proceedings, International Conference on Finite Element Methods in Engineering, University of New South Wales, Australia, August 1974, pp. 349-364.

Huizer, A. and Shrive, N.G., (1984), "Loss of Prestress in Post-Tensioned Masonry Walls", International Symposium on Reinforced and Prestressed Masonry, Edinburgh, 1984, pp. 381-391.

Jessop, E.L., Baker, L.R., Ameny, P. and Khalil, K.R., (1978a), "Moisture, Thermal, Elastic and Creep Properties of Masonry", Dept. of Civil Engg., Research Report No. CE78-16, The University of Calgary, 1978.

Jessop, E.L., Shrive, N.G. and England, G.L., (1978b), "Elastic and Creep Properties of Masonry", Proceedings, The North American Masonry Conference, Boulder, Colorado, 1978, pp. 12.1-12.17.

Kabir, A.F., (1976), "Non-Linear Analysis of Reinforced Concrete Panels, Slabs and Shells for Time-Dependent Effects", Ph.D. Thesis, The University of California, Berkeley, 1976.

Khalil, M.R.A., (1983), "Three-Dimensional Stress Analysis of Hollow Masonry", Ph.D. Thesis, University of Calgary, 1983.

Lenczner, D., (1969), "Creep in Model Brickwork", Designing, Engineering and Constructing with Masonry Products, Johnson, F.B. (ed.), Gulf Publishing Company, 1969, pp. 58-67.

Lenczner, D., (1971), "Creep in Brickwork", Proceedings, Second International Brick Masonry Conference, The British Ceramic Research Association, 1971, pp. 44-49.

Lenczner, D., (1974), "Creep in Concrete Blockwork Piers", The Structural Engineer, Vol. 52, No. 3, March 1974, pp. 97-101.

Lenczner, D., (1981), "Brickwork: A Guide to Creep", The Journal of Masonry Construction, Vol. 1, No. 4, 1981, pp. 127-133.

Lenczner, D., (1983), "Loss of Prestress in Post-Tensioned Brickwork Walls and Columns", Proceedings, The British Ceramic Society, International Symposium on Load Bearing Brickwork, November 1983.

Lenczner, D. and Davis, P., (1984), "Loss of Prestress in Post-Tensioned Brickwork Walls and Columns", International Symposium on Reinforced and Prestressed Masonry, Edinburgh, 1984, pp. 76-89.

Lenczner, D. and Salahuddin, J., (1976), "Creep and Moisture Movements in Brickwork and Blockwork", Proceedings, Conference on Performance of Building Structures, Glasgow, 1976, pp. 369-383.

Lenczner, D., Salahuddin, J. and Wyatt, K., (1975), "Effect of Stress on Creep in Brickwork Piers", Proceedings, The British Ceramic Society, No. 24, September 1975, pp. 1-9.

Loov, R.E., (1984), Personal Communications.

Magura, D.D., Sozen, M.A. and Siess, C.P., (1964), "A Study of Stress Relaxation in Prestressing Reinforcement", Prestressed Concrete Institute Journal, 9, No. 2, 1964, pp. 13-57.

Neville, A.M., Dilger, W.H. and Brooks, J.J., (1983), "Creep of Plain and Structural Concrete", Construction Press, London and New York, 1983.

Owen, D.R.J. and Hinton, E., (1980), "Finite Elements in Plasticity", Pineridge Press Limited, Swansea, U.K., 1980.

PCI Committee on Prestress Losses, (1975), "Recommendations for

Estimating Prestress Losses", Prestressed Concrete Institute Journal, 20, No. 4, 1975, pp. 43-75.

Pian, T.H.H., (1964), "Derivation of Element Stiffness Matrices by Assumed Stress Distributions", AIAA Journal, Vol. 2, No. 7, 1964, pp. 1333-1336.

Poljakov, S.V., (1962), "Some Problems on Creep in Ordinary and Reinforced Masonry Members", International Council for Building Research, Studies and Documentation, Paris, 1962.

Shrive, N.G., (1982), "The Failure Mechanism of Face-Shell Bedded (Ungrouted and Unreinforced) Masonry", International Journal of Masonry Construction, Vol. 2, No, 3, 1982.

Shrive, N.G. and England, G.L., (1981), "Elastic, Creep and Shrinkage Behaviour of Masonry", The International Journal of Masonry Construction, Vol. 1, No. 3, 1981, pp. 103-109.

Simbeya, K.W., (1985), "Stresses in Masonry due to a Concentrated Load", M.Sc. Thesis, The University of Calgary, 1985.

Suter, G.T., Naguib, E.M.F. and Bowes, W.H., (1983), "Stress Analysis of Masonry Walls Subjected to a Concentrated Amount of Prestressing", Proceedings, Third Canadian Masonry Symposium, Edmonton, June 1983.

Sutherland, W.H., (1970), "AXICRP-Finite Element Computer Code for Creep Analysis of Plain Stress, Plain Strain and Axisymmetric Bodies", Nuclear Engineering and Design, Vol. 11, 1970, pp. 169-285.

Tatsa, E., Yishai, O. and Levy, M., (1973), "Loss of Steel Stresses in Prestressed Concrete Blockwork Walls, "The Structural Engineer, Vol. 51, No. 5, May 1973, pp. 170-180.

US Bureau of Reclamation, (1956), "Creep of Concrete Under High Intensity Loading", Concrete Laboratory Report No. C-820, Denver, Colorado, April 1956, 6 pp.

Wyatt, K., Lenczner, D. and Salahuddin, J., (1975), "The Analysis of Creep Data for Brickwork", Proceedings, The British Ceramic Society, No. 24, September 1975, pp. 11-19.

Zienkiewicz, O.C., (1977), "The Finite Element Method in Engineering Science", McGraw-Hill Book Company, 1977.

APPENDIX

APPROXIMATE ANALYTICAL SOLUTION METHOD

In the present analysis,

$E(t) = E(t_o) = E$

where E is the modulus of elasticity, t_o is the age at initial loading and t is any time or age.

Further, $E_u = E_m$

where E_m is the modulus of elasticity of mortar and E_u is the modulus of elasticity of block unit.

Let $E_u = E_m = E_o$ . .

For the wall model of Figure 6.26, one basic assumption is made that plane section remains plane at all times.

In the Vertical Plane (x-z plane):

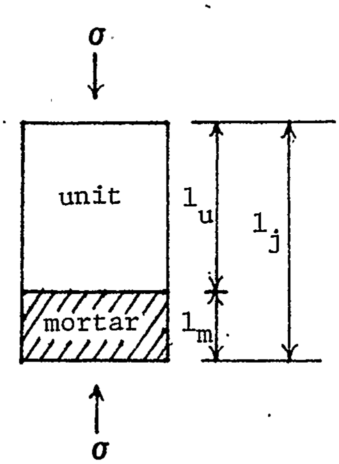

In 'z' direction, ℓ_u is the block unit portion length, ℓ_m is the mortar portion length and ℓ_j is the combined length. Subscript 'm' represents mortar, 'u' indicates block unit and the combined effect is represented by 'j'.

(A) Instant Change in Length (Elastic Analysis):

i.e. at time $t = t_o$,

$$\Delta\ell_j^e(t_o) = \Delta\ell_u^e(t_o) + \Delta\ell_m^e(t_o)$$

where $\Delta\ell^e$ is the change in length due to elastic analysis.

$$\frac{\Delta \ell_j^e(t_o)}{\sigma} = \frac{\ell_u}{E_o} + \frac{\ell_m}{E_o} = \frac{\ell_j}{E_o} \tag{A.1}$$

(B) Time Dependent Change in Length:

i.e. at time $t > t_o$,

(a) Creep Analysis:

$$\Delta \ell_j^c(t) = \Delta \ell_u^c(t) + \Delta \ell_m^c(t) \tag{A.2}$$

where $\Delta \ell^c$ is the change in length due to creep analysis.

$$\Delta \ell_j^c(t) = E_o \; \Delta \ell_j(t_o) \; C_j(t,t_o) \tag{A.3a}$$

$$\Delta \ell_u^c(t) = \sigma \ell_u \; C_u(t,t_o) \tag{A.3b}$$

$$\Delta \ell_m^c(t) = \sigma \ell_m \; C_m(t,t_o) \tag{A.3c}$$

where C_j is the specific creep of the combined action of unit and mortar.

From Equations (A.2) and (A.3),

$$C_j(t,t_o) = \frac{\sigma}{E_o \Delta \ell_j^e(t_o)} \left[\ell_u \; C_u(t,t_o) + \ell_m C_m(t,t_o)\right] \tag{A.4}$$

From Equations (A.1) and (A.4),

$$C_j(t,t_o) = \frac{1}{\ell_j} \left[\ell_u \; C_u(t,t_o) + \ell_m \; C_m(t,t_o)\right] \tag{A.5}$$

(b) Shrinkage Analysis:

$$\Delta \ell_j^s(t) = \Delta \ell_u^s(t) + \Delta \ell_m^s(t)$$

where $\Delta \ell^s$ is the change in length due to shrinkage.

$$\ell_j \; \varepsilon_j^s(t,t_s) = \ell_u \; \varepsilon_u^s(t,t_s) + \ell_m \; \varepsilon_m^s(t,t_s)$$

$$\varepsilon_j^s(t,t_s) = \frac{1}{\ell_j} \, [\ell_u \; \varepsilon_u^s(t,t_s) + \ell_m \; \varepsilon_m^s(t,t_s)] \qquad (A.6)$$

<u>In the Horizontal Plane</u> (x-y plane)

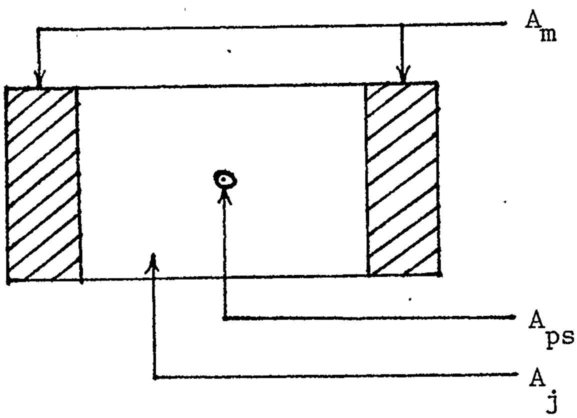

In x-y plane, A_j is the area of combined portion of unit and mortar (combined action is because of x-z plane), A_m is area of mortar only and A_{ps} is the area of prestressing steel.

(A) Instant Time Analysis :

i.e. at time $t = t_o$,

for only prestressing load,

$P_{ps} = -(P_j + P_m)$

where P_{ps} is the prestressing force, P_j is the vertical load shared by combined portion (non-shaded area) and P_m is the vertical load shared by mortar portion (shaded area). Subscript 'ps' represents prestressing steel.

Since $E_m = E_j = E_o$,

$$\sigma_j(t_o) = \sigma_m(t_o) = \frac{-P_{ps}}{A} \qquad (A.7)$$

where $A = A_j + A_m$ and σ is the stress.

(B) Time Dependent Changes:

i.e. at time $t > t_o$,

$\Delta P_j + \Delta P_m + \Delta P_{ps} = 0$

Thus,

$$\Delta\sigma_{ps} = -\frac{1}{A_{ps}} (A_j\ \Delta\sigma_j + A_m\ \Delta\sigma_m) \tag{A.8}$$

where ΔP is the change in force and $\Delta\sigma$ is the change in stress.

$$\Delta\varepsilon_{ps}(t) = \frac{\Delta\sigma_{ps} - \Delta\bar{\sigma}_{pr}}{E_{ps}} \tag{A.9a}$$

$$\Delta\varepsilon_j(t) = \sigma_j(t_o)\ C_j(t,t_o) + \varepsilon_j^s(t,t_o) + \frac{\Delta\sigma_j}{E_o} + \Delta\sigma_j\chi\ C_j(t,t_o) \tag{A.9b}$$

$$\Delta\varepsilon_m(t) = \sigma_m(t_o)\ C_m(t,t_o) + \varepsilon_m^s(t,t_o) + \frac{\Delta\sigma_m}{E_o} + \Delta\sigma_m\chi\ C_m(t,t_o) \tag{A.9c}$$

where $\Delta\varepsilon(t)$ is the total time dependent change in strain at time t, $\Delta\sigma$ is the change in stress, $\Delta\sigma_{ps}$ is the change in stress in the prestressed steel due to combined effects of creep, shrinkage and relaxation, $\Delta\bar{\sigma}_{pr}$ is the reduced relaxation and χ is the aging coefficient.

For definitions and understanding of the different terms, the text by Ghali and Favre (1986) can be referenced.

Since plane section remains plane,

$$\Delta\varepsilon_{ps}(t) = \Delta\varepsilon_j(t) = \Delta\varepsilon_m(t) \tag{A.10}$$

From Equations (A.8), (A.9) and (A.10),

$$\Delta\sigma_{ps} = \frac{1}{\beta}[\alpha_j + \alpha_m)\Delta\bar{\sigma}_{pr} + \alpha_j\ E_{ps}\ \sigma_j(t_o)C_j(t,t_o)$$

$$+ \alpha_j\ E_{ps}\ \varepsilon_j^s(t,t_o) + \alpha_m\ E_{ps}\ \sigma_m(t_o)C_m(t,t_o)$$

$$+ \alpha_m\ E_{ps}\ \varepsilon_m^s(t,t_o)] \tag{A.11}$$

where

$$\beta = (1 + \alpha_j + \alpha_m)$$

$$\alpha_j = \frac{A_j\ \bar{E}_j}{A_{ps}\ E_{ps}} \quad \text{and} \quad \alpha_m = \frac{A_m\ \bar{E}_m}{A_{ps}\ E_{ps}}$$

$$\bar{E}_j = \frac{E_o}{1 + \chi\ E_o\ C_j(t,t_o)}$$

$$\bar{E}_m = \frac{E_o}{1 + \chi\ E_o\ C_m(t,t_o)}$$

For the present analysis, χ has been taken equal to 0.8 and

$$\Delta\bar{\sigma}_{pr} = \chi_r\ \Delta\sigma_{pr}$$

where χ_r is the reduced relaxation coefficient and $\Delta\sigma_{pr}$ is the intrinsic relaxation. To calculate $\Delta\sigma_{pr}$, Equation (3.24) or (3.25) may be used. For χ_r values, tables and graphs of the text by Ghali and Favre (1986) were used.

Thus, approximate prestress loss values were calculated by Equation (A.11).